A Study of the Effect of Machine Parameters on Defects Produced in EOS Additive Manufacturing Builds

A Dissertation Presented for the
Doctor of Philosophy
Degree
The University of Tennessee, Knoxville

Tina White Malone
May 2023

Acknowledgements

Andrew Chaloupka
Erin Lanigan
William Battle
Brian West
Erin Richardson
Catherine Bell
Brady Kimbrel
Rachel Bardsley
Colton Katsarelis
James Morgan
Richard Boothe
Pat Salvail
Bryan Tucker
Ching Hua Su

A special thanks to Dr. Yu, my advisor, and all of my committee.

Preface

Numerous studies have been conducted to look at the defects produced by additive manufacturing, using various types of equipment. This study is limited to materials built on an EOS (Electro Optical System) 3D printer using an EOS in situ monitoring system.

Abstract

[5]Additive Manufacturing (AM) is defined in the American Society for Testing and Materials (ASTM) standard F2792 as “a process of joining materials to make objects from 3D model data, usually layer upon layer, as opposed to subtractive manufacturing methodologies. It provides an advanced method for building complex geometries and parts for high performance with a significant cost savings. [55]It’s advantages include the reduced need for tools and molds commonly used in manufacturing, a large reduction in wasted material, much shorter manufacturing cycles for the building of hardware, and its uniquely inherent ability to produce much more complex shapes. Polymers, metals, ceramics, and composites can all be built using some method of AM.

The use of standardized vendor parameters for additive manufacturing builds has resulted in numerous defects in the as-built parts. This study looked at HR-1 products built on an EOS M290 DMLS 3D printer. The builds were monitored using an EOS in-situ monitoring system to identify when “problems” began to occur and it compares the “problems” with the results of post build computed tomography inspections. It also looked at the defects produced and evaluated them versus the additive manufacturing process parameters.

Table of Contents

List of Tables

List of Figures

List of Equations

Chapter 1

Introduction and General Information

[5]Additive Manufacturing (AM) is defined in the American Society for Testing and Materials (ASTM) standard F2792 as “a process of joining materials to make objects from 3D model data, usually layer upon layer, as opposed to subtractive manufacturing methodologies. Lu[13] et al and Li[14] label it a “bottoms up” approach, as opposed to the traditional, top-down approach of subtractive manufacturing. It provides an advanced method for building complex geometries and parts for high performance with a significant cost savings. [55]It’s advantages include the reduced need for tools and molds commonly used in manufacturing, a large reduction in wasted material, much shorter manufacturing cycles for the building of hardware, and its uniquely inherent ability to produce much more complex shapes. [5]The ASTM standard divides the additive methodologies into 7 categories: Binder Jetting, Material Extrusion, VAT Photopolymerization, Material Jetting, Sheet Lamination, Directed Energy Deposition (DED), and Powder bed fusion (PBF). Polymers, metals, ceramics and composites can all be built using some method of AM. Table 1.1 shows the categories, provides a description of the methodologies of the AM process, and gives some examples of the types of AM.

According to Yao Chen, et al, AM is particularly adept at providing “low-cost, short cycle, and rapid prototyping of large and complex metal structures for aerospace and

Table 1.1 Categories of the Additive Manufacturing Process [5, 55]

AM Technology	Description	Examples
Material extrusion	Material is selectively dispensed through an orifice or nozzle.	Fused Deposition Modeling (FDM)
Vat photopolymerization	Pre-deposited photopolymer in a vat is selectively cured by light-activated cross linking of adjoining polymer.	Stereolithography apparatus (SLA) Digital light processing (DLP) Continuous liquid interface production (CLIP)
Binder jetting	A liquid bonding agent is selectively deposited to join powder material	Three-dimensional printing (3DP) Binder Jetting (BJ) Powder bed and ink-jet head (PBIH)
Material jetting	Droplets of build material are selectively deposited.	Material jetting (MJ) Drop on demand (DOD)
Sheet lamination	Sheets of material are bonded to form an object.	Laminated object manufacturing (LOM)

Table 1.1 Continued.

AM Technology	Description	Examples
Powder bed fusion	Thermal energy selectively fuses regions of a powder bed.	Selective laser sintering (SLS) Direct metal laser sintering (DMLS) Electron beam melting (EBM) Selective heat sintering (SHM) Laser beam melting (LBM)
Directed energy deposition	Wire or powder is blown from a nozzle and melted by an electron beam or laser.	Laser metal deposition (LMD) Electron beam free-form fabrication (EBF) Laser engineered net shaping (LENS) Directed laser deposition (DLD) Direct metal deposition (DMD)

defense equipment, such as spacecraft, missiles and satellites." But it cannot produce the ideal mechanical properties and surface roughness for many of the requirements that are needed to benefit most applications. According to [6]Everton, et al, the state of the art for AM machine tools has greatly improved from the earlier versions of the 1980's, but problems with porosity, cracking, thermal management, and material supply do continue to persist and have been attributed to "…a lack of in-process, monitoring and closed loop control algorithms used to manage machine operations." In Everton's report, it is stated that this rapid uptake of AM is demonstrated by figures shown in the Wohler report which is "a compendium of commercial activity relating to AM." [47]The 2013 document reports a growth rate of 38.9% to "$2.015 billion for the AM services market". Which demonstrates that the interest in AM and associated processes continue to persist, and further, that sustaining technologies such as in-situ monitoring, are becoming important research areas as well.

[15]Selective Laser Melting (SLM) is an additive manufacturing process that is relatively mature and has been the subject of much research for utilization to manufacture metallic hardware. A CAD model is developed which provides data to slice the design into thin layers and direct the machine to follow a scan path with each layer. Layer by layer the process continues until the part is built. Figure 1.1 shows a schematic of an SLM setup, from reference 16. In an article by [7]Alldredge, et al, an approach for system planned for use in this study. Their approach is described as one that "…allows for the detection of anomalies in real time, enabling corrective action to potentially be taken, or

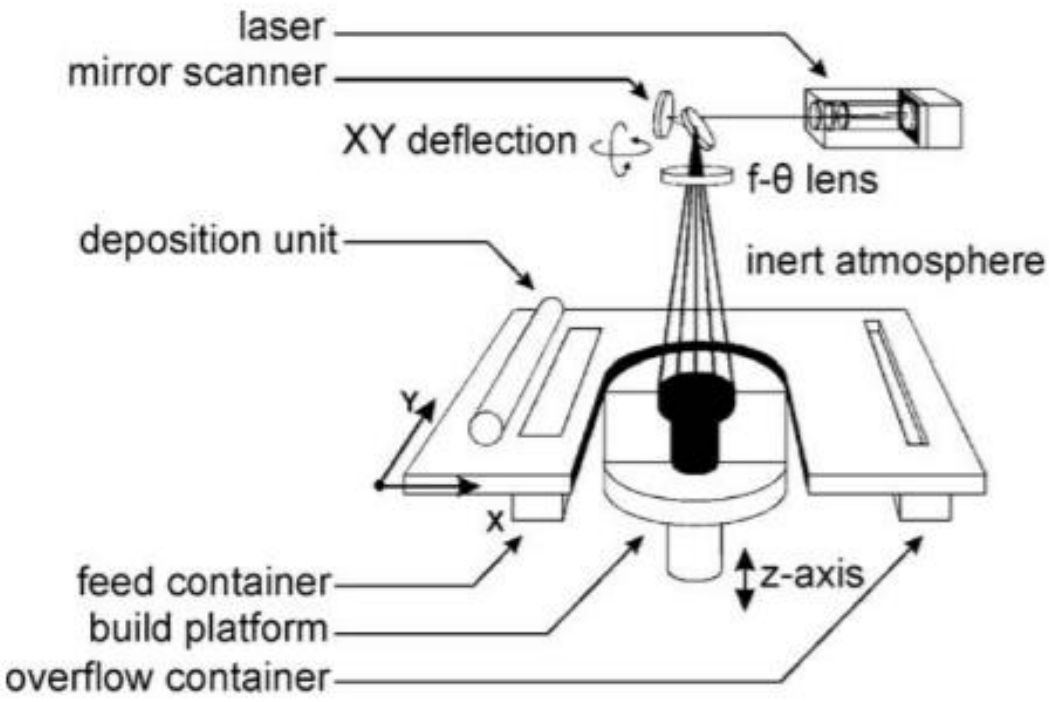

Figure 1.1 A Schematic Layout of an SLM Setup [16]

parts to be stopped immediately after the error, saving material and time."

[8]In an article by Freedman that was published in December of 2011, Prabhjot Singh, manager of GE's Additive Manufacturing Lab is quoted as saying that, "…We still don't understand why a part comes out slightly differently on one machine than it does on another, or even on the same machine on a different day." These words were also quoted in another article by [9]Dunsky in September of 2014 and Dunsky added, "In large part, that assessment is still accurate today." I too can say, based on my research into this subject, it is still not completely known as to why this occurs. There is still work left to be done. Dunsky also quotes Dr. Florian Bechmann, head of development at OEM equipment maker Concept Laser GmbH (Lichtenfels, Germany), as saying that increasingly in metal AM machines, "customers expect active process monitoring and series production capability, i. e., producibility at an industrial level." According to him, "In-situ, real time monitoring" of these processes would address these concerns but the technology still has a long way to go to achieve that goal. Although systems now exist to perform that task, they still are not commonly accepted for use for this purpose by industry.

[6]Process, condition, or "in-situ" monitoring as used in conventional machine tools relies on force, position, and acoustic sensing to gather data needed to make an assessment. In order to accomplish this ability in AM an entirely new or at least a different usage of existing technology was needed to achieve this goal. Much research went into developing processes and technologies that could potentially provide useful data to

evaluate an ongoing process without requiring the eventual “ex-situ” inspection and analysis. The final quality and homogeneity of AM parts are often identified as inadequacies with AM and continuing research is needed to address this problem.

This study looks at HR-1 products built on an EOS M290 DMLS 3D printer. The powder used is HR-1, which is variation of a high strength Fe-Ni alloy developed by NASA in the 1990’s to resist high pressure hydrogen embrittlement, oxidation, and corrosion. The typical composition and certified composition for the HR-1 powder is provided in Table 1.2. The powder used was 44 micron (Lot # HRA9) ordered from Pratt & Whitney – HMI Metal Powders. The builds were monitored using an EOS in situ monitoring system to identify when “problems” began to occur and they were compared with the results of limited computed tomography inspections. X-rays were also taken of the separated specimens prior to any testing. The comparison helped to identify which “problems” equate to real defects post build. The purpose was to develop a process through which one can identify defects as they are forming and then stop the build before a part is completed, thereby eliminating wasted time and money. It is feasible and this study shows that it can be done.

Currently and for years in fact, much of the structure and properties of AM built components have been optimized by a “trial and error approach”[61]. This is true for much developmental material and/or manufacturing work. For this effort a DOE was designed using Minitab software and three of the most significant build parameters.

Table 1.2 Composition of HR-1 (all values in %).

	Fe	Ni	Co	Cr	Mo	V	W	Ti	Al
Typical	Balance	34	3.3	15	2	0.3	1.8	2.5	0.3
Certified	Balance	33.91	3.79	14.66	1.83	0.302	1.6	2.41	0.243

.

These are laser power, scan speed and hatch spacing. Levels were chosen that bound or include the levels that are currently being used for processing the HR-1 material. The builds were evaluated using in-situ monitoring. Build pieces were characterized by post build NDE methods including x-ray of all the specimens and some limited computed tomography. The original plan included mechanical behavior methods but due to issues during the builds, these tests were not completed. Metallography and microscopy was completed on a limited number of samples. The in-situ results showed that some of the runs were very hot and some were cold, but did not indicate specific defects.

1.1 Benefits of Additive Manufacturing

When new parts, items, widgets, if you will, are being developed, a methodology is broadly used that begins with a design. It may or may not be well thought out in the beginning, how that design will be built and then certified for use. A lot depends on the final use. Eventually, materials will be chosen and a plan will be developed as to how the part will be manufactured and evaluated for the given purpose. Ideally the plan should also include how to prevent or respond to defects in the manufacturing process which will invariably occur in the beginning of the product development. Solutions to these problems must be developed because there will be a cost associated with every problem. A cost of either time or monetary loss. Standard manufacturing processes for materials usually involve a lot of wasted material or material that must be recycled. Literally tons of chips can be generated when parts are machined from large pieces of metal or other materials, and these chips must be disposed of or recycled in some manner which then introduces more cost into the process. Using additive manufacturing

eliminates a lot of this waste making it a very desirable alternative from the standpoint of less wasted material and time. But it also brings into play other issues that must be dealt with. Inconsistencies or defects occurring during the AM process can add back in a significant amount of cost, if it is required that widgets be tossed aside and/or recycled. This too can introduce a significant amount of cost into the process.

Additive manufacturing is generally selected for building hardware, as an effort to save time and money. It is expected that the issue with defects will eventually be minimized to the point that both the cost and time savings can be realized. But that is only a part of the equation. Usually, a material is first selected to meet the requirements of the widget to be built. The requirements may include any number of factors. Frequently strength is among those requirements, but not always. When strength is important, the method of manufacture makes a significant difference. AM generally makes a difference in the strength of a material. This process affects other properties as well.

A material is then chosen that is expected to meet the requirements for the widget. Sometimes there is data in the literature to assess what processes may be used to build with and may or may not include AM data. Sometimes the material and process will be selected in concert. A comparative study will likely be performed to select both the material and the process and there may be many other factors that come into play. But of late, more and more items are chosen to be manufactured by additive manufacturing for the savings that it affords.

The use of in-situ monitoring can also provide significant benefit to using the AM process. There is still a lot of work to be done to completely utilize the benefits provided by AM. But using in-situ monitoring potentially allows for a greater degree of certainty in the success of the final product.

1.2 In-Situ Monitoring

[55]AM is particularly well suited for aerospace and defense applications that need to be low cost and are produced in minimal numbers. Things like spacecraft, missiles and satellites fall into this category. They are mostly complicated items and are built only a few at a time. But right now, AM is not able to consistently produce the parts with the mechanical properties and surface roughness needed for these applications, while producing them defect free.

[55]The requirements for AM include rapid, low cost detection and the ability to adapt to the type of structure being produced as well as the specific conditions of the AM product such as rough surface condition and multiple defect types. It would definitely be a plus to be able to detect problems or defects in process thereby presenting the opportunity to eliminate defects altogether.

Traditionally, parts are built first and then tested and/or inspected. Tests and inspections may occur at different points in the manufacturing process including raw materials, machined or as built and so on. At least some of these tests and inspections would invariably be required for any part that is being built by any process. But a reduction in

some of the post build non-destructive inspections or tests could be accomplished by using in-situ monitoring. That is, the parts could be observed while being built, therefore knowing exactly what is being constructed and perhaps eliminating the need for many of the post build inspections. This would greatly minimize the necessity of dealing with imperfect parts and/or recycling parts that do not meet the design criteria. This study will focus first on determining the cause of defects produced in the process and then on the use of in-situ monitoring to minimize the defects remaining in the hardware at the end of the additive manufacturing process. It will develop a method for choosing parameters that will not cause defects to start with in the final material condition as well as visualizing what defects would exist based on the results from in-situ monitoring and thereby enable a process that could be stopped when the first real problem occurs. Then the methodology can be further extrapolated for use with other materials.

In-situ monitoring of materials during AM processing focuses on abnormal phenomena occurring during the process. Then the phenomena can be used to predict when a defect is occurring. Post build testing with standard non-destructive evaluations such as computed tomography can then be used to establish a relationship between the process conditions that have occurred and the final part quality.[55] The plan was to use the data that I collected to develop a model that could be used to assess the defect generation during the process of manufacturing the AM specimens during this study. Unfortunately, some of those abnormal phenomena occurred which limited the ability to model the data. This will be discussed in greater detail in a later chapter.

1.3 Cost and Time Benefits

The benefit to both cost and time will be substantial. When a piece of hardware is built, numerous moderate defects can be introduced during a single build cycle. Or one large defect can be introduced at any time during the build cycle. Either way, once a substantial defect is introduced, all the time and material used to complete that build cycle is wasted as well as any additional time or funds used to do additional testing and preparation for the post build tests. Since the production of a defect can be detected during the build process and if it can be shown to be of sufficient magnitude so as to warrant stopping the process, then significant savings can be achieved by doing so. This is already done to an extent when developing the unique process for a piece of hardware. However, defects and issues still occur down the road no matter how well the process is developed, and a substantial savings can still be had by knowing what is meant by the problems detected by in-situ, during even a well characterized process.

1.4 Benefits for In-Space Builds

The benefit to be had for using in-situ in the space environment is even more significant. Every ounce/gram of material that is carried into space for the purpose of building an item, is needed in space and has a much more significant, several fold, cost attached to it. Any amount of waste that can be avoided is huge compared to wastes here on Earth. We can and do produce a lot of waste here on Earth, but that is a luxury we cannot afford when working and building hardware in space.

[52]There are currently about 29,000lbs of hardware spares and replacement units on the International Space Station (ISS), staged and ready to keep work going up there. Another 39,000lbs are sitting here, ready to be launched at any time and as they are needed. Typically, about 7,000lbs are launched yearly. A testbed using 3D printing is currently being used on the ISS to develop a way to manufacture all those necessary parts in space. NASA's next step will be to apply the use of AM to the longer duration missions to the Moon and Mars where moving hardware from earth is a much greater engineering obstacle. The ability to use in-situ monitoring to improve productivity of AM is very nearly a necessity in space. Carrying cargo into space that may become useless hardware containing defects which cannot be repaired is a major roadblock. It is necessary that the hardware built in space be as near perfect as possible so that the time and materials spent building it, will not be wasted. The cost of the excess cargo alone, that is going into space, is prohibitive. It is a waste that cannot be afforded. A methodology such as in-situ monitoring is needed to make it possible to prevent such waste by stopping a process just as soon as it becomes evident that it will not result in usable hardware. This study will enable a process that will do just that. It will allow for stopping an AM built before a lot of time and material waste has occurred thereby minimizing the impact of that waste.

Chapter 2

Literature Review

2.1 Parameters for Additive Manufacturing

According to Zhang, et al[1] there are many parameters utilized for the SLM (selective laser melting) process that when improperly chosen will inevitably cause defects. These include laser power, scan speed, hatch spacing, layer thickness, powder materials, chamber environment, and others. In this report, they identify porosities, incomplete fusion holes, and cracks, as the three most common classifications of defects in SLM structures. According to their article, the major process factors that are related to defect formation are laser energy input, powder material, and scan strategy and they discuss defect formation in terms of these factors.

Zhang, et al, also suggested that the rapid melting and then solidification that occurs during SLM builds causes a high cooling rate that ultimately yields a part that has a fine-grained microstructure and better tensile properties. But they say the parts will also have a “directional effect” which causes severe anisotropy. Additionally, they say that the defects that are formed in the horizontal direction will significantly reduce the load-bearing cross sectional area resulting in lower strength.

Sciammarella[2], conducted a study using a DOE of laser power, travel speed, and powder feed rate to measure the influence of thermal conditions and how they would define the microstructure and micro-hardness of the material produced. His conclusion

was that it is possible to achieve a suitable microstructure with a small percentage (1.1%) of porosity while maintaining a micro-hardness that is equivalent to standard wrought 316L. He achieved this by building with a powder flow to travel speed ratio the same as the power level. This minimized the heat input for the build.

Another study by Hanzl*[3] looked at the influence of hatch angle, building direction, layer thickness and overlap rate on the mechanical properties of SLM (selective laser melting) mechanical properties. This study showed that the properties were influenced by the building direction but were not affected by other parameters such as layer thickness and overlap rate.

A report by Hossein[11] reviews the types of defects that occur during additive manufacturing and the mechanisms that cause them. It also looks at how to detect the defects and an evaluation of the properties and metrology of the materials once they are manufactured. This report similarly looks at process parameters, powder and substrate characteristics, material parameters, and processing mechanisms, as well as the microstructural anomalies produced therein. The report describes seven defects/phenomenon that occur during the additive process. These are defined as: Microstructural anomalies, porosity including general porosity, gas porosity, and porosity due to lack of fusion, anisotropy and shade stability, inclusions, geometrical anomalies, balling phenomenon, cracks (and similar linear features), defects in the powder materials, and finally, defects in functionally graded materials manufactured by AM methods. Similarly, the report states that the generation of defects is related to

process parameters which in this case include laser power, scan speed, layer thickness, spacing of scan lines, powder feed rate, powder size distribution, and surface chemistry. Even so, the combined influence of these and other parameters is still not well understood and this author states that robust process models are still needed to reach a clear understanding of the defects produced.

There are many articles and research reports that discuss the types of defects found in additively manufactured hardware. These include articles by Thijs[16] and Aboulkhair.[18]. A study by Fulga[12], et al, discusses an approach for the identification of in-line defects and failures during additive manufacturing powder bed fusion (AM PBF) processes using the example of the selective laser sintering (SLM) process. For AM in an industrial environment he says, "…statements about product quality are indispensable". Documented compliance as far as geometric tolerances and physical parameters are a requirement and the sooner they can be obtained the better, for making the AM as efficient as possible. Meaning that in-situ monitoring would be greatly beneficial to the certification processes. One aspect identified the need for a study of the condition of the feedstock, i.e. the reusability of the powder while another addresses the levels of the process parameters used in manufacturing. The elements deemed pertinent in this study are: Laser power, Scan speed, scan line, temperature profile, layer thickness, laser exposure style, hatch distance, and atmosphere. The next level of this work was expected to be a rigorous DOE to identify valid conclusions allowing a ranking of these factors that influence quality by causing in-line defects and failing parts.

2.2 Types of Defects

According to Zhang[1] the types of defects found in additive hardware include porosity, incomplete fusion, and cracks. There is an additional type of defect described by Yao Chen[55] called balling.

Zhang has said that porosity is formed when gas that is present between or within the powder particles dissolves in the molten pool before it solidifies. The cooling rate is high during solidification and once the gas is dissolved, it can't come back out before the solidification process is completed, thereby causing the porosity. Gas is always available to be dissolved into the powder.

[19]The spherical porosities are attributed by Gong et al, to gas that is generated by high laser energy being applied to the molten pool causing gas bubbles due to vaporization of the low melting point additions in the alloy. The SLM solidification rate of the molten pool does not allow gas bubbles enough time to reach the liquid surface and escape into the environment. Thus the high energy input or perhaps inconsistent processing parameters may cause spherical porosity that is distributed in a completed part. These defects are difficult at best to completely prevent but can certainly be minimized. [55]Pores can also be generated from a lack of fusion within the part as it is being built. Figure 2.1 shows examples of porosity type defects found in SLM and EBM Ti-6Al-4V materials.

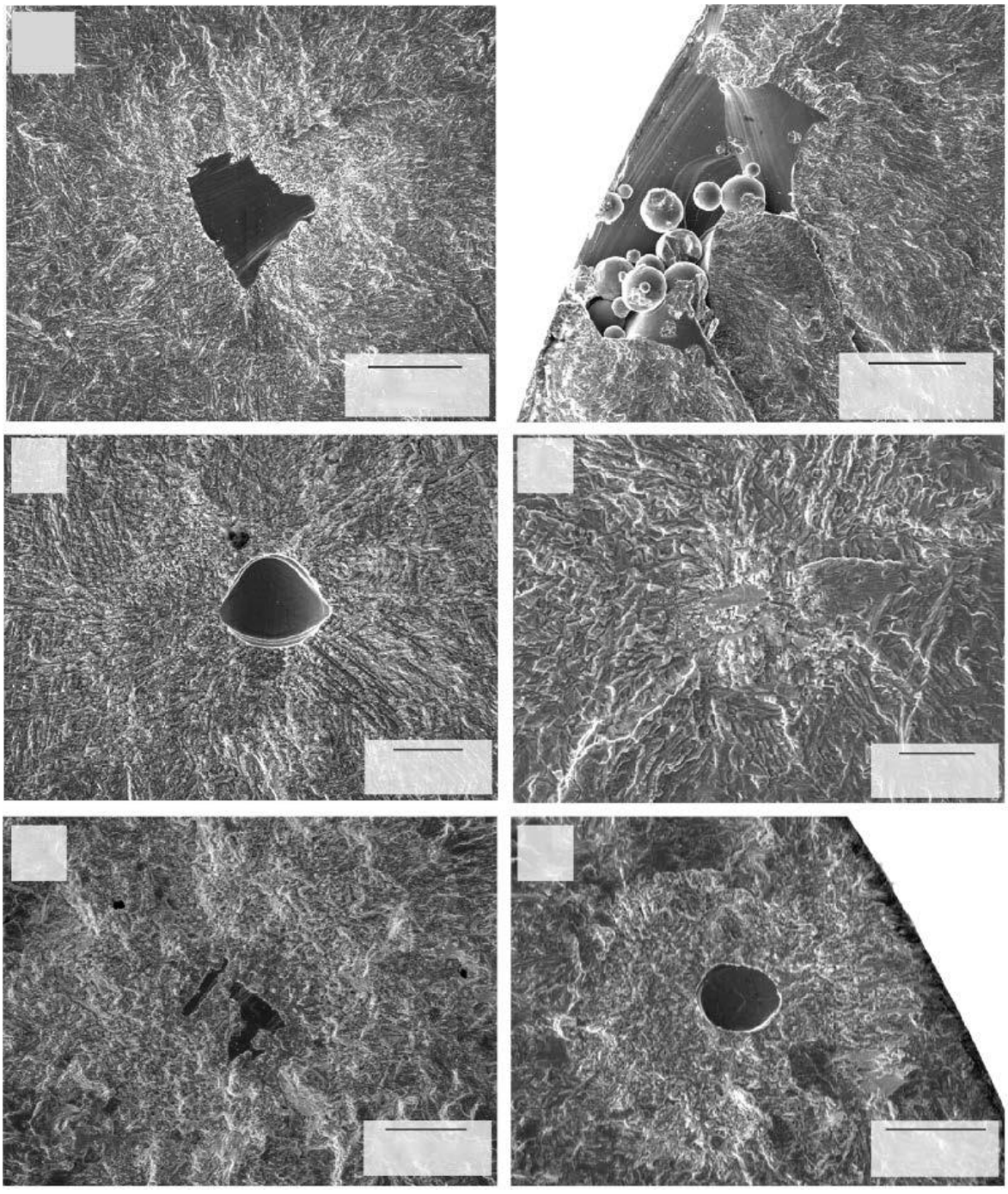

Figure 2.1 Examples of porosity type defects in SLM and EBM Ti- 6Al-4V materials [57]

[19,20,21]Another type of defect that occurs in the AM parts is incomplete fusion. These are believed to result from inadequate energy during processing. Inadequate energy during the SLM process may also result in not fully melting the metal powder causing the next layer to be incompletely fused to the first. This can result in defects containing incompletely melted powder. Figures 2.2 and 2.3 show some examples of lack of fusion defects in selective laser melting (SLM) of AlSi10Mg [64].

[24, 25, 26]Because of the rapid melting and solidification during the SLM process, a large temperature gradient can occur and may cause crack initiation and propagation. Cracks are another form of defect that can occur in AM builds.

[55]Figure 2.4 shows some examples of liquation and cracking that occurred in Inconel 738. Superalloys tend to be more vulnerable to cracking, but it is said that the cracking can be reduced by preheating the substrate and having a more desirable ambient environment. The internal defects or cracks that tend to occur in AM components have been shown to occur mainly from thermal stresses during the forming process. Many studies have shown that cracks may be generated when liquid films form on grain boundaries in a heat affected zone or when tensile stresses have formed in parts.[23, 57-60] These occurrences can be the result of the process parameters used in the AM processing. [55]Cracks may also form as the result of thermal stresses being trapped inside the component and then released. These stresses are formed due to variations in the temperature of the metal powder and while it is melting. Balling or metal ball

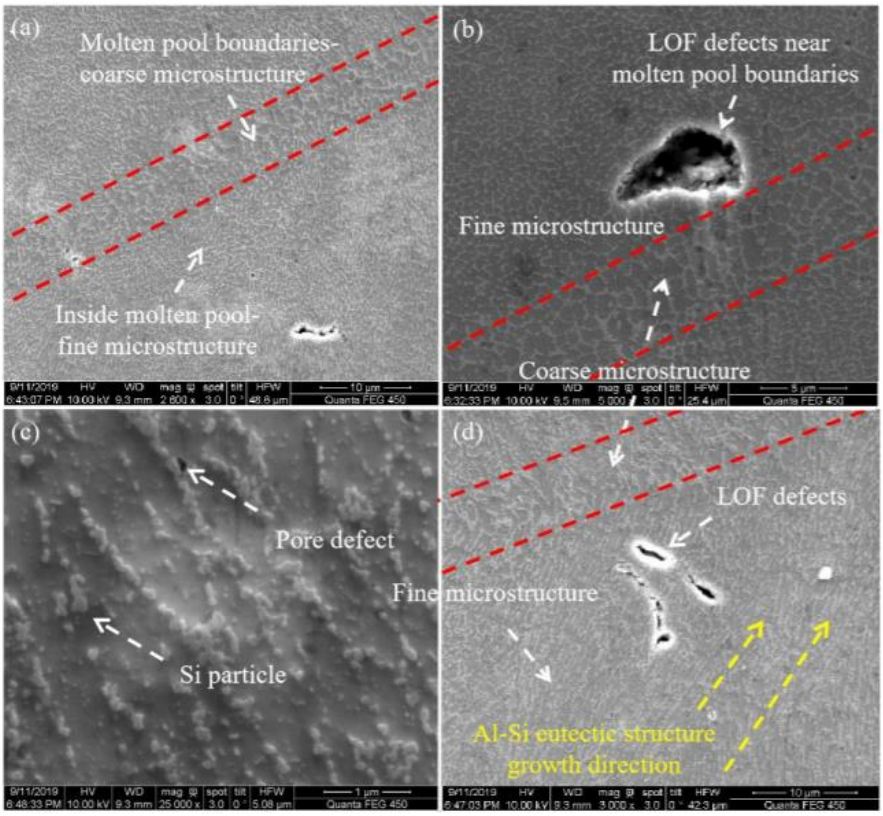

Figure 2.2 Typical Microstructure of Selective Laser Melting (SLM) AlSi10Mg alloy including LOF Defects [64]

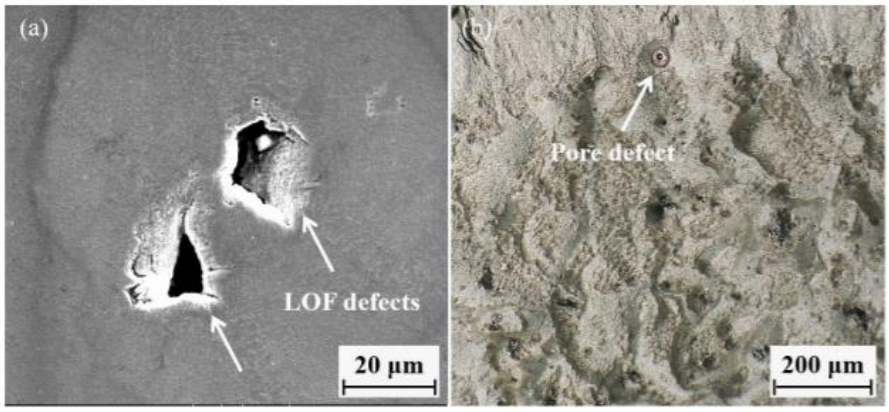

Figure 2.3 Typical defects of selective laser melting (SLM) AlSi10Mg alloy: (a) Lack of fusion (LOF) defect; (b) Pore defect. [64]

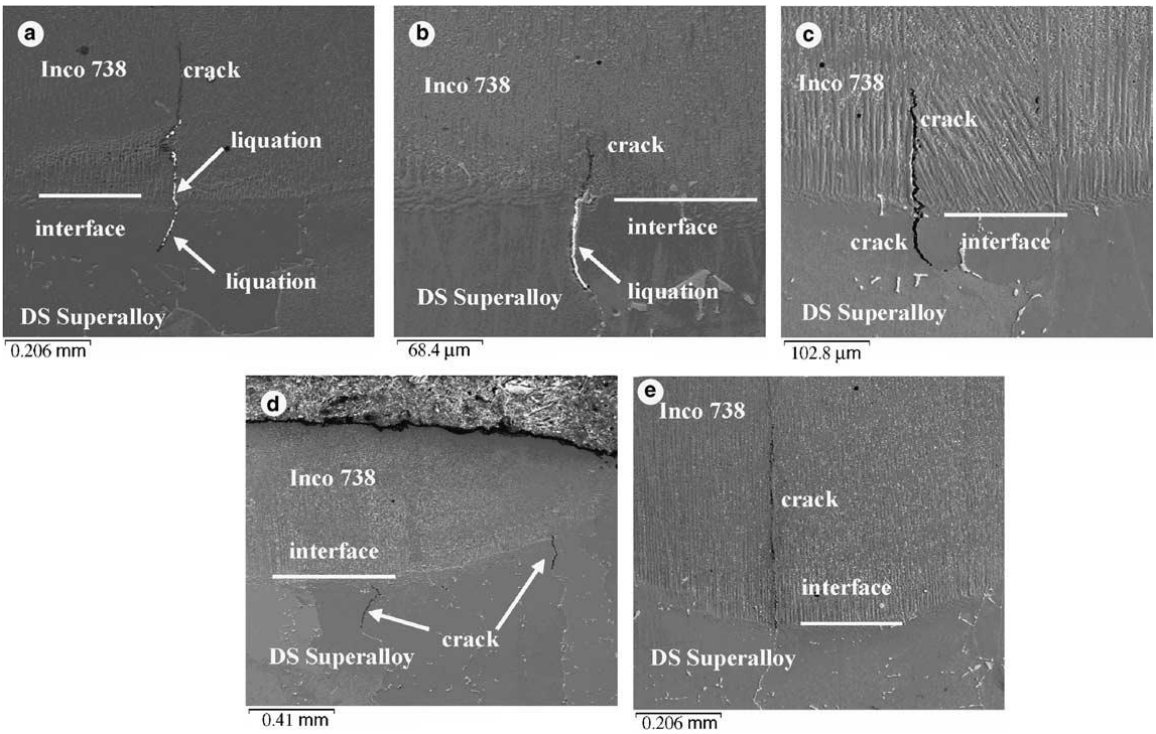

Figure 2.4 Examples of various liquation and cracking phenomenon in Inco 738 superalloy [55]

formation is described as occurring when material from the molten layer solidifies into spherical balls instead of a more uniform solid layer. This may be caused by interactions between the metal powder and the molten metal pool and may severely impede the connections of interlayers.

2.3 Defects and Process Parameters

There are many process parameters and other criteria that have an impact on SLM processes and the resulting defect formation. [18]Aboulkhair, et al have divided these factors into four groups: 1) laser related, 2) scan-related, 3) powder related, and 4) temperature related and each group contains a number of parameters, or criteria as depicted in Figure 2.5.

2.3.1 Laser Related

[1]The input of laser energy results in melting of the metal powder. The laser energy combined with the characteristics of the powder may have a significant impact on what defects may occur. The energy being applied to the material is a direct result of the combination of laser power, scan speed, hatch spacing, and layer thickness. If the scan speed is low and laser power is high, then more powder is melted and may result in porosity defects from the entrapped gas in the powder. When the rapid solidification of the SLM process occurs, the molten low melting point constituents may not have time to escape and can be solidified into the metal.

[24, 26, 27] This condition of the high laser energy can also result in high residual thermal stress which upon solidification can result in cracking. The higher the energy input, the

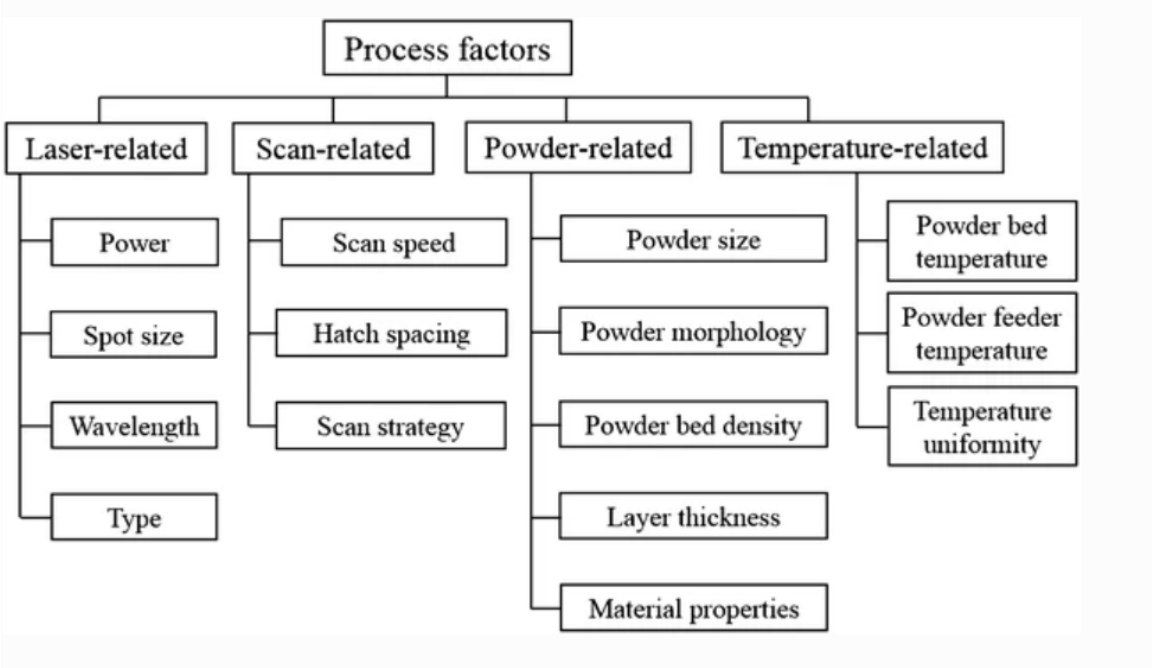

Figure 2.5 Factors involved in SLM process. [18]

worse this condition becomes. Beginning with micro cracks and continuing into cracks that are much worse as the metal undergoes much more severe shrinkage. [1]Conversely, when the scan speed is high and the laser power is low, powders may not be fully melted resulting in an incomplete fusion of adjacent tracks in the SLM or incomplete fusion defects liken to lack of fusion in weldments. There could also be an occurrence of a larger than normal powder layer that could result in inadequate penetration, liken to a lack of penetration defect that occurs in weldments. This would be due to the inadequacy of the laser energy that is input here.[19, 20, 26, 28]

[1]An equation that describes the energy density E, or energy that is input into the system, has also been used to describe the average energy that is applied during the deposition of material in an SLM process.

$$E = \frac{P}{vht}$$ **Equation 2.1**

where: E is the energy density in J/mm^3,
P is the laser power in watts,
v is the scan speed in mm/s,
and, t is the layer thickness in mm.

This equation has been used widely in the characterization of SLM processes and will be used in this study as well. It will allow a determination of the impact of the

parameters described above. [16, 19, 29] The specific level of the energy density needed depends on the specific material among other things. But it has been shown that an increase in the energy density is related to the defects that will be produced and can be used as an aid in selection of at least a starting point for SLM parameters.[1]

2.3.2 Powder Related

The morphology and size of metal powders is known to influence the flowability of the powder as it is introduced into the powder bed and therefore defect formation. In addition, the method of production of a powder, and the gas contained in the material will also influence defect formation. Though these aspects of the powder are very important they will not be considered as a part of this study and a single powder will be used.

2.3.3 Scan Strategy

Several different scan strategies have been tried with SLM and can affect both the amount of heat transfer that occurs and how the powder melts and solidifies.[1] This may have a major effect on how and where defects occur. There are at least three strategies that are being used for SLM processes. These are unidirectional, zigzag, and cross-hatching.[16] Unidirectional and zigzag are known to result in unstable laser power and reduced scan speed at the beginning and end of the scan which can cause higher laser energy and therefore more defects formation.[31] Defect accumulation and propagation may be reduced by a more balanced energy input as would be the case when a cross-hatching scan strategy is used.[1]

Three additional scan strategies have been developed for fabricating SLM parts. These are island[32], interlayer staggering and orthogonal scan strategies.[33,34] These three scan strategies are depicted in Figure 2.6.[16]

For the island strategy, the filled layer is initially divided into islands that are both random and continuous. Layers following the island are moved a bit to avoid putting all the defects in one place. This also tends to balance the thermal residual stress so that cracking is reduced. In this case, defects tend to be found near the interface between the islands and the following layers.[1,32] The island strategy is depicted in Figure 2.7. The schematic illustrates how (a) each layer is divided into islands and scanned, and (b) how the layers are effectively displaced to achieve the goal of minimizing defects.

Yang, et al[33,34] used interlayer staggering and orthogonal strategies in their studies to remove or reduce defects found in the tracks between scans. The overlapping zone between the tracks is used to ensure that the powder in the next layer is adequately melted which helps to balance the energy applied and reduces defects. Interlayer staggering and orthogonal scanning is depicted in Figure 2.8.

2.4 Defects and the Impact on Mechanical Properties

It is well known that defects cause a stress concentration in materials which can lead to reduced strength and possibly failure.[1] Cracks may form or they may already exist and propagate through the part. The degree of the impact varies depending on the type of

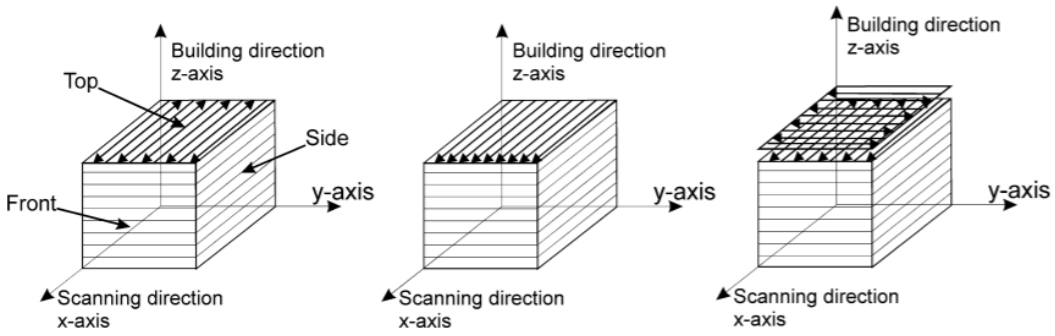

Figure 2.6 Scan Strategies [16]

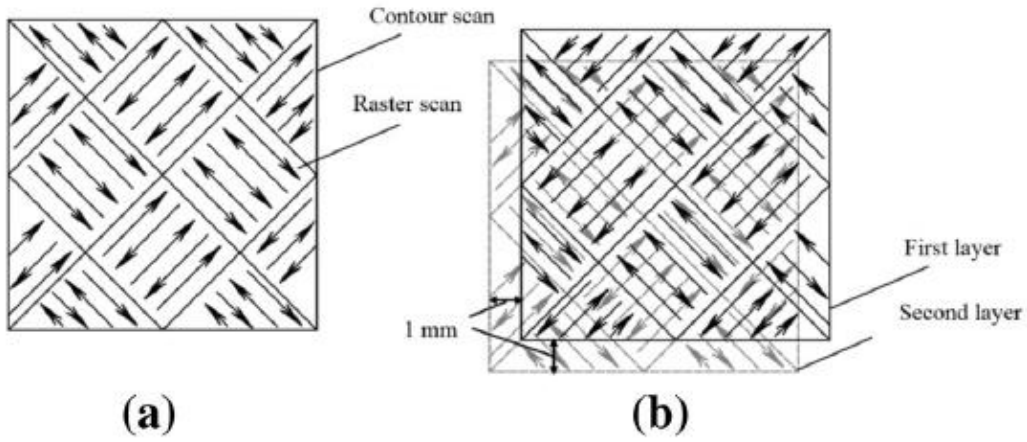

Figure 2.7 Island Strategy Examples [34], (a) each layer is divided into islands and raster scanned, and (b) the successive layers are displaced by 1 mm.

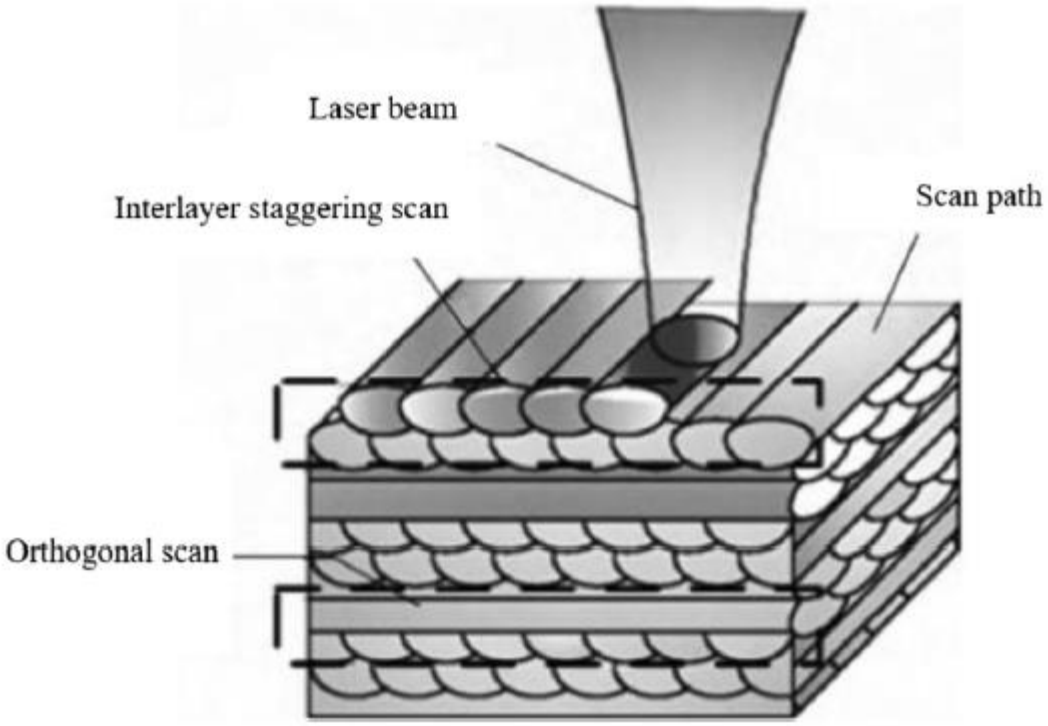

Figure 2.8 Interlayer Staggering and Orthogonal Scan Strategy [34]

defect and how it progresses. The following sections look at discussions of how the different properties are affected by any defects that are found in a structure.

2.4.1 Tensile Properties

It has already been discussed that during the SLM process, powders melt and solidify rapidly due to the high rate of cooling which ultimately produces a finer microstructure. The finer microstructure provides improved tensile strength when compared to the more traditional wrought materials. However, ductility measurements, such as elongation, can be significantly reduced. Data presented in references 35, 36, 37, and 38 shows that SLM produces parts with a finer grain microstructure and better tensile properties than that of traditional wrought materials. Data from these articles were combined in Table 1 of reference 1 to show this improvement. The table also shows the ductility of the material via elongation measurements which clearly shows the decrement when compared with traditional wrought materials. Wu[39] attributes this decrease, in part, to defects contained in the SLM parts.

2.4.2 Fatigue Properties

[1]Defects are detrimental to the fatigue life of any part and impacts SLM parts as well. Defects serve as crack initiation sites and points of stress concentration that will ultimately reduce the fatigue life of a part. References 40, 41, 42, 43, 44, and 45 all present data for Ti6Al4V that demonstrates this phenomenon as it relates to SLM produced materials and represents the summary of the data that Zhang used to develop Figure 2.9.

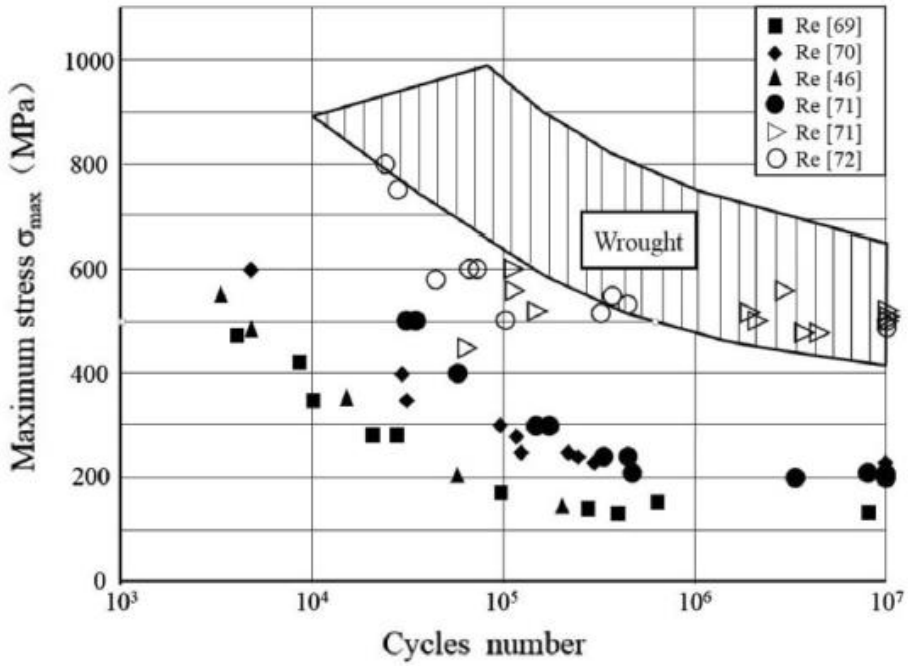

Figure 2.9 Summary of Fatigue Data for Ti6Al4V SLM Parts Containing Defects [1]

2.5 In-situ Monitoring Technology

Figure 2.10 shows a depiction of the EOS process for in-situ monitoring and feedback control of the selective laser powder processing.[46] [6]There was a report written in 2012 by the UK (United Kingdom) AM special interest group (SIG), called “Shaping our national competency in additive manufacturing.” It discussed the issue of non-robustness of additive manufacturing stating that it was “a key barrier to the adoption of AM in the UK.” [48]The “limited control and monitoring of processes, in-situ” was deemed to be a serious barricade to the employment of AM. [49]The need for in-situ monitoring and control was also documented by the United States National Institute of Standards and Technology (NIST) in 2013 in their “Measurement science roadmap for metal-based additive manufacturing.”

Table 2.1 shows a list of some of the technologies that are now available for in-situ monitoring. Most manufacturers of AM machines now offer some semblance of controls for the machines that they produce, as an add-on.

[6]Powder bed fusion is an AM process that uses either a laser or an electron beam to melt and solidify a spreading of loose powder on a build platform. In this case a laser is used. As each layer is continuously melted and fused to the next layer, the platform is lowered and once again covered with powder. This is the process used by the EOS

M290 which was used to build the specimens for my study. As has already been discussed, a wide range of discontinuities occur during the AM process and are known

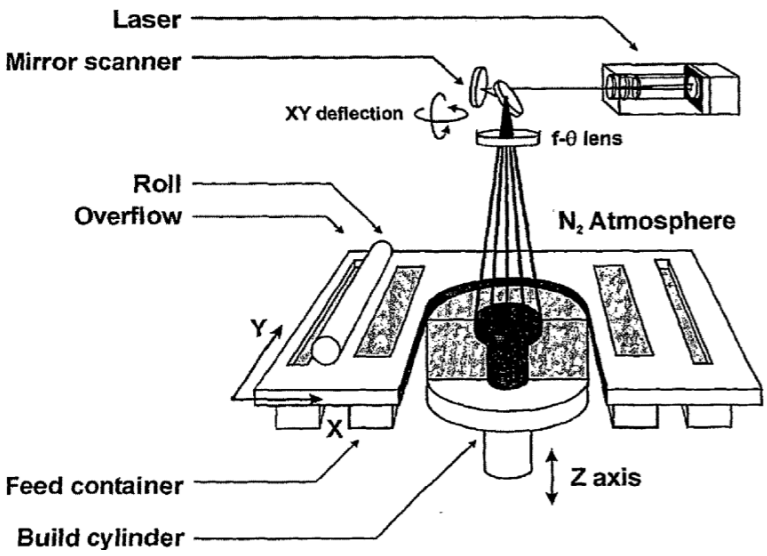

Figure 2.10 Depiction of EOS Process for In Situ Monitoring [46]

Table 2.1 In Situ Monitoring Technologies

In-situ measurement 'modules' available from AM machine manufacturers and measurement specialists.

AM process	Machine manufacturer	'Module' name	Failure mode monitored	Parameter altered	Equipment
EB-PBF	Arcam	LayerQam™	Porosity	N/A	Camera
L-PBF	B6 Sigma, Inc. (specialist)	PrintRite3D® INSPECT™	Unknown	N/A	Thermocouple and high-speed camera
	Concept Laser	QM melt pool	Melt pool monitoring	Laser Power	High-speed CMOS-camera
	EOS	N/A	Unknown	N/A	Camera
DED	DEMCON	LCC 100	Melt pool monitoring	Laser Power	Camera
	DM3D Technology	DMD closed-loop feedback system	Melt pool monitoring and build height	Laser Power	Dual-colour pyrometer and three high-speed CCD cameras
	Laser Depth	LD-600	Depth measurement	Laser Power	Inline coherent imaging
	Promotec	PD 2000	Melt pool monitoring	N/A	CMOS-camera
		PM 7000	Melt pool monitoring	N/A	1D photo detector
	Stratonics	ThermaViz system	Melt pool temperature	Laser Power	Two-wavelength imaging pyrometer

to be tied to the input parameters. Numerous non-destructive in-situ methods have been looked at for laser and EB PBF. Visual and thermographic methods are both common and the EOS uses both. There are other, more novel techniques that have also been looked at. [50]Purtonen, et al provides a discussion of monitoring and adaptive control in their paper on laser processes.

2.6 Additive Manufacturing in Space

[51]The 3D Printing Media Network has said that AM will have a "key role in enabling the future of human space travel and interplanetary colonization." It is already being utilized for reducing the cost of satellites and making rockets that are both lighter and more efficient. One of the biggest challenges that any space endeavor will face is the huge cost of sending payload into space which can be greatly impacted by utilizing AM materials. AM can be a very effective tool in reducing the total weight of a payload or spacecraft thereby reducing the need for more powerful launch vehicles.

The future will not only bring more space travel but also more manufacturing in space. The more traveling into space that occurs the more production of hardware in space that will occur and additive manufacturing along with in-situ monitoring will be key to pursuing these endeavors. According to the 3D Media Network, "…AM has the potential to be one of the key elements that will help the commercial space industry grow into maturity. …no technology can deliver on-location, distributed manufacturing of complex parts more efficiently than additive manufacturing." There are already projects that are funded by NASA and ESA for the purpose of exploring the use of various AM methods

for building the infrastructure that will soon be required to make the trip to the Moon and later to Mars.

[52]In 2014 under a project called “In-Space Manufacturing”, NASA began leading the development of technologies that will eventually enable the use of AM on-demand as astronaut teams return to the moon and go further to also explore far reaching locations such as Mars. A 3D printer stationed on board the ISS was utilized to build tools via a design that was transmitted from Earth. These items were built from polymer powder but metal 3D printing is also in the works.

2.7 Benefits of the In-Situ Monitoring Methodology

[53]According to Alldredge, et al, in 2018, “One of the major challenges in metal additive manufacturing is developing *in-situ* sensing and feedback control capabilities to eliminate build errors and allow qualified part creation without the need for costly and destructive external testing.” This is just one article that has spoken to the need for in-situ monitoring. They also say that once this methodology is “realized and validated,” in-situ can provide real time feedback, process optimization, residual stress control, and parameter optimization. It will also make it feasible to qualify AM parts, develop new AM materials, control both the microstructures and properties, reduce the need for support structures and improve dimensional accuracy and surface roughness of the parts produced. Which will then cause AM’s use to be more readily adopted and proliferate.

Chapter 3

Problem Definition

This chapter discusses the definition of the problem that is addressed by the subject of my dissertation.

3.1 Defects Occurring in Additive Manufacturing Built Hardware

The use of standardized vendor parameters for additive manufacturing builds sometimes results in numerous defects in the as built parts. The standardized vendor parameters are developed for a specific material and may work very well in some cases. But usually, it is necessary to make modifications for specific parts, i. e. parts are not always producible with the standard AM parameters, so modifications are required to achieve a part with limited defects. Some of the parameters that were considered for use in this study are laser power, scan speed, hatch spacing, layer thickness, powder materials, and chamber environment. When adjusted slightly from the standards, these parameters guaranteed that defects were achieved in the final product, making it possible to do a good comparison between build material with and build material without defects. Unfortunately, all the material produced had at least some porosity and I believe that is the norm because HIP is standardly used post process along with the standard heat treatment. The preliminary parameter choices were power, scan speed, hatch spacing, and layer thickness, but to limit the study to only one panel three parameters were used. Due to the problems with the first and later builds, data was collected from part of three builds. The first build was very short. The second build was

restarted and continued with build #3 and finally the fourth build was almost complete. So, the original plan to replicate the evaluation in two separate builds did not happen. But in some cases, more than one panel was assessed with extra material that was available.

As was previously discussed in Chapter 2, the defects typically occurring in SLM builds are porosity, incomplete or lack of fusion, and cracks. It was expected that each of these types of defects would be observed in the panels that were built in this study, but only porosity was found in the final material product. The parameters were chosen based on a partially optimized set of parameters that was expanded by about 10%, to achieve defects. The defects that were found within the build were evaluated against the observations of the in-situ monitoring system.

[54]An EOS M 290 located at Marshall Space Flight Center was used to build the test panels. The EOS M 290 is an industrial 3D printer. Figure 3.1 shows a picture of the EOS M 290. The M 290 is a DMLS printer which uses a 400W Yb fiber laser scanning up to 7.0 m/s with a focusing diameter of 0.004 in. The high beam quality of the laser spot is regarded as exceptional producing detail resolution ideal for manufacturing highly complex DMLS components that are expected to ensure homogeneous part properties from part to part, job to job, and machine to machine. It uses a 32A/400V power supply and consumes up to a maximum of 8.5 kW with an average consumption of 2.4 kW. The system software includes a CAM tool, EOSPRINT, for developing and managing each job, a module for inputting desired parameters called EOS Parameter

Figure 3.1 EOS M290 DMLS Printer

Editor, for application specific optimization of parameters and a comprehensive monitoring suite called EOSTATE which includes five different monitoring systems. These monitoring systems include system, laser, powder-bed, melt-pool, and exposure (optical tomography).

Additive manufacturing is beginning to be more and more widely used, however, there continues to be issues with defects. Processes can be developed to minimize them, but a great deal of parts, materials, and time, can still be wasted even with a process that is well developed. These wastes equate to a significant amount of both time and financial expense. To achieve parts with zero defects, a great deal of time, material and money can be expended while still building parts with defects.

In-situ monitoring is a process that has been developed to characterize problems as they occur within an AM build. The problems identified by in-situ have not been adequately studied and fully characterized to show clearly which defects are meaningful and substantially impact the usefulness of a structure, and which are merely minor anomalies. As a result, strategies to stop a build when problems occur and thereby prevent a lot of the waste have not yet been developed and are not being fully utilized.

It is theorized that this can be done by correlating the problems identified by in-situ monitoring with defects found by other post process non-destructive evaluations and verified by the evaluation of microscopy and materials properties. It was the goal of this effort to optimize a set of processing parameters for HR-1 for a set of test coupons that

will minimize the defects found in the final product. But the mechanical testing could not be completed as a result of the in-process issues that occurred and will be discussed more in chapter 4. It was also a goal of this effort to correlate the defects and other anomalies found by in-situ monitoring with any defects found by post process non-destructive evaluation (NDE) but no defects were detected by post process NDE. But I was still able to show how in-situ can be used to stop a process that is going to result in a useless part.

In addition, additive manufacturing is slated to have a very important role in establishing a long-term human presence in space, enabling future space travel and eventually interplanetary colonization beginning with a return trip to the moon and later travel to and extended visits to Mars. The use of AM for developing these missions is already almost certainly guaranteed but in-situ monitoring would significantly improve the ability of a service station-like post on the moon to aid those future missions to Mars by being able to monitor while building the hardware needed for excursions beyond the earth atmosphere. Thereby saving vast amounts of time for traveling to and from space.

3.2 A 3D Model Based on Transient Heat Transfer and Fluid Flow

[61, 62] In 2018, Mukherjee, et al, published a pair of reports on work leading to a 3D transient heat transfer and fluid flow model for multiple layers and hatches of the powder bed fusion (PBF) process. The model, according to Mukherjee, solves the equations of conservation of mass, momentum, and energy and uses the solution to obtain transient temperature fields, cooling rates and solidification parameters needed

to "...fabricate defect free, structurally sound and reliable components based on these principles." Mukherjee used this solution to develop a nondimensional number that can quantify the effects of parameters studied in the literature and the effects of these parameters on the lack of fusion (LOF) defects. This is the equation for that number:

$$Lr = \frac{\rho(Cp\ \Delta T + L)}{\frac{\eta P}{\pi r^2 v}}\ F\left(\frac{t}{d}\right)\left(\frac{h}{\omega}\right)^2 \qquad \textbf{Equation 3.1}$$

Where: ρ = density = kg/m^3
C_p = specific heat = J/kg K
$\Delta T = T_L - T_S$ = K where T_L and T_S are the liquidus and solidus temperatures of the alloy in question

L = Latent heat of fusion for the alloy = J/kg
η = Absorptivity of the laser beam
P = laser beam power = W
v = laser scanning speed = m/s
r = laser beam radius = m
F = Fourier number
t = layer thickness = m
h = hatch spacing = m
d = molten pool depth = m
ω = molten pool half-width = m

[62]Part II of Mukherjee's work presents his model and calculates the temperature field and molten pool dimensions for three alloys built using PBF, five hatches and three layers to avoid having the LOF defects.

Chapter 4

Research Methodologies

This chapter will discuss the design of the experiment conducted, the test methods used, the specimens tested, the analyses performed after testing, and the flow of the work done. The EOS M290 DMLS Printer was used with NASA-HR-1 alloy. HR-1 is a nickel based super alloy that was derived from JBK-75 and developed for high hydrogen environment embrittlement (HEE) resistance.

4.1 Flow of Testing Research

Figure 4.1 presents a chart describing the flow of experimentation that was originally planned for this dissertation. Some things had to be changed during the course of the experimentation because of problems that occurred during processing of the builds. There were additional builds that were made but some of the testing was not conducted as a result.

Additional builds were made but tensile tests were not performed and measurement blocks were not evaluated. X-ray was performed on all coupons and CT was only done on two of the specimens.

4.2 The Design

This section discusses the design of the experiment that was conducted to evaluate the defects produced by varying the process parameters outside of the standard

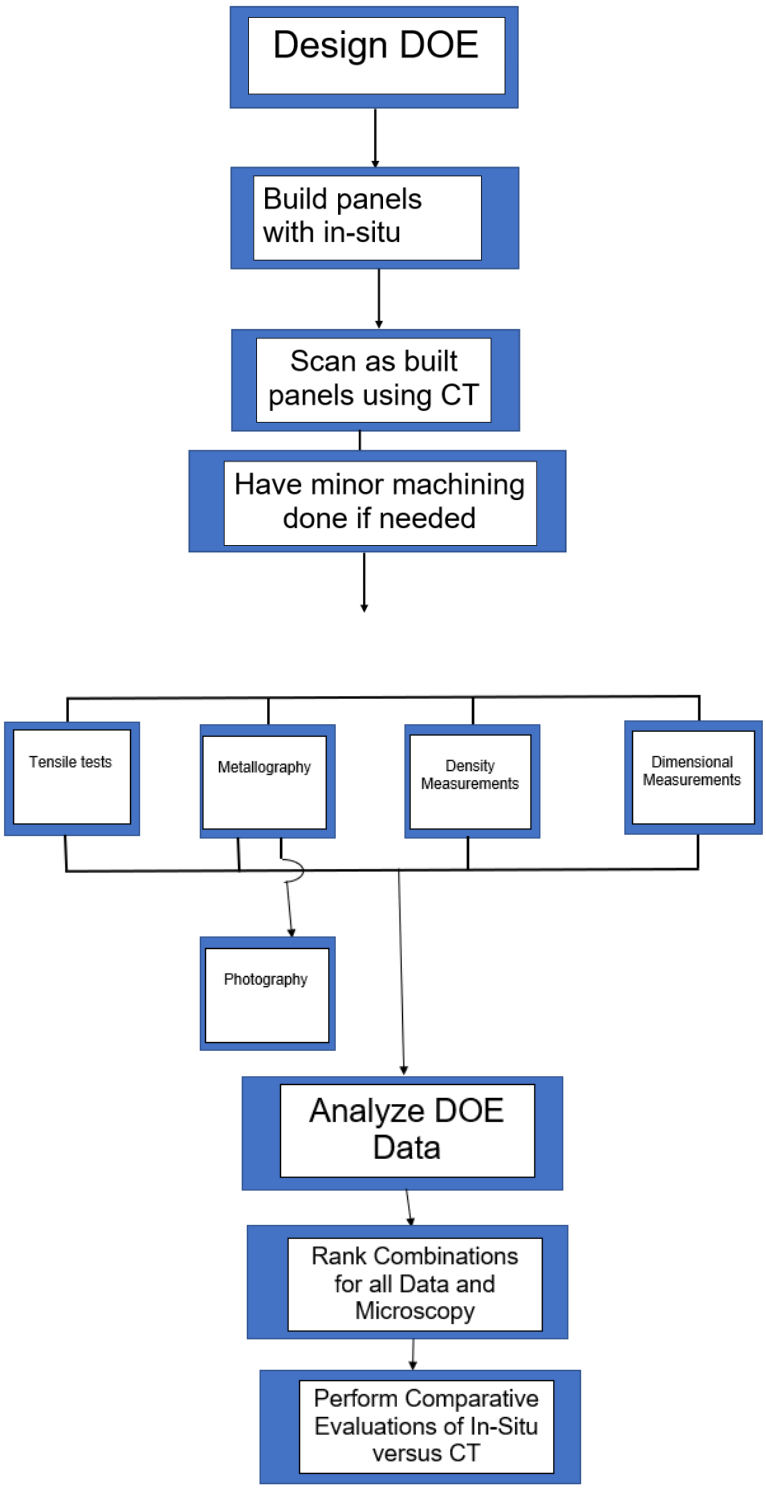

Figure 4.1 The Flow of the Research

parameters currently in use for HR-1. The selected DOE used three process parameters. These were laser power, scan speed, and hatch spacing. Two panels of the DOE were built because of the problems encountered during the build process but they were not entirely complete. In every case the machine stopped during the build process. But the last two builds were close to being complete.

Table 4.1 shows the design of the experiment. It was a Plackett-Burman factorial design with two replicates and 4 center points per replicate, for a total of 32 runs. Thirty-two is the maximum number of runs that I could get from a single AM panel. Unfortunately, two of the combinations had to be eliminated after the first build, to get the build close to finishing. This will be discussed further in Chapter 6.

[66]A Plackett-Burman experimental design is generally used to identify the most important factors early in the experimentation phase when complete knowledge about the system is not available. It was developed in 1946 by statisticians Robin L. Plackett and J.P. Burman. This is an efficient screening method to identify the active factors using as few experimental runs as possible. In Plackett-Burman designs, main effects tend to have complicated confounding relationships with two-factor interactions and therefore are mainly used to study main effects, only when it can be assumed that two-way interactions are negligible. In this case I am using a full factorial Plackett-Burman design which will result in no confounding. Two replicates of three factors at two levels resulting in no confounding of two factor interactions. There will also be four center-points in each replicate to represent the set of parameters that are currently in use with

Table 4.1 Plackett-Burman 32 Runs

Standard Order	Run Order	Point Type	Laser Power (W)	Scan Speed (mm/s)	Hatch Spacing (mm)
4	1	1	340	860	0.14
12	2	1	230	860	0.1
10	3	1	340	860	0.1
14	4	0	285	1080	0.12
5	5	1	340	1300	0.1
3	6	1	230	1300	0.14
1	7	1	340	860	0.14
7	8	1	230	1300	0.14
11	9	1	230	1300	0.1
15	10	0	285	1080	0.12
9	11	1	230	860	0.1
13	12	0	285	1080	0.12
16	13	0	285	1080	0.12
8	14	1	230	860	0.14
6	15	1	340	1300	0.14
2	16	1	340	1300	0.1
17	17	1	340	860	0.14
26	18	1	340	860	0.1
22	19	1	340	1300	0.14
27	20	1	230	1300	0.1
24	21	1	230	860	0.14
31	22	0	285	1080	0.12
19	23	1	230	1300	0.14
25	24	1	230	860	0.1
20	25	1	340	860	0.14
30	26	0	285	1080	0.12
28	27	1	230	860	0.1
29	28	0	285	1080	0.12
21	29	1	340	1300	0.1
32	30	0	285	1080	0.12
18	31	1	340	1300	0.1
23	32	1	230	1300	0.14

the HR-1 material. This design should have enabled fitting of a first-order models (detecting linear effects) and provided information on the existence of second-order effects (curvature) by using the center points. Unfortunately, the problems with the builds and having to eliminate two combinations made this impossible. Ideally statistical methods such as analysis of variance would have also been used to analyze the results of the test program. But instead, analysis of the DOE results includes trend analysis and ranking of the combinations.

The M290 machine comes with pre-settings for some different materials but also can be adjusted to other settings for most parameters. The team at MSFC has been using the settings for IN 718 because it is very close to HR-1. But the parameters are not completely optimized. They have been looking at adjustments to parameters but have not completed the optimization for HR-1. The hope was to use the IN 718 parameters or their best set of parameters at the time, for the center-points and increase/decrease by about 10% to get the high/low levels of the factors. It has been said that this will certainly result in some defects, and it did. But porosity was the main defect that was produced. LOF did occur in one set of combinations (Run #23). These defects were measured and compared with the in-situ and metallography results.

Each test set included two tensile coupons, two metallography coupons and one measurement coupon for a total of 5 parts. The specimen build layout shown in Figure 4.2 was designed using the EOS software. Each build plate is approximately 250 mm by

250 mm. Table 4.2 shows the calculated energy density for each of the combinations in the DOE.

The plan was to have two tensile coupons for each combination, one to be tested as built and another to be machined and tested. To achieve the standard properties, the machined samples are also HIP-ed (hot isostatic pressed) and heat treated. Unfortunately, the as-built specimens were not sufficiently completed in the builds to be able to run them and the other specimens could not be machined due to funding constraints, so they were not tested either. Two metallography coupons intended for as built and post process preparation were also built but somehow their identity was lost at the machine shop. The partial as built samples were used for metallography since they had retained identities throughout the process. Eight of the tensile coupons were sent to be heat treated and HIP-ed but did not get finished in time to be machined and tested. The dimensional blocks did not have measurements made on them either. However, all the specimens were x-rayed and CT was performed on two of the tensile coupons.

Figure 4.3 shows the build layout with the run number superimposed on each set of coupons with the types identified. This figure was originally developed by Rachel Bardsley of EM42 to visually match some hotspots on the build plate of the last build, (Build #4).

4.3 The EOS in-situ Monitoring System

The EOS[4] in-situ monitoring system uses two different technologies to monitor metal

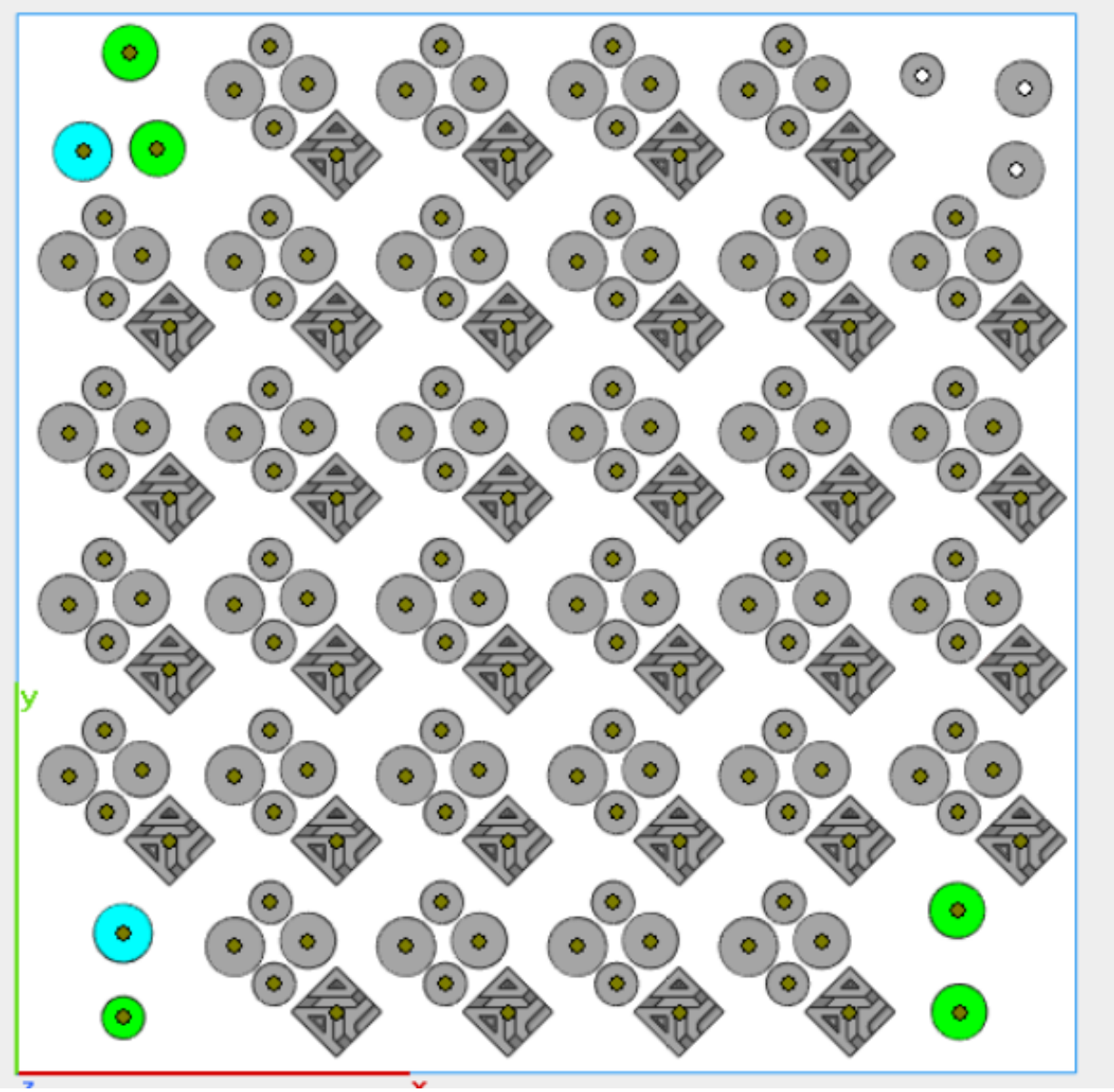

Figure 4.2 Specimen Build Plate Layout (build plate is 250 mm x 250 mm).

Table 4.2 Calculated Energy Densities for the DOE

Standard Order	Run Order	Point Type	Laser Power (W)	Scan Speed (mm/s)	Hatch Spacing mm)	energy density (J/m^3)
4	1	1	340	860	0.14	70.60
12	2	1	230	860	0.1	66.86
10	3	1	340	860	0.1	98.84
14	4	0	285	1080	0.12	54.98
5	5	1	340	1300	0.1	65.38
3	6	1	230	1300	0.14	31.59
1	7	1	340	860	0.14	70.60
7	8	1	230	1300	0.14	31.59
11	9	1	230	1300	0.1	44.23
15	10	0	285	1080	0.12	54.98
9	11	1	230	860	0.1	66.86
13	12	0	285	1080	0.12	54.98
16	13	0	285	1080	0.12	54.98
8	14	1	230	860	0.14	47.76
6	15	1	340	1300	0.14	46.70
2	16	1	340	1300	0.1	65.38
17	17	1	340	860	0.14	70.60
26	18	1	340	860	0.1	98.84
22	19	1	340	1300	0.14	46.70
27	20	1	230	1300	0.1	44.23
24	21	1	230	860	0.14	47.76
31	22	0	285	1080	0.12	54.98
19	23	1	230	1300	0.14	31.59
25	24	1	230	860	0.1	66.86
20	25	1	340	860	0.14	70.60
30	26	0	285	1080	0.12	54.98
28	27	1	230	860	0.1	66.86
29	28	0	285	1080	0.12	54.98
21	29	1	340	1300	0.1	65.38
32	30	0	285	1080	0.12	54.98
18	31	1	340	1300	0.1	65.38
23	32	1	230	1300	0.14	31.59

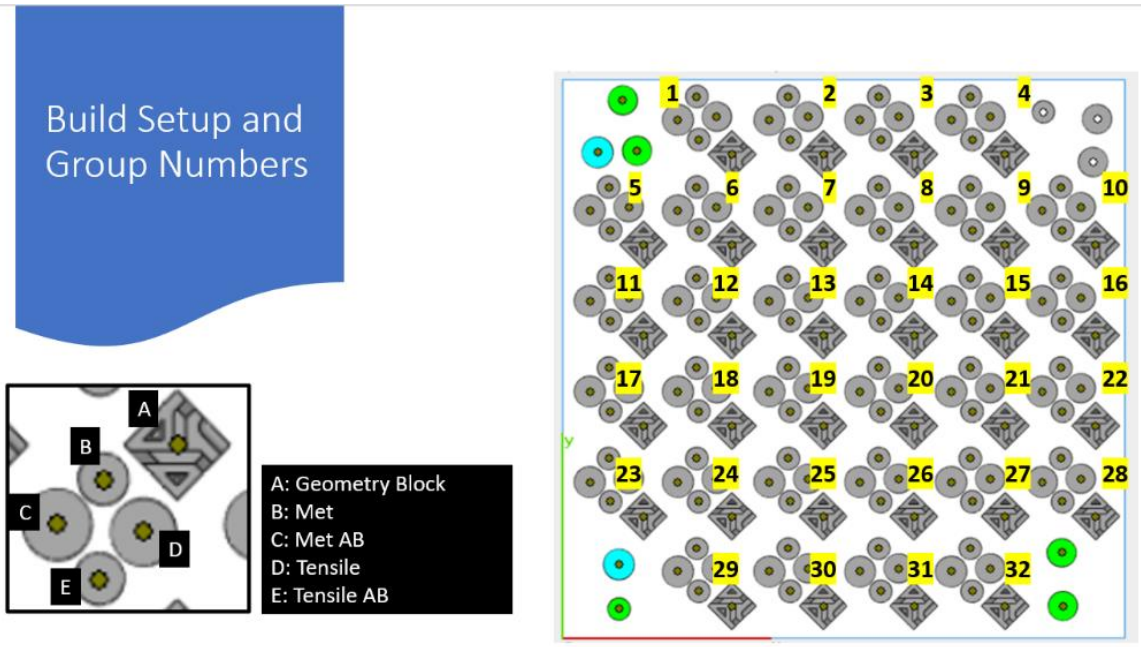

Figure 4.3 Randomized Layout for the DOE Study

systems. The first is called EOSTATE Melt-pool Monitoring and uses a photodiode in the laser path. It is used to provide high resolution and in-depth visibility into the melt pool to measure the light that is emitted from it. The second is called EOSTATE Exposure OT and uses a camera that is something like a thermal imaging camera, to collect near infrared spectrum light emissions. Both systems are touted as being able to detect deviations in the process before they can lead to defects. These processes were to be utilized to observe the building of a set of specimens manufactured as identified in section 4.2. Once built the panels were separated into the individual specimens required, identified, and then used for the following test methods.

After building, the specimens were to be finalized with minimal machining if required and inspected using computed tomography to evaluate and compare to the issues identified by in-situ monitoring. All the specimens were x-rayed and two were sent for CT. Results are provided in Chapter 6. They were then to be tested according to the procedures described in the following sections and each set of data would be analyzed as a part of the DOE using the Minitab software to determine the best set of parameters for the build. Instead, trend analyses and ranking, were performed and the results are included in Chapter 6. In addition, the results of the in-situ monitoring were compared with the metallographic results and evaluated to determine whether the build should have been stopped at any point during processing. The combinations were randomly located on the panels and the analyses considers whether the location on the panel could possibly have anything to do with a defect occurring at that location.

4.4 Test Methods

There were five samples included in each set. There were two tensile coupons, one to be tested as built and another to be machined and tested. To achieve the standard properties, the machined samples are also HIP-ed (hot isostatic pressed) and heat treated. Two metallography coupons were also intended for evaluation in the as-built, and, post process heat treated and HIPed condition. The final block that was built was a dimensional block. The dimensional blocks were developed by a summer student in the test lab a few years ago. Their actual purpose is to evaluate how well the actual dimensions compare to the design dimensions, which is another measure of how well the process is optimized. All the samples were built and were available to evaluate the defects that were revealed in the in-situ data.

As was already stated, CT (computed tomography) was used to compare to the in-situ results to determine what defects may have shown up during processing. Tension testing was also planned to verify the impact of the defect on mechanical properties and metallography was used to look at what the defects really are, i. e. porosity, incomplete fusion, or cracks. Most of the defects that were found, turned out to be porosity.

The dimensional blocks were developed a few years ago. Three block designs to include in each build on the M290 machine. The purpose was to verify the dimensional accuracy of the build. Although this will not necessarily benefit this work, it did provide additional material to look for defects in and it would have been interesting to look at the

dimensional variation due to the change in the parameters. Perhaps this will also show an impact on the dimensional stability due to an increase in the defect population.

Density measurements were performed on the tensile blanks intended for mechanical testing. These measurements provided another way to look for the existence of defects, especially porosity. Testing was performed in our chemistry laboratory.

Previously, a study was conducted using density measurements in lieu of other methods to evaluate defects at NASA's Marshall Spaceflight Center by Dr. Tracie Prater. She developed a DOE looking at layer thickness at 2 levels and, power, speed, and hatch spacing at 3 levels, and measured and analyzed the final density of the resulting AM product. Analysis in this study included matrix plots, correlation and regression analyses which showed only subtle and intuitive relationships between the build parameters and the density measurements. It was anticipated that looking at larger differences in the build parameters would add definition to these relationships. The small changes in these parameters were not enough to show significant changes in density. Density was used as an additional methodology to correlate the difference due to the parameter changes and analyzing the test results using these same methodologies would likely be beneficial. Dr. Prater's study used all three methods of density measurement at MSFC. Future work was recommended to perform metallography on her density blocks, but that has not been reported on. Metallography was done for some of the blocks in the study.

There were extra metallography blocks included in this study, based on metallography that has been developed to support a specification that was developed at MSFC. The specification is EM20 MSFC Technical Standard “Specification for Control and Qualification of Laser Powder Bed Fusion Metallurgical Processes”, which is available for public release with unlimited distribution.

A direct comparison of the computed tomography defects and defects identified via in situ monitoring was performed. Two CT’s and eight metallography samples were conducted to review and evaluate the defects for their detrimental impact on properties. The two CT’s evaluated were from the hottest parameter conditions available. Figure 4.2 shows the DOE that was developed and built for this work. Figure 4.3 is a picture of the layout developed for the AM panel that was built. It includes enough sample blocks for the full matrix plus a few extras.

Specimen Configurations:

Figure 4.4 shows the tensile coupon configuration that is typically used for testing AM properties in MSFC labs. Tensile coupons are sometimes machined post build and sometimes they are tested as built. The ideal plan for any hardware would be to avoid as much machining as possible, however the surface condition of the AM parts impacts its behavior in service. It may not be possible to completely avoid all machining. Figure 4.5 presents a comparison of two models of the as built tensile coupons that are used for testing as built and machining prior to test. These samples were not completed when the build shut down prematurely so the “as built’ coupon was used for metallography

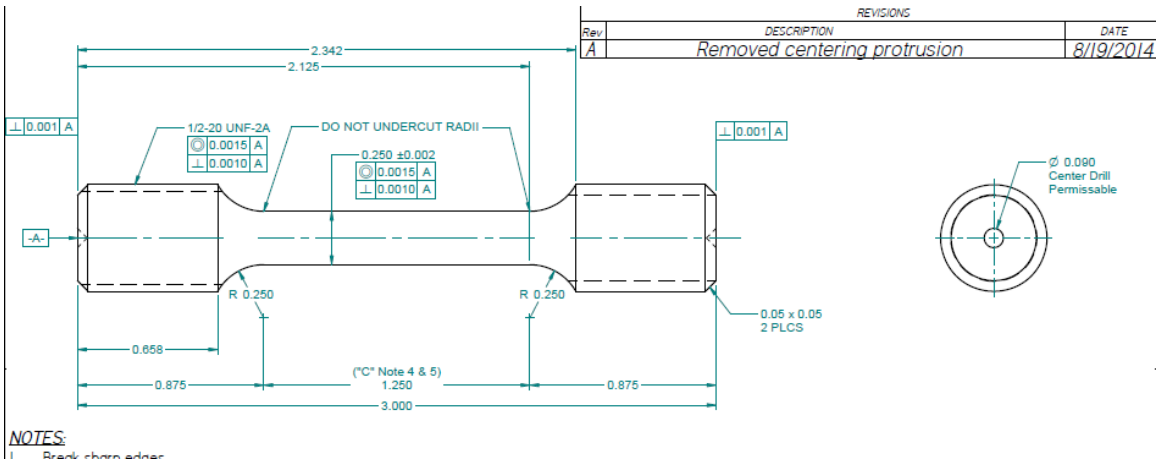

Figure 4.4 Additive Manufacturing Tensile Configuration

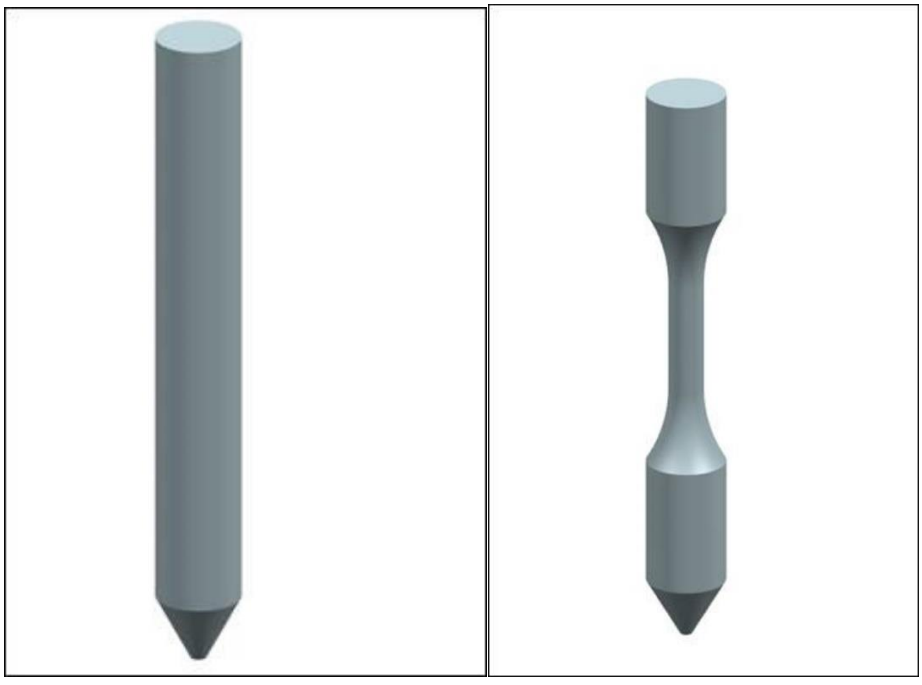

Figure 4.5 Models of Tensile Coupons Used for Testing: A) to be machined and then tested, and B) to be tested as built.

and the density measurements were made on the to be machined tensile coupons. The “as built” coupon is normally tested without any post build processing. The machined coupon is normally hot isostatic pressed (HIP-ed) and heat treated prior to machining and testing. Eight of the to be machined coupons were heat treated but not tested.

Figure 4.6 shows a model of one of the samples intended for metallography blocks. The two metallography blocks are the same, just configured differently within the sample block to show differences in the microstructure. The metallography block lost traceability at the machine shop so I used eight of the incomplete as built tensile coupons to perform the metallography on. The plan was to look at each microstructure and any/all defects that had occurred in the other samples from each block, after the data was collected for them. The metallography samples were processed and etched in the same way that they are standardly processed and the specimens were evaluated and measured using ImageJ. All significant defects were documented photographically for comparison with the information provided by the in-situ monitoring system.

Figure 4.7 shows a model of the density blocks that are standardly used at MSFC for AM work. Studies have been conducted using density as a measure of the defectiveness of AM products, i. e. comparisons between the normal density of a material and the density of the as built samples for evaluation. This method was also used to assess the defects produced by the DOE.

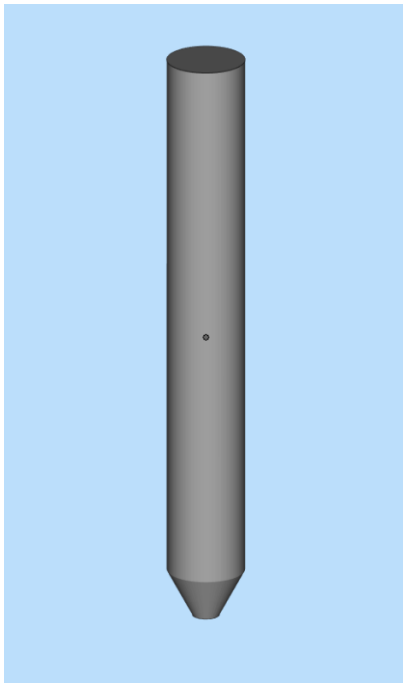

Figure 4.6 Model of Metallography Block

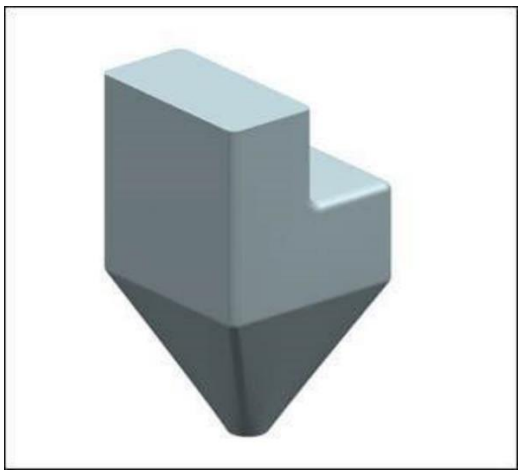

Figure 4.7 Model of Density Block

Figure 4.8 shows a set of dimensional blocks that were designed by a summer student at MSFC a few summers ago. Their purpose is to show how well dimensions in a variety of configurations, compare to the design dimensions which is another measure of how well the process is optimized. They also show how well the dimensions can be achieved using AM processing. The plan for this study was to look at one of the dimension block measurements for variations due to the DOE parameters and the resulting defects studied here. The sample was intended to be measured using a Keyence 3D Microscope system as depicted in Figure 4.9 and are still available to be measured. The Keyence microscope is an all-in-one microscope for observation, measurement, and image capture. It has a large depth-of-field and provides built in two dimensional and 3-dimensional measurement tools that can be utilized without touching the article to be measured.

These samples were also x-rayed to look for defects. A few of the samples were also CT'd to look for defects. The kind of CT System that was used, a North Star X5000 CT System, is shown in in Figure 4.9.

[17]Computed tomography provides a scan of an object as it is penetrated by an x-ray beam. It provides a three-dimensional density map of the object. It is built up of two-dimensional projection images of the part that are built up onto an array. The slices allow users to visualize, measure and evaluate the internal structure and the defects present inside of an object.

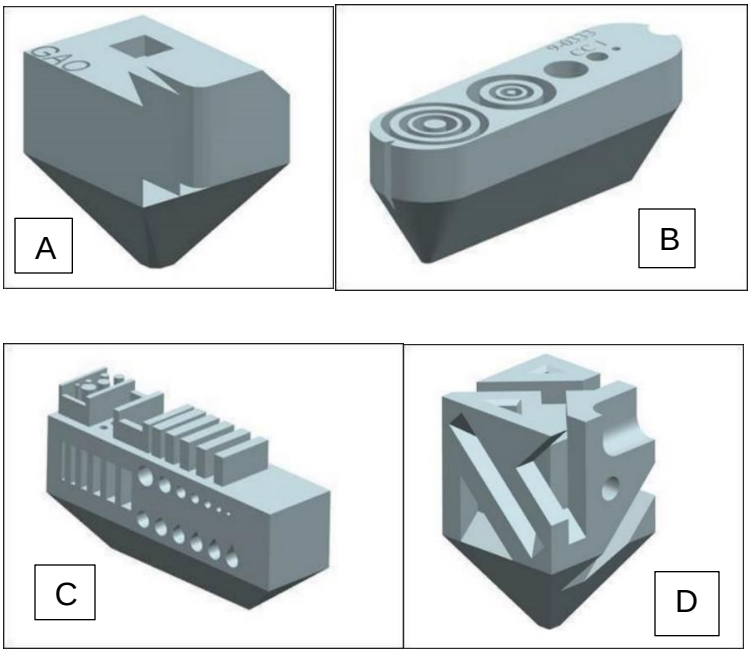

Figure 4.8 Models of Dimension Blocks

Figure 4.9 Keyence 3D Microscope System

A North Star X5000 CT system was used for evaluation of the test panel once it is built. In that system, there are two x-ray tubeheads: one is higher energy to get through larger parts, which leads to lower resolution (mini-focus), and one is lower energy to achieve higher resolution on small parts (up to ~1” diameter for most metals), that one is called micro-focus. Both are used with a digital detector array. The part is placed between the x-ray tubehead and the detector array on a turntable that rotates the parts. X-ray images are captured as the part is rotated around and the resulting images are reconstructed into a 3D representation of the part with any internal density changes. Since the samples are small, the micro focus will be used. I should be able to identify the size of the defects or defective areas by the density changes identified with the CT, which will provide a binary number for the final metric. Figure 4.10 shows a picture of a North Star X5000 CT System.

4.5 In-Situ Monitoring System

The in-situ monitoring system on the M290 machine is an EOState Monitoring Suite. It includes both MeltPool Monitoring and Exposure Optical Tomography. The MeltPool Monitoring includes both on-axis and off-axis photodiodes. Here are the specs for the MeltPool Monitoring:

- On-axis and off-axis photodiodes
- Samples melt emission @400-900nm
- For each layer: .png, .h5, .mpm
    - PNGs are a binary mask of parts
    - Export TIFs for layer images
    - All layers, all data: ~10-100 GB

The Exposure OT uses a Complementary metal-oxide semiconductor camera. Here are the specs for the exposure OT:

4.10 North Star X5000 CT System

- Optical tomography CMOS camera
- Integrated melt emission @900 nm
- Data export options:
    - RAW 32-bit uncompressed
    - TIFF 16-bit uncompressed
        - 20-40 GB total
    - TIFF 8-bit uncompressed
    - JPG compressed

The system includes software for both types of monitoring and data will be collected for both. It will be a large amount of data because this panel run will probably take about 5 days to complete, but the group already has a system set up for storing the data at MSFC. It will be stored and analyzed according to their current standard procedures. There are specific Vendor supplied software for viewing and analyzing data from each of the systems. These are:

EOSTATE Exposure OT® Monitoring software for laser-sintering systems[67]
EOSTATE MeltPool® Monitoring software for laser-sintering systems[68]

It is my plan to be there as much of the time as is logical to view the build process and the final analysis of the data. I want to identify the locations and size of the areas suspected to contain defects so that I can compare that to the CT and metallography results. I may also be able to measure the density of the defective areas and compare that with the density of defects in the metallography coupons. I think that either the density of defects or for effective area may be the best numerical way to use this data to perform an ANOVA analysis. It does depend somewhat on how much defects I get or how bad they are. I would also like to use the types of defects in some way. If there are obviously different types for different runs in the DOE, that may be an indicator of the problem as well.

[65]The EOSTATE Exposure OT system is an optional accessory provided for the EOS M 290 laser sintering system and is used to monitor and document the building process. It is a part of the system previously referred to as the M290 and will be used during the building of the test panel for this study. It includes a high-resolution camera that will capture the entire building area and acquires the process light emitted in the near-infrared range. During the build process, a sequence of images will be obtained, the exposure of a layer is then combined with them (e.g. formation of integral or maximum), and the result saved as an image for each layer of the build. The combined image is then evaluated for irregularities and deviations that could be defects in the final product. Based on the layer and location within the panel, the images can be correlated with the defects that are identified by computed tomography and any that are found via metallography.

4.6 Analysis and Ranking of Results Methodology

Trend analysis was performed on the density data and metallography data and plots of the data is included in Chapter 6. A set of rankings for each set of tests was also performed and is included in chapter 6.

Chapter 5

An Evaluation by the Mukherjee Number

The [61, 62] Mukherjee number was utilized to assess the measured results of this dissertation using Mukherjee's philosophy.[61,62] In 2018 H. L. Mukherjee, et al, published two articles discussing the modeling of powder bed fusion and the mitigation of lack of fusion defects in PBF additive manufacturing by using this model. His work was based on the premise that the trial-and-error method typically used for optimization of processes and properties could be better accomplished using theoretical models defined by heat transfer and fluid flow. Such a three-dimensional model for multiple layers and hatches of the PBF process was developed in his first article. The second article utilized the model that he had developed to mitigate lack of fusion defects in four different alloys manufactured by PBF. To accomplish this, he built panels using five hatches and three layers.

Mukherjee LOF results are indicated following:

1 LOF voids are inversely proportional to the scanning speed,

2 Amount of LOF is directly proportional to the layer thickness and the hatch spacing,

3 Laser spot radius, absorptivity of the laser beam at the powder bed, the molten pool width and depth, and the rate of heat transfer also govern the occurrence of LOF defects in PBF.

So as a result, Mukherjee developed a non-dimensional LOF number to quantify the effects of these parameters on LOF. That is the number that was presented in Chapter 3. Use of the Mukherjee number is presented in section 5.1

Calculating the Numbers:

For each of the variations built in this DOE experiment, the Mukherjee number was calculated according to the Equation 3.1.

The Mukherjee number will provide an expected risk of having LOF for each of the combinations included in the DOE, which can be compared to the in situ results. It will be developed for comparison with the rankings in Chapter 4 from the in-situ evaluation and test results to determine how well the numbers correlate with the actual outcome of the testing and analysis results.

Numbers required for the equation are assembled and calculated below:

Density $\rho = 8.07$ g/cc $= 0.292$ lb/in^3 $= 8.07$ g/cm^2(8.07 g/10^{-4}m^2)

$= 8.07 \times 10^4$ g/m^2(10^{-3}kg/g)

$= 80.7$ kg/m^2

Specific Heat c_p = see graph in Figure 5.1

Liquidus Temperature $T_L = 2579$ F $= 1688.2$ K

Solidus Temperature $T_S = 2426$ F $= 1603.2$ K

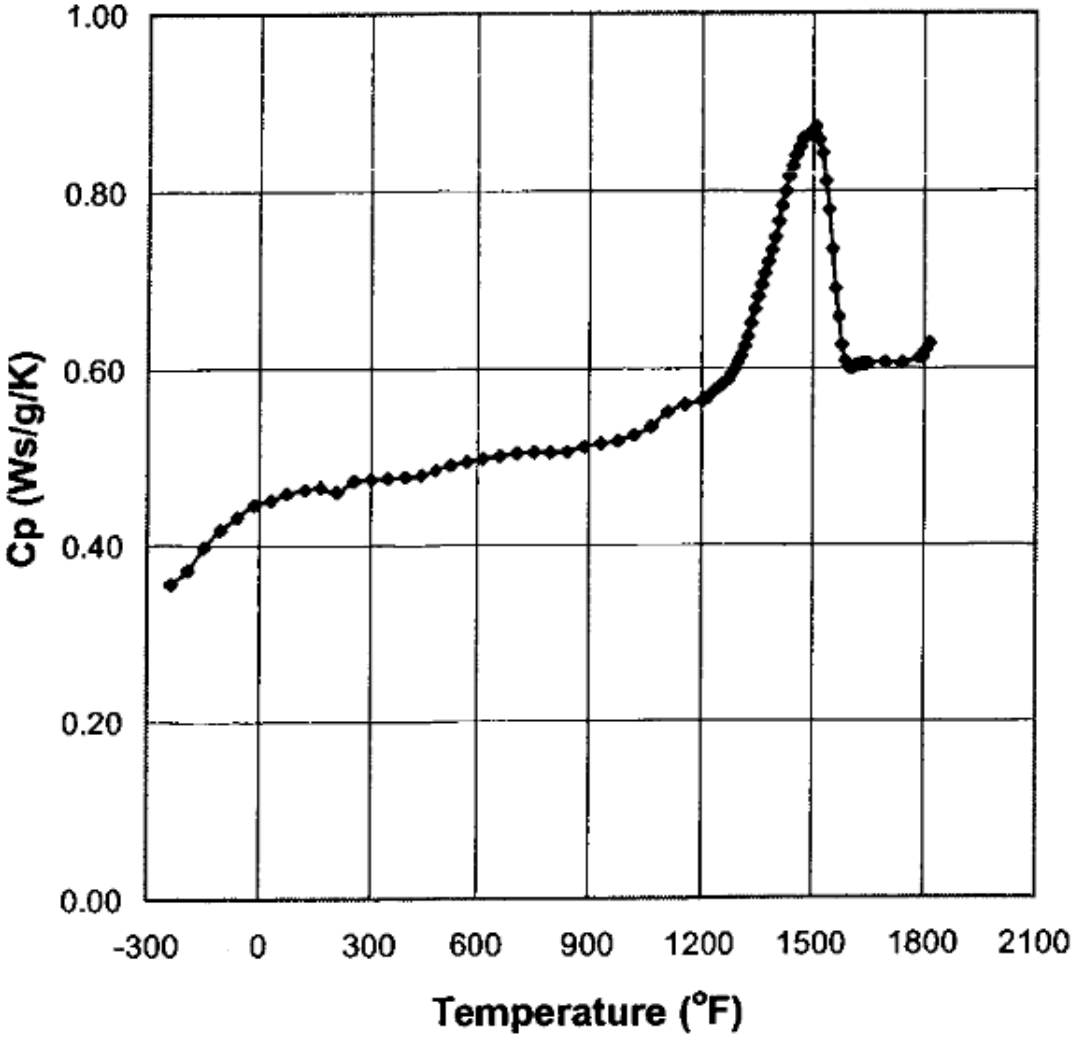

Figure 5.1 Specific Heat Plot from ASM Handbook (72)

$\Delta T = 85$ K

Latent Heat of Fusion for the alloy HR-1 is calculated in Table 5.1. Elemental values were used from reference 70.

Latent Heat of Fusion L = 316.131 kJ/kg

Absortivity values for the laser beam impinging on the Hr-1 were estimated from Figure 5.2 values for 316L stainless steel.

Power of laser beam P = see Table 5.2, W = kg m^2/s

Scanning speed v = see Table 5.2, mm/s = 10^{-3}m/s

Radius of laser beam r = 40 μm = 40 x 10^{-6}m

Fourier number was calculated as by Mukherjee in his paper.

$$F_o = \frac{\alpha t}{L^2}$$ **Equation 5.1**

η_{230} = 0.76 kg/kJ

η_{285} = 0.755 kg/kJ

η_{340} = 0.75 kg/kJ

Table 5.1 Calculation of Latent Heat of Fusion for HR-1 (70)

	HR-1 Typical Composition (%)	Atomic Weight (g/mol)	Latent Heat of Fusion (kJ/kg)	LHF % contribution
Al	34	27	396	134.64
Cr	15	52	394	59.1
Co	3.3	58.9	275	9.075
Fe	41	55.8	247	101.27
Mo	2	95.9	375	7.5
Ti	0.3	47.9	390	1.17
W	1.6	184	190	3.04
V	0.3	50.9	112	0.336
			Total	316.131

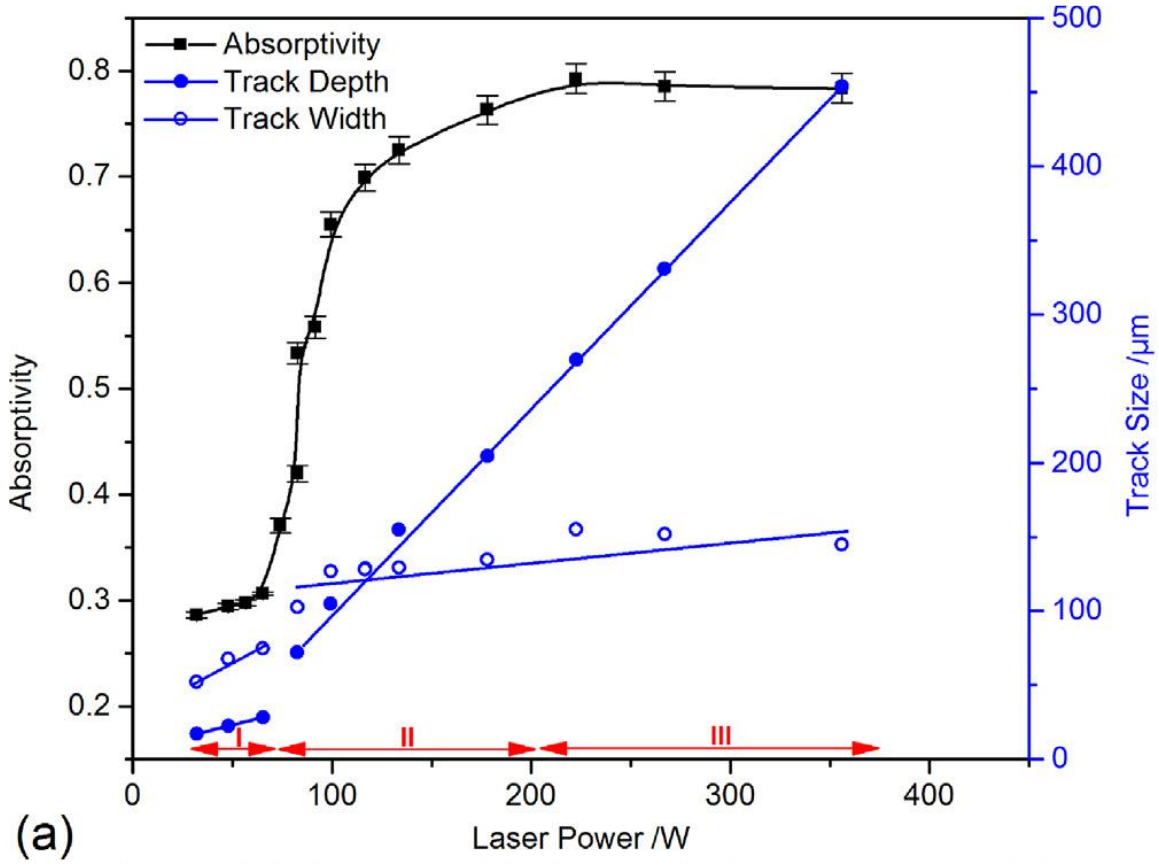

Figure 5.2 Absorptivity versus Laser Power for 316L Stainless Steel (71)

where α = thermal diffusivity

t = time

L = length

According to Mukherjee's conversion

$t / L = \alpha / v$, where v = laser scanning speed

so, F can be expressed as $F = \alpha / (vl)$

where l = the molten pool length

so, assuming that the molten pool length, depth and width are symmetrical

and therefore equal, l = 150 – 200 μm 175×10^{-6}m

Molten Pool Half Width ω = 75 – 100 μm 87.5×10^{-6}m

Molten Pool Depth d = 150 – 200 μm 175×10^{-6}m

Using the average value in the calculation

The maximum available α is about 0.2 ft^2/hour, from Figure 5.3, at 1200 F.

$0.2(0.3048^2)/60 = 61.94 \mu m^2/s(10^{-6}) = 61.94 \times 10^{-6} m^2/s$

So, assuming α =0.2, then, $F = 61.94 \times 10^{-6}/175v = 0.3539 \times 10^{-6}/v$

$F_{860} = 0.3539/860 = 411.5 \times 10^{-3}\ m^2/s^2$

$F_{1080} = 0.3539/1080 = 327.7 \times 10^{-3}\ m^2/s^2$

$F_{1300} = 0.3539/1300 = 272.2 \times 10^{-3}\ m^2/s^2$

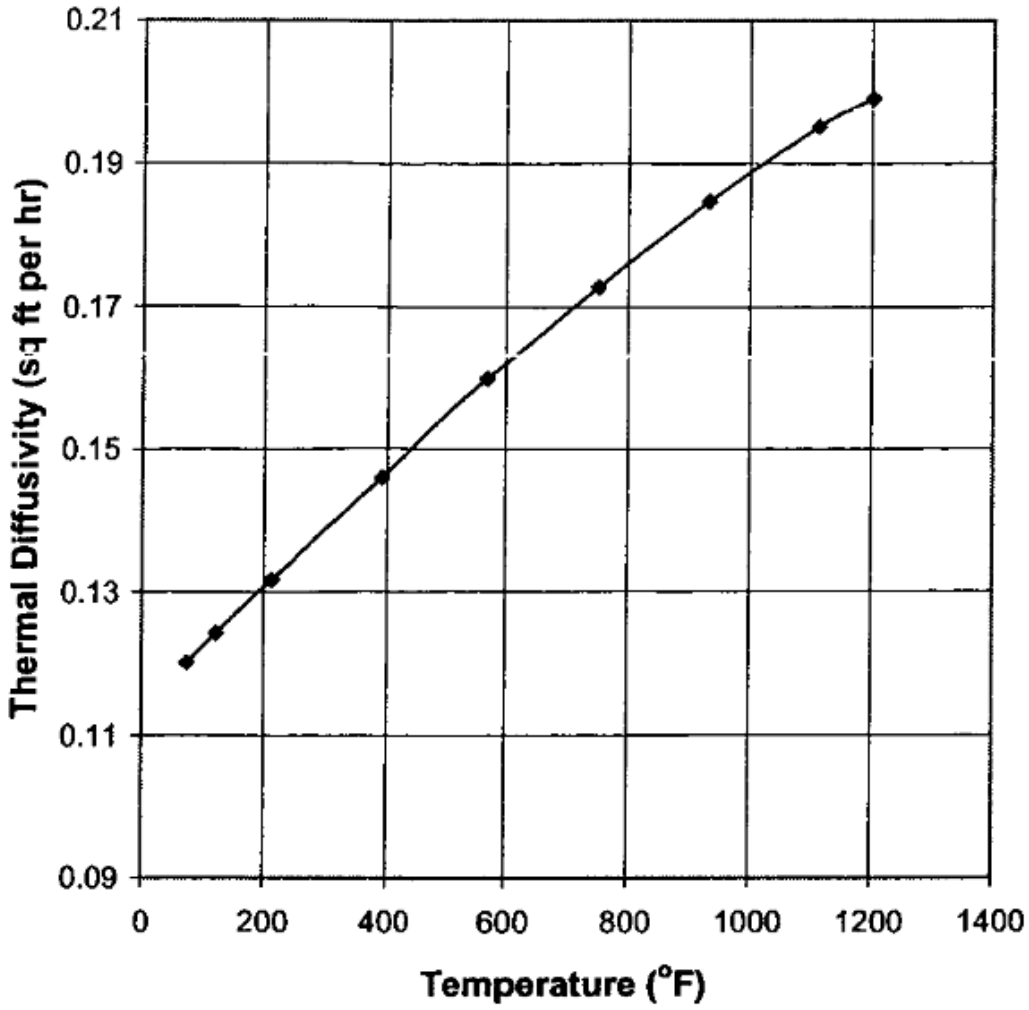

Figure 5.3 Thermal Diffusivity from ASM Handbook. (72)

Layer thickness $t = 40\ \mu m = 40 \times 10^{-6}$

Hatch Spacing h = see Table 5.2

Table 5.2 shows the calculated values for the Mukherjee number tabulated with the values used for the calculation and Table 5.3 shows the ranking of the combinations based on the calculated Mukherjee number. A typical value for density was used for these calculations.

The blacked-out numbers in Table 5.4 and 5.5 were samples that were damaged either during the processing or post processing and could not be used for the analysis. Tables 5.4 and 5.5 shows similar calculations and ranking using the density values developed in this study.

Table 5.2 Mukjerjee Calculations.

Standard Order	Run Order	Point Type	Laser Power, P (kg/m^2)	Scan Speed, v ($x10^{-3}m/s$)	Hatch Spacing, h ($x10^{-3}m$)	Energy Density (J/m^3)	Absorptivity, η (kg/J)	Fourier Number, F (m^2/s^2)	Radius of Laser Beam, r ($x10^{-6}m$)	Laser Thickness, t (x10-6 m)	Molten Pool Depth, d (x10-6 m)	Molten Pool half width, ω (x10-6 m)	ΔT (K)	Density, ρ (kg/m^2)	Specific Heat at ~1800 F, c_p (Ws/g/K)	Latent Heat of Fusion, L (kJ/kg)	Mukherjee number
4	1	1	340	860	0.14	70.60	0.75	411.5	40	40	175	87.5	85	80.7	0.64	316.131	0.002104808
12	2	1	230	860	0.1	66.86	0.76	411.5	40	40	175	87.5	85	80.7	0.64	316.131	0.00601821
10	3	1	340	860	0.1	98.84	0.75	411.5	40	40	175	87.5	85	80.7	0.64	316.131	0.004125424
14	4	0	285	1080	0.12	54.98	0.755	327.7	40	40	175	87.5	85	80.7	0.64	316.131	0.005353936
5	5	1	340	1300	0.1	65.38	0.75	272.2	40	40	175	87.5	85	80.7	0.64	316.131	0.009427471
3	6	1	230	1300	0.14	31.59	0.76	272.2	40	40	175	87.5	85	80.7	0.64	316.131	0.007016781
1	7	1	340	860	0.14	70.60	0.75	411.5	40	40	175	87.5	85	80.7	0.64	316.131	0.002104808
7	8	1	230	1300	0.14	31.59	0.76	272.2	40	40	175	87.5	85	80.7	0.64	316.131	0.007016781
11	9	1	230	1300	0.1	44.23	0.76	272.2	40	40	175	87.5	85	80.7	0.64	316.131	0.01375289
15	10	0	285	1080	0.12	54.98	0.755	327.7	40	40	175	87.5	85	80.7	0.64	316.131	0.005353936
9	11	1	230	860	0.1	66.86	0.76	411.5	40	40	175	87.5	85	80.7	0.64	316.131	0.00601821
13	12	0	285	1080	0.12	54.98	0.755	327.7	40	40	175	87.5	85	80.7	0.64	316.131	0.005353936
16	13	0	285	1080	0.12	54.98	0.755	327.7	40	40	175	87.5	85	80.7	0.64	316.131	0.005353936
8	14	1	230	860	0.14	47.76	0.76	411.5	40	40	175	87.5	85	80.7	0.64	316.131	0.003070515
6	15	1	340	1300	0.14	46.70	0.75	272.2	40	40	175	87.5	85	80.7	0.64	316.131	0.004809934
2	16	1	340	1300	0.1	65.38	0.75	272.2	40	40	175	87.5	85	80.7	0.64	316.131	0.009427471
17	17	1	340	860	0.14	70.60	0.75	411.5	40	40	175	87.5	85	80.7	0.64	316.131	0.002104808
26	18	1	340	860	0.1	98.84	0.75	411.5	40	40	175	87.5	85	80.7	0.64	316.131	0.004125424
22	19	1	340	1300	0.14	46.70	0.75	272.2	40	40	175	87.5	85	80.7	0.64	316.131	0.004809934
27	20	1	230	1300	0.1	44.23	0.76	272.2	40	40	175	87.5	85	80.7	0.64	316.131	0.01375289
24	21	1	230	860	0.14	47.76	0.76	411.5	40	40	175	87.5	85	80.7	0.64	316.131	0.003070515
31	22	0	285	1080	0.12	54.98	0.755	327.7	40	40	175	87.5	85	80.7	0.64	316.131	0.005353936
19	23	1	230	1300	0.14	31.59	0.76	272.2	40	40	175	87.5	85	80.7	0.64	316.131	0.007016781
25	24	1	230	860	0.1	66.86	0.76	411.5	40	40	175	87.5	85	80.7	0.64	316.131	0.00601821
20	25	1	340	860	0.14	70.60	0.75	411.5	40	40	175	87.5	85	80.7	0.64	316.131	0.002104808
30	26	0	285	1080	0.12	54.98	0.755	272.2	40	40	175	87.5	85	80.7	0.64	316.131	0.006445572
28	27	1	230	860	0.1	66.86	0.76	411.5	40	40	175	87.5	85	80.7	0.64	316.131	0.00601821
29	28	0	285	1080	0.12	54.98	0.755	327.7	40	40	175	87.5	85	80.7	0.64	316.131	0.005353936
21	29	1	340	1300	0.1	65.38	0.75	272.2	40	40	175	87.5	85	80.7	0.64	316.131	0.009427471
32	30	0	285	1080	0.12	54.98	0.755	327.7	40	40	175	87.5	85	80.7	0.64	316.131	0.005353936
18	31	1	340	1300	0.1	65.38	0.75	272.2	40	40	175	87.5	85	80.7	0.64	316.131	0.009427471
23	32	1	230	1300	0.14	31.59	0.76	272.2	40	40	175	87.5	85	80.7	0.64	316.131	0.007016781

Table 5.3 Ranked by Mukherjee Number

Standard Order	Run Order	Point Type	Laser Power, P (kg/m^2)	Scan Speed, v ($x10^{-3}m/s$)	Hatch Spacing, h ($x10^{-3}m$)	Mukherjee number
4	1	1	340	860	0.14	0.002104808
1	7	1	340	860	0.14	0.002104808
17	17	1	340	860	0.14	0.002104808
20	25	1	340	860	0.14	0.002104808
8	14	1	230	860	0.14	0.003070515
24	21	1	230	860	0.14	0.003070515
10	3	1	340	860	0.1	0.004125424
26	18	1	340	860	0.1	0.004125424
6	15	1	340	1300	0.14	0.004809934
22	19	1	340	1300	0.14	0.004809934
14	4	0	285	1080	0.12	0.005353936
15	10	0	285	1080	0.12	0.005353936
13	12	0	285	1080	0.12	0.005353936
16	13	0	285	1080	0.12	0.005353936
31	22	0	285	1080	0.12	0.005353936
29	28	0	285	1080	0.12	0.005353936
32	30	0	285	1080	0.12	0.005353936
12	2	1	230	860	0.1	0.00601821
9	11	1	230	860	0.1	0.00601821
25	24	1	230	860	0.1	0.00601821
28	27	1	230	860	0.1	0.00601821
30	26	0	285	1080	0.12	0.006445572
3	6	1	230	1300	0.14	0.007016781
7	8	1	230	1300	0.14	0.007016781
19	23	1	230	1300	0.14	0.007016781
23	32	1	230	1300	0.14	0.007016781
5	5	1	340	1300	0.1	0.009427471
2	16	1	340	1300	0.1	0.009427471
21	29	1	340	1300	0.1	0.009427471
18	31	1	340	1300	0.1	0.009427471
11	9	1	230	1300	0.1	0.01375289
27	20	1	230	1300	0.1	0.01375289

Table 5.4 Mukjerjee calculations using measured densities from Chapter 6

Standard Order	Run Order	Point Type	Laser Power, P (kg/m^2)	Scan Speed, v ($x10^{-3}m/s$)	Hatch Spacing, h ($x10^{-3}m$)	Energy Density (J/m^3)	Absorptivity, η (kg/J)	Fourier Number, F (m^2/s^2)	Radius of Laser Beam, r ($x10^{-6}m$)	Laser Thickness, t (x10-6 m)	Molten Pool Depth, d (x10-6 m)	Molten Pool half width, ω (x10-6 m)	ΔT (K)	Density, ρ (kg/m^2)	Specific Heat at ~1800 F, c_p (Ws/g/K)	Latent Heat of Fusion, L (kJ/kg)	Mukherjee number
4	1	1	340	860	0.14	70.60	0.75	411.5	40	40	175	87.5	85	80.85453	0.64	316.131	0.002108839
12	2	1	230	860	0.1	66.86	0.76	411.5	40	40	175	87.5	85	81.10122	0.64	316.131	0.006048132
10	3	1	340	860	0.1	98.84	0.75	411.5	40	40	175	87.5	85		0.64	316.131	
14	4	0	285	1080	0.12	54.98	0.755	327.7	40	40	175	87.5	85	80.99506	0.64	316.131	0.005373511
5	5	1	340	1300	0.1	65.38	0.75	272.2	40	40	175	87.5	85	80.84289	0.64	316.131	0.009444164
3	6	1	230	1300	0.14	31.59	0.76	272.2	40	40	175	87.5	85	78.73299	0.64	316.131	0.006845751
1	7	1	340	860	0.14	70.60	0.75	411.5	40	40	175	87.5	85	80.84855	0.64	316.131	0.002108683
7	8	1	230	1300	0.14	31.59	0.76	272.2	40	40	175	87.5	85		0.64	316.131	
11	9	1	230	1300	0.1	44.23	0.76	272.2	40	40	175	87.5	85	80.89758	0.64	316.131	0.013786561
15	10	0	285	1080	0.12	54.98	0.755	327.7	40	40	175	87.5	85	81.1226	0.64	316.131	0.005381973
9	11	1	230	860	0.1	66.86	0.76	411.5	40	40	175	87.5	85	80.93951	0.64	316.131	0.006036072
13	12	0	285	1080	0.12	54.98	0.755	327.7	40	40	175	87.5	85	80.95473	0.64	316.131	0.005370836
16	13	0	285	1080	0.12	54.98	0.755	327.7	40	40	175	87.5	85	81.14119	0.64	316.131	0.005383206
8	14	1	230	860	0.14	47.76	0.76	411.5	40	40	175	87.5	85	80.82538	0.64	316.131	0.003075286
6	15	1	340	1300	0.14	46.70	0.75	272.2	40	40	175	87.5	85	80.42062	0.64	316.131	0.004793283
2	16	1	340	1300	0.1	65.38	0.75	272.2	40	40	175	87.5	85	81.07255	0.64	316.131	0.009470993
17	17	1	340	860	0.14	70.60	0.75	411.5	40	40	175	87.5	85	75.87584	0.64	316.131	0.001978985
26	18	1	340	860	0.1	98.84	0.75	411.5	40	40	175	87.5	85		0.64	316.131	
22	19	1	340	1300	0.14	46.70	0.75	272.2	40	40	175	87.5	85	68.81934	0.64	316.131	0.004101816
27	20	1	230	1300	0.1	44.23	0.76	272.2	40	40	175	87.5	85	80.97918	0.64	316.131	0.013800468
24	21	1	230	860	0.14	47.76	0.76	411.5	40	40	175	87.5	85	80.8403	0.64	316.131	0.003075854
31	22	0	285	1080	0.12	54.98	0.755	327.7	40	40	175	87.5	85	81.14489	0.64	316.131	0.005383452
19	23	1	230	1300	0.14	31.59	0.76	272.2	40	40	175	87.5	85	78.77317	0.64	316.131	0.006849245
25	24	1	230	860	0.1	66.86	0.76	411.5	40	40	175	87.5	85	81.23234	0.64	316.131	0.00605791
20	25	1	340	860	0.14	70.60	0.75	411.5	40	40	175	87.5	85		0.64	316.131	
30	26	0	285	1080	0.12	54.98	0.755	272.2	40	40	175	87.5	85	81.14708	0.64	316.131	0.006481281
28	27	1	230	860	0.1	66.86	0.76	411.5	40	40	175	87.5	85	81.04048	0.64	316.131	0.006043601
29	28	0	285	1080	0.12	54.98	0.755	327.7	40	40	175	87.5	85	81.05401	0.64	316.131	0.005377422
21	29	1	340	1300	0.1	65.38	0.75	272.2	40	40	175	87.5	85	81.15409	0.64	316.131	0.009480519
32	30	0	285	1080	0.12	54.98	0.755	327.7	40	40	175	87.5	85	65.91774	0.64	316.131	0.004373226
18	31	1	340	1300	0.1	65.38	0.75	272.2	40	40	175	87.5	85	80.93921	0.64	316.131	0.009455416
23	32	1	230	1300	0.14	31.59	0.76	272.2	40	40	175	87.5	85	77.66342	0.64	316.131	0.006752753

Table 5.5 Ranked by Mukherjee Number using measured densities from Chap. 6

Standard Order	Run Order	Point Type	Laser Power, P (kg/m^2)	Scan Speed, v ($x10^{-3}m/s$)	Hatch Spacing, h ($x10^{-3}m$)	Energy Density (J/m^3)	Mukherjee number
10	3	1	340	860	0.1	98.84	
7	8	1	230	1300	0.14	31.59	
26	18	1	340	860	0.1	98.84	
20	25	1	340	860	0.14	70.60	
17	17	1	340	860	0.14	70.60	0.001978985
1	7	1	340	860	0.14	70.60	0.002108683
4	1	1	340	860	0.14	70.60	0.002108839
8	14	1	230	860	0.14	47.76	0.003075286
24	21	1	230	860	0.14	47.76	0.003075854
22	19	1	340	1300	0.14	46.70	0.004101816
32	30	0	285	1080	0.12	54.98	0.004373226
6	15	1	340	1300	0.14	46.70	0.004793283
13	12	0	285	1080	0.12	54.98	0.005370836
14	4	0	285	1080	0.12	54.98	0.005373511
29	28	0	285	1080	0.12	54.98	0.005377422
15	10	0	285	1080	0.12	54.98	0.005381973
16	13	0	285	1080	0.12	54.98	0.005383206
31	22	0	285	1080	0.12	54.98	0.005383452
9	11	1	230	860	0.1	66.86	0.006036072
28	27	1	230	860	0.1	66.86	0.006043601
12	2	1	230	860	0.1	66.86	0.006048132
25	24	1	230	860	0.1	66.86	0.00605791
30	26	0	285	1080	0.12	54.98	0.006481281
23	32	1	230	1300	0.14	31.59	0.006752753
3	6	1	230	1300	0.14	31.59	0.006845751
19	23	1	230	1300	0.14	31.59	0.006849245
5	5	1	340	1300	0.1	65.38	0.009444164
18	31	1	340	1300	0.1	65.38	0.009455416
2	16	1	340	1300	0.1	65.38	0.009470993
21	29	1	340	1300	0.1	65.38	0.009480519
11	9	1	230	1300	0.1	44.23	0.013786561
27	20	1	230	1300	0.1	44.23	0.013800468

Chapter 6

Results and Discussion

6.1 Results

The results section includes or at least refers to all of the tabulated data**,** including in-situ results, CT results, photos of the defects, metallography photos, and density comparisons to fully dense standard material.

The main goal was to build specimens with defects to correlate with the results observed by in-situ monitoring and to determine whether one can in fact observe defects as the part is being built, thereby stopping the process before a huge waste of time and material occurs. Additionally, there is also effort underway to use the results from in-situ to certify hardware. So, there is value added in corelating the test results with the more standard NDE approach. It was said by the people using AM every day, that using a 10% decrease/increase in the parameters discussed would guarantee some defects in the samples which has proven to be true.

HIP is known to resolve some of the defects so it would have been nice to have completed the post process tensile tests. Perhaps those tests can be completed later. Work is currently ongoing to develop in-situ for use in certification of hardware, but it can also be used to prevent building a lot of defective hardware. In other words, it will make it possible to stop a build with the knowledge that whatever is being built would

have been useless if completed. Actual defects would have occurred had the process continued. Based on these findings in-situ can be used in that way, but there is still work to be done.

6.2 Discussion

6.2.1 DOE Runs

Three runs were attempted of the DOE on the M290 machine. Problems were encountered on each of the runs and the machine was restarted to try and complete the test sequences.

Build #1 stopped early in the build and was restarted more than once and it was finally decided that the reason was that two of the combinations were just too hot to build without causing the system to stop. The energy density in part groups 3 and 18 was just too high to prevent collisions during layers. The energy density was 98.8 J/mm^3. See Figure 4.2 for the calculated energy density for each of the combinations. The build failed at layer 111 due to scraping of the re-coater blade. This was heard during earlier layer's but it was unknown what the sound was at the time and it eventually led to a collision.

Figure 6.1 shows the last in-situ scan of Build # 1. The two hot runs can obviously be seen as being very bright on the picture. There are also four runs that are very dark. These runs are quite cold. They are 6, 8, 23 and 32. These are the worst runs in the DOE. Metallography was performed on 23 which can be seen later in these results. It

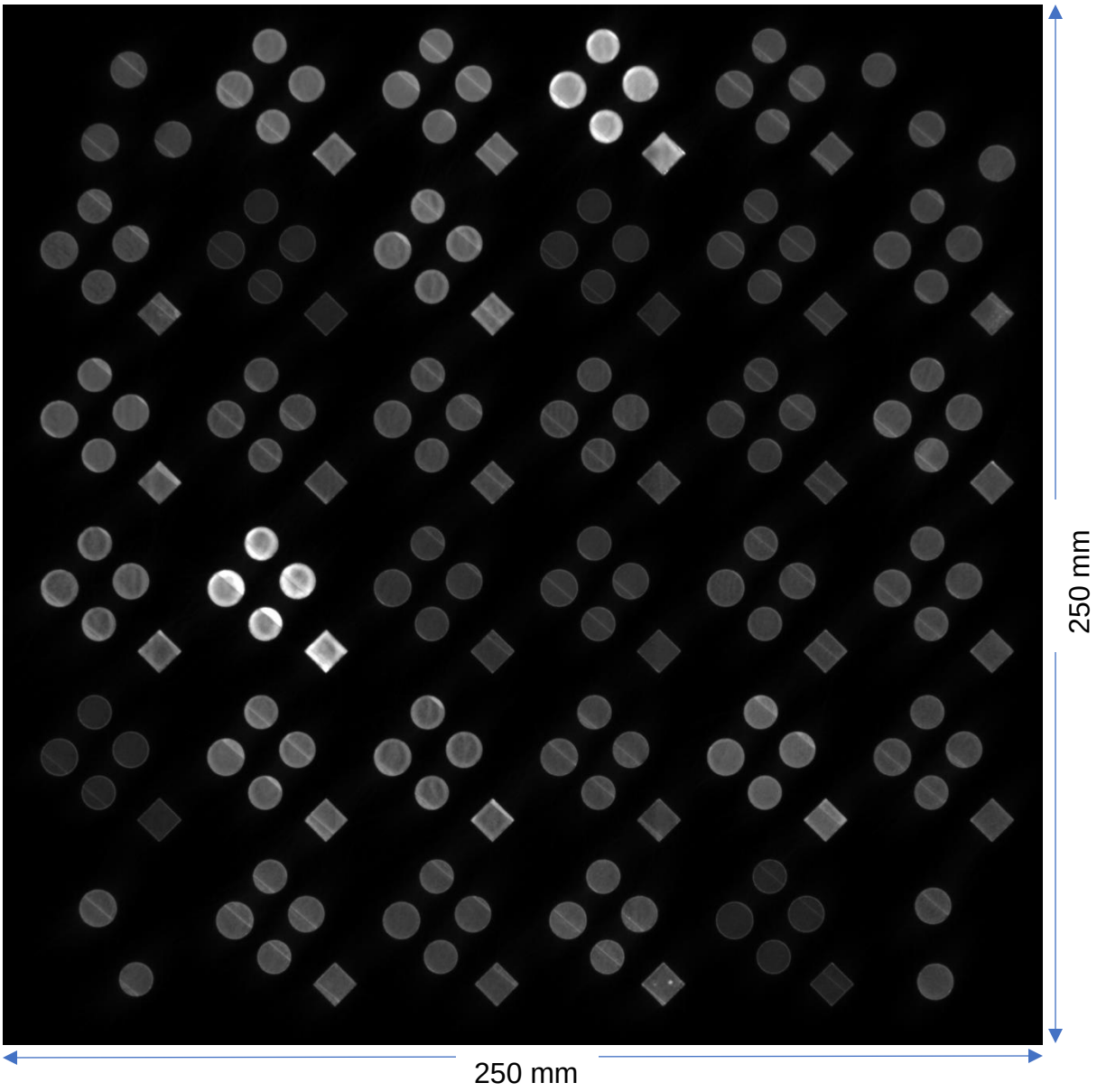

Figure 6.1 Last In-Situ Scan of Build #1 (250 mm x 250 mm).

was the most defective of the runs observed and can be identified by in situ as one of the coldest runs. Although the extent varies, all the other runs are obviously in between the worst case hot and cold runs. This finding is also possible by looking at the energy density calculated prior to a build. Hot builds typically have a high energy density and cold builds have a low energy density. The common goal is to aim for an energy density around 50 to achieve the best material. Unfortunately, builds with an energy density around 50 will still contain some porosity as will be seen in the metallography later.

A new build was started without the hot combinations. Part groups 3 and 18 were eliminated from the build to prevent collisions. But Run #2 failed similarly at layer 113 due to scraping of re-coater blade, which again, led to a collision that caused the system to stop. Figure 6.2 shows the last scan in Build #2. Build #2 also has hot spots in the last scan but it is not completely clear why that occurred.

Because of the issues with builds #1 and #2, build #3 was started at layer 150 and much of the support was eliminated, in an effort to distribute the heat better. The re-coater caught on the part at layer 1569, 1611, and there was a couple of fill tank errors that also occurred. A re-coater collision finally occurred at layer 1684 and the build had to be ended to evaluate for fixes to the fill tank error problem.

In Build #4, runs 3 and 18 were again removed due to the re-coater issues and the build was started at layer 130. Build #4 failed similarly with build #3 and bent T5AB causing the build to stop. The pause was not observed immediately, meaning that the build

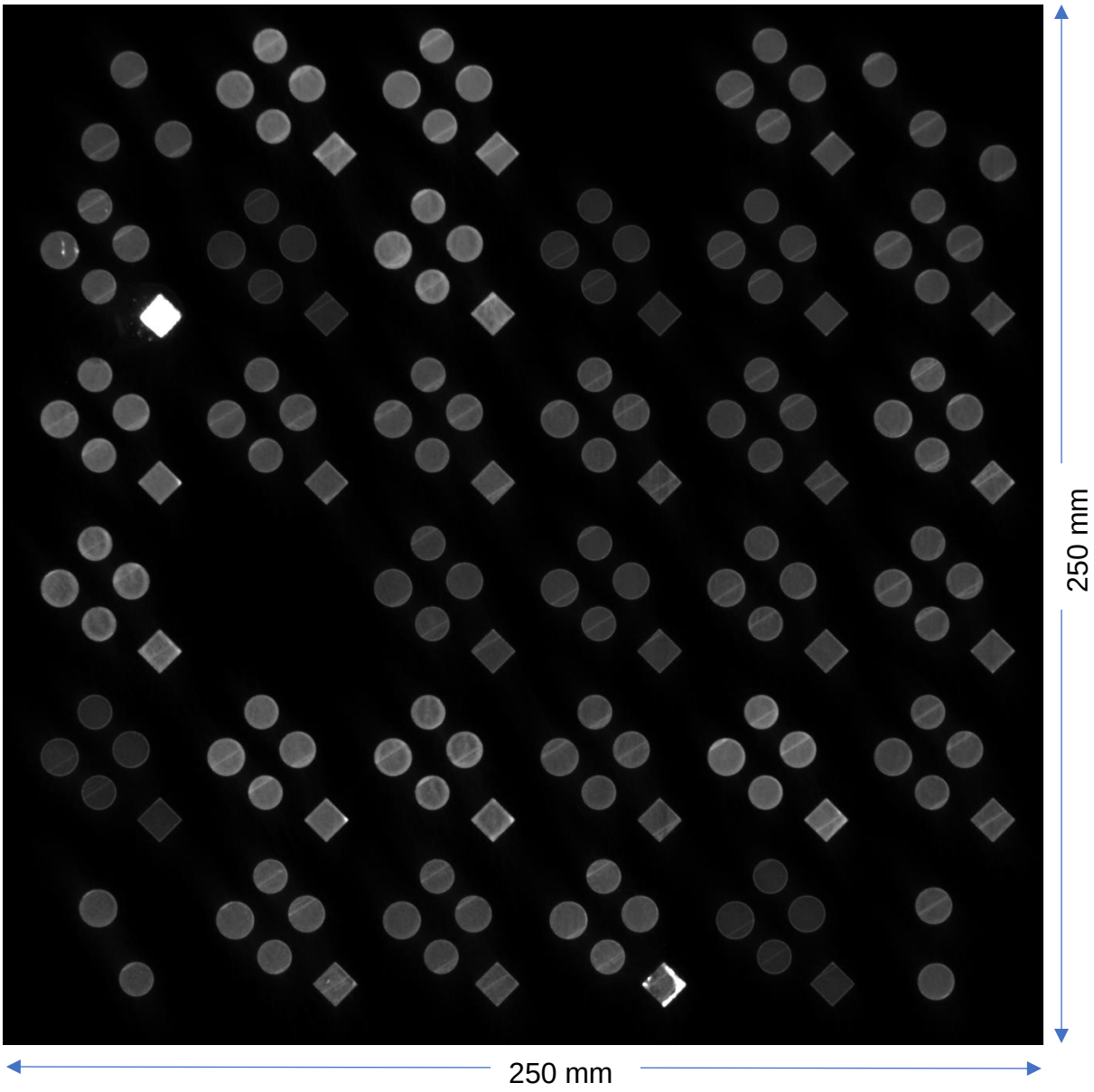

Figure 6.2 Last in situ scan of Build #2 (250 mm x 250 mm).

could not be restarted at that point. The problem seems to be at T5 (sets 5, 16, 29, and 31, see the build layout in Figure 4.2.2. The Exposure Software showed an unusual hot spot at T7 which from visual observation of the machine was around layer 1510-1530, see Figure 6.3. The T7 location does appear to be among the hotter locations. Figure 6.4 shows a larger picture of layer 1511 so that the hot spot is easier to see. This hot spot was measured at 63.76 and lines up with a defect on T5. The defect appears to be a sheared off burnt layer from a tensile specimen. The theory is that the T7 parts created this piece of shrapnel and the re-coater deposited it on T5. Figure 6.5 shows a picture of the tensile with the embedded shrapnel. There may be a general hot spot in the upper left of the build plate. It was decided that we could not attempt the build again until we can find a way to resolve this continuing problem. Some of the coupons from both Build #3 and #4 were still usable for my study.

6.2.2 X-rays

X-rays were made of Builds #3 and #4 to help determine which samples to evaluate using CT. The x-rays of Build #3 are shown in the following figures. Nothing abnormal was identified in the measurement samples shown in Figure 6.6.

Figures 6.7 and 6.8 depict the as-built tensile coupons or at least what would have been the as-build tensile coupons if the build had been completed. Figure 6.7 is scaled so that the detail on the thicker part can be seen. Figure 6.8 is re-scaled so that the detail on the thinner part can be seen.

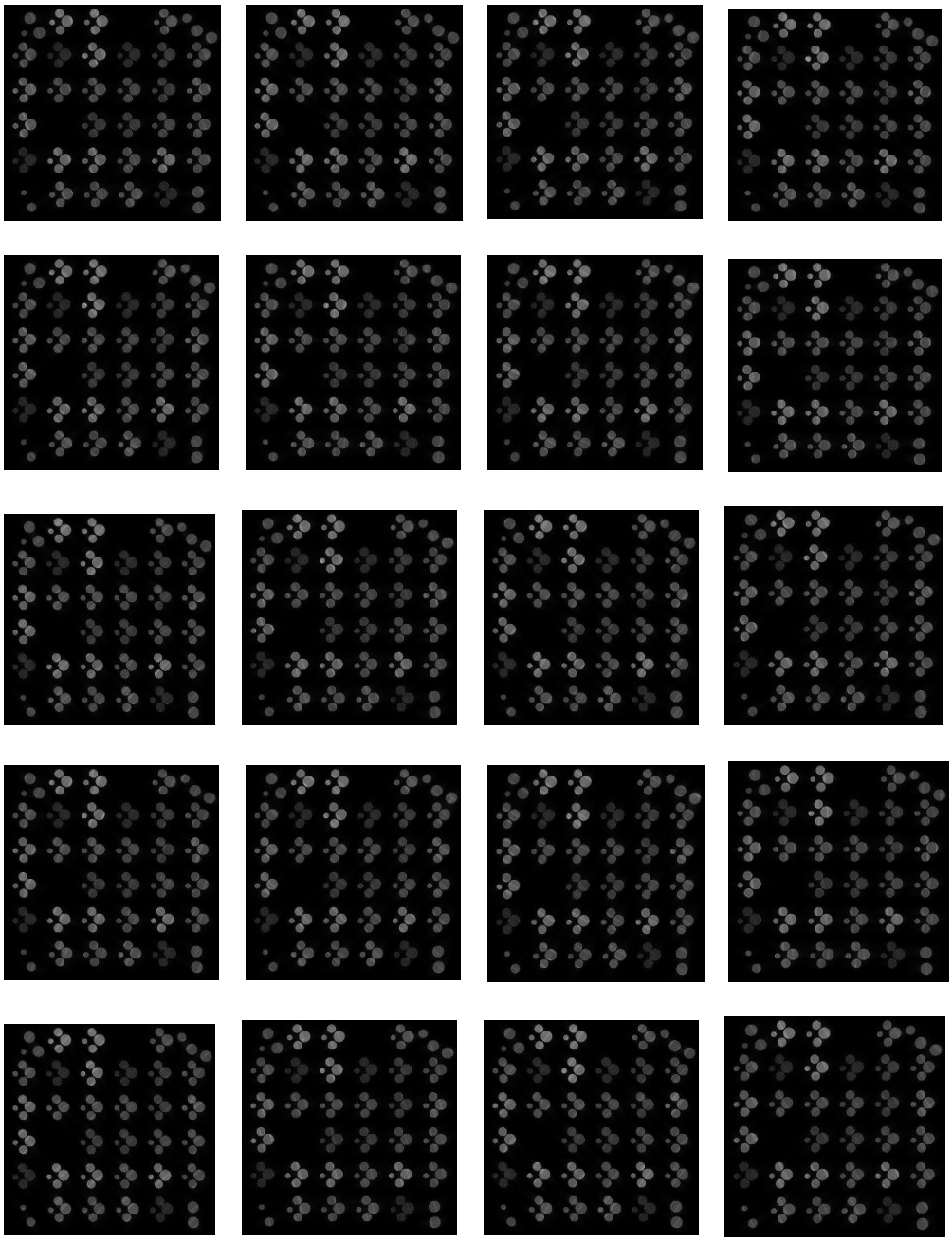

Figure 6.3 In-Situ Scans of Layers 1510-1530 of Build #4 (each scan is 250 mm x 250 mm)

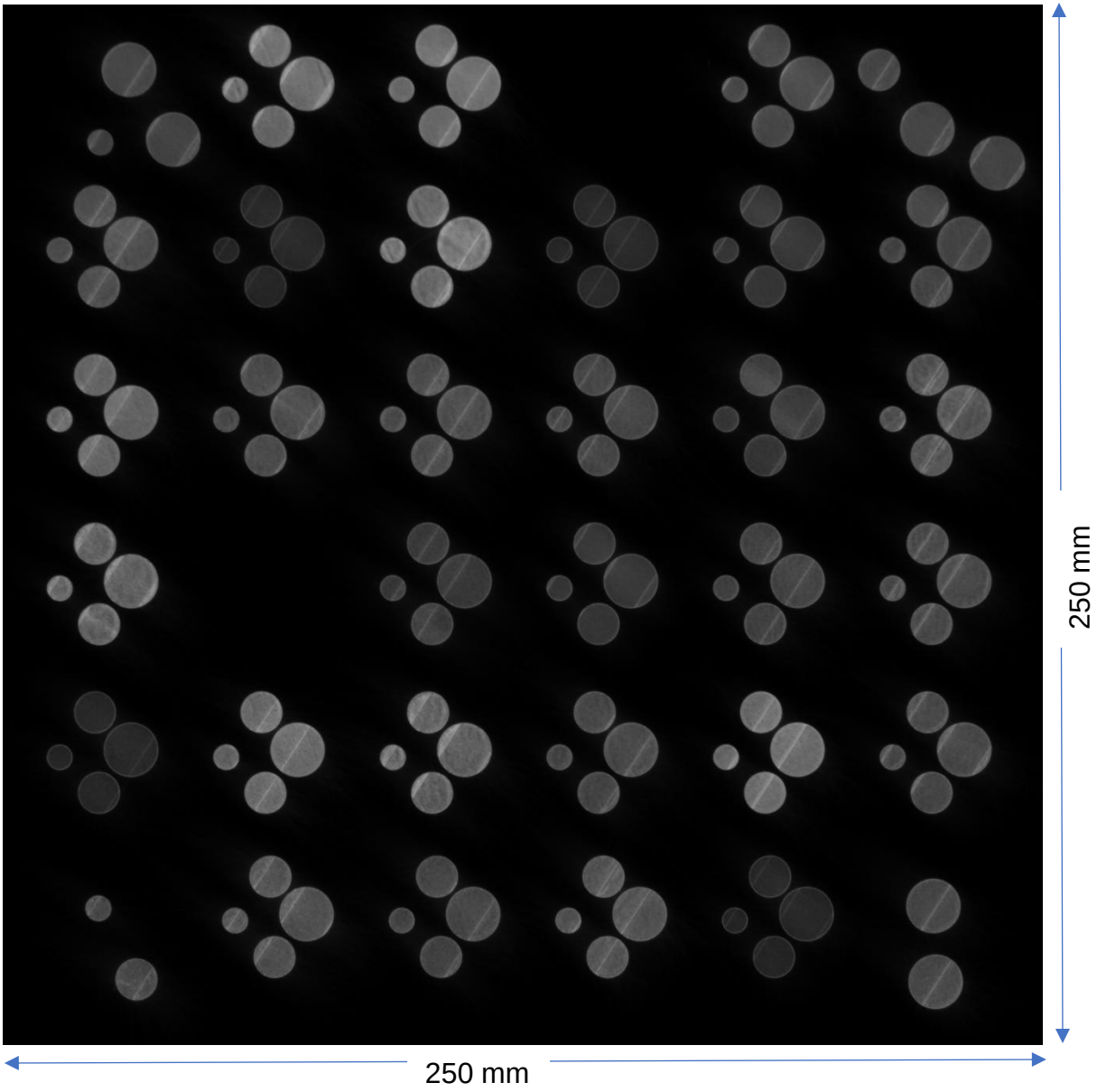

Figure 6.4 In-Situ Scan 1511 of Build #4 (250 mm x 250 mm)

Figure 6.5 Photograph of Tensile Embedded with Shrapnel from Overheating.

Figure 6.6 X-ray of Build #3 Measurement Samples

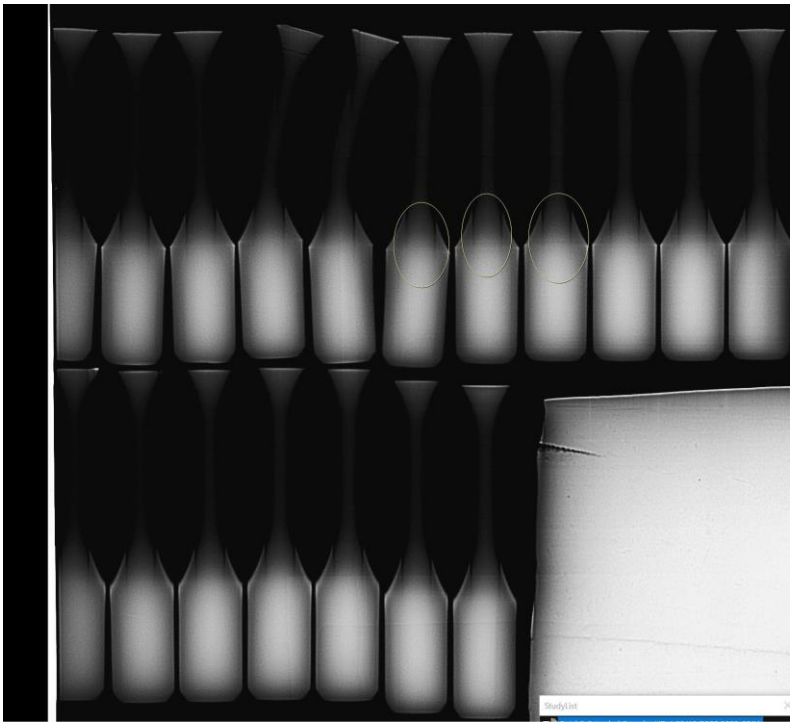

Figure 6.7 X-ray of Build #3 As Built Tensile’s

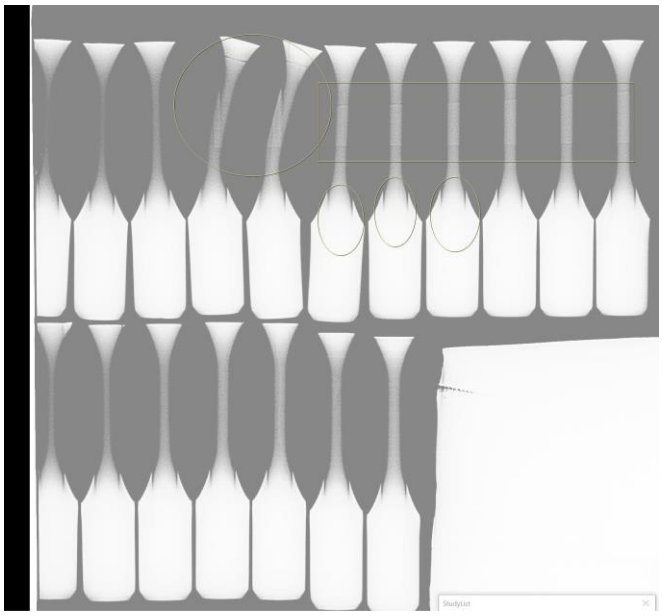

Figure 6.8 X-ray of Build #3 As Built Tensiles (samples are 2 3/8 - 2 5/8 inches long).

Figure 6.9 shows the metallography coupons from build #3. The metallography coupons have linear, circumferential indications noted on many of them. This might correlate to hotter combinations in the in-situ results. But because the identities were lost on these samples it is impossible to say for sure.

The tensile blanks T1-32 were found to have linear circumferential indications in 6, 8, 9, 23, 25, and 32. All of the tensile blanks are shown in Figure 6.10.

X-rays of the rest of Build #4 are shown in the following figures (Figures 6.11 and 6.12). Nothing abnormal was identified in any of the build #4 specimens by x-ray.

6.2.3 In-Situ Monitoring Results

For build #3 there are 1684 images provided by the system. Each of these images shows 30 sets of the samples for the 30 DOE runs that were ultimately included in the build. Two were eliminated because of the heat problems/issues encountered during the build processing. It also includes 10 samples that are standardly included with each build completed at MSFC in the EM42 laboratories. The additional samples are witness specimens, kept by EM42 to verify build consistency. Each set includes 6 tensile coupons, 2 high cycle fatigue coupons, and 2 metallography bars all built with nominal HR-1 parameters.

Figure 6.13 is the first image from Build #3. Each Scan is 250 mm x 250 mm. You can see that the variation in intensity follows the heat generated by the combination of

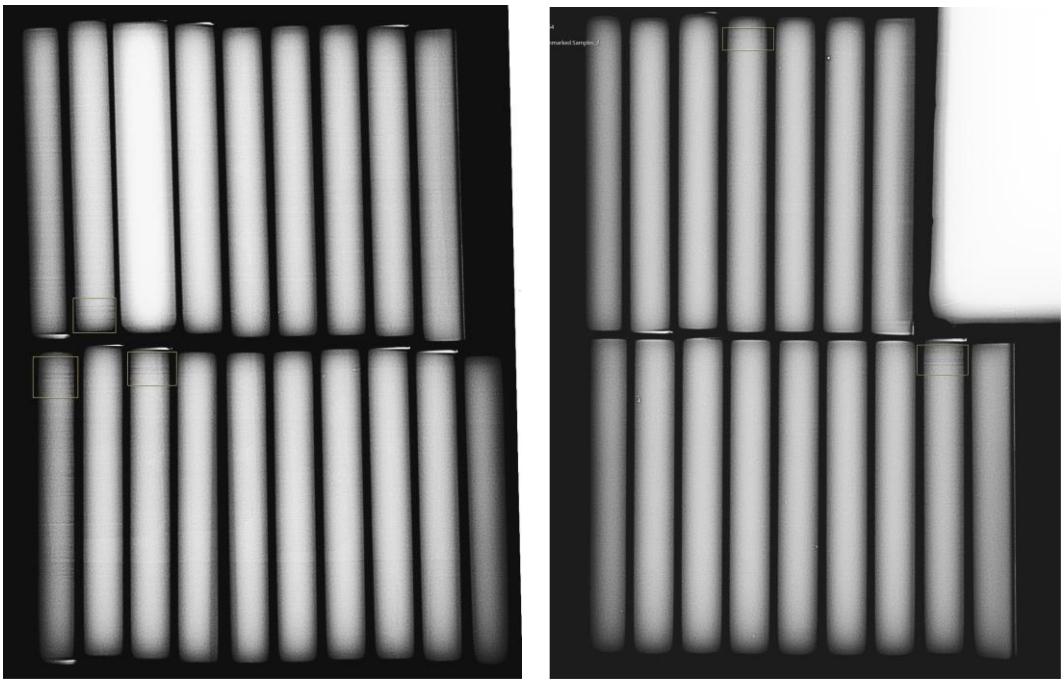

Figure 6.9 Unidentified metallography coupons from Build #3 (samples are 2 3/8 - 2 5/8 inches long).

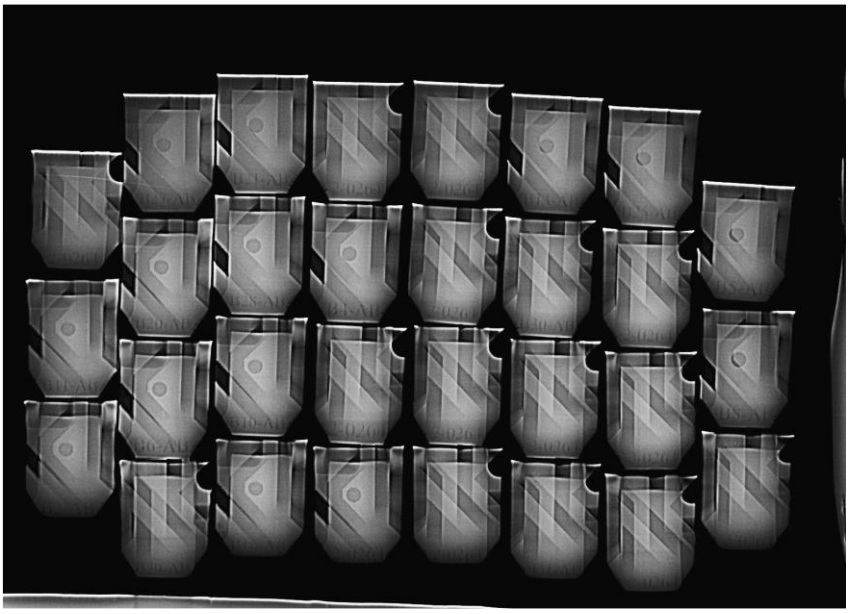

Figure 6.10 X-ray of Build #4 Measurement Samples (samples are 5/8 x 5/8 inch).

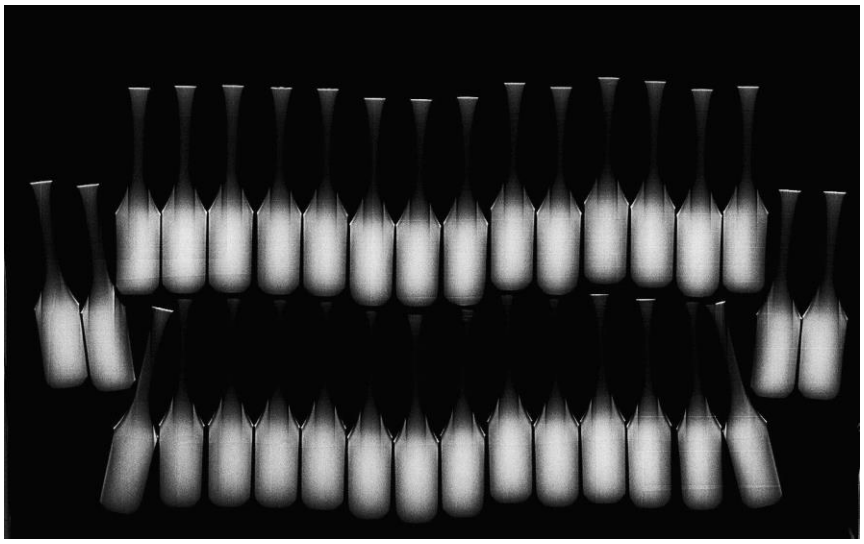

Figure 6.11 X-ray of Build #4 As Built, Tensile coupons (samples are 2 3/8 - 2 5/8 inches long).

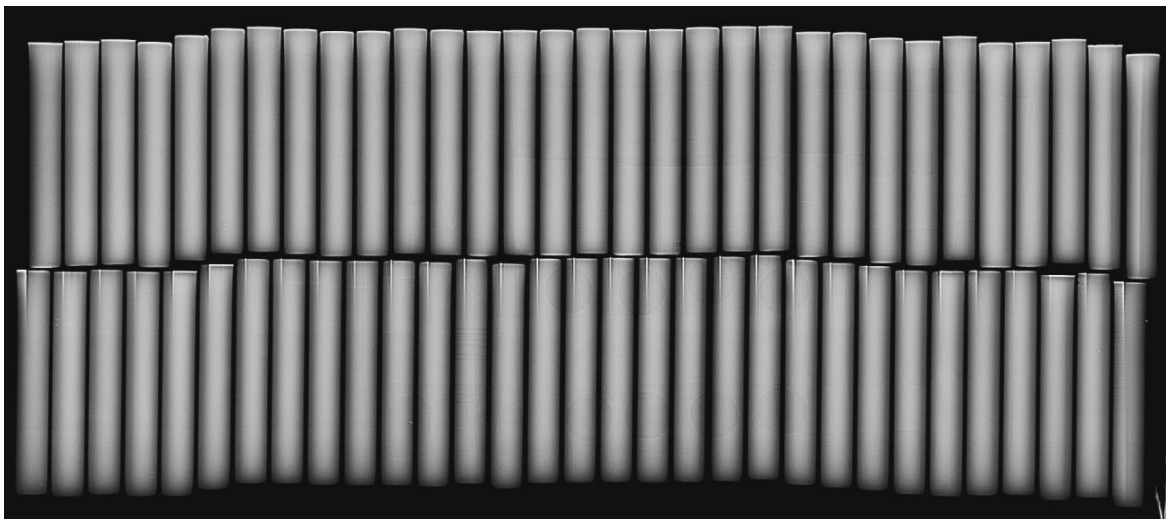

Figure 6.12 X-ray of Tensile Blanks for Machining and Heat Treating. (samples are 2 3/8 - 2 5/8 inches long).

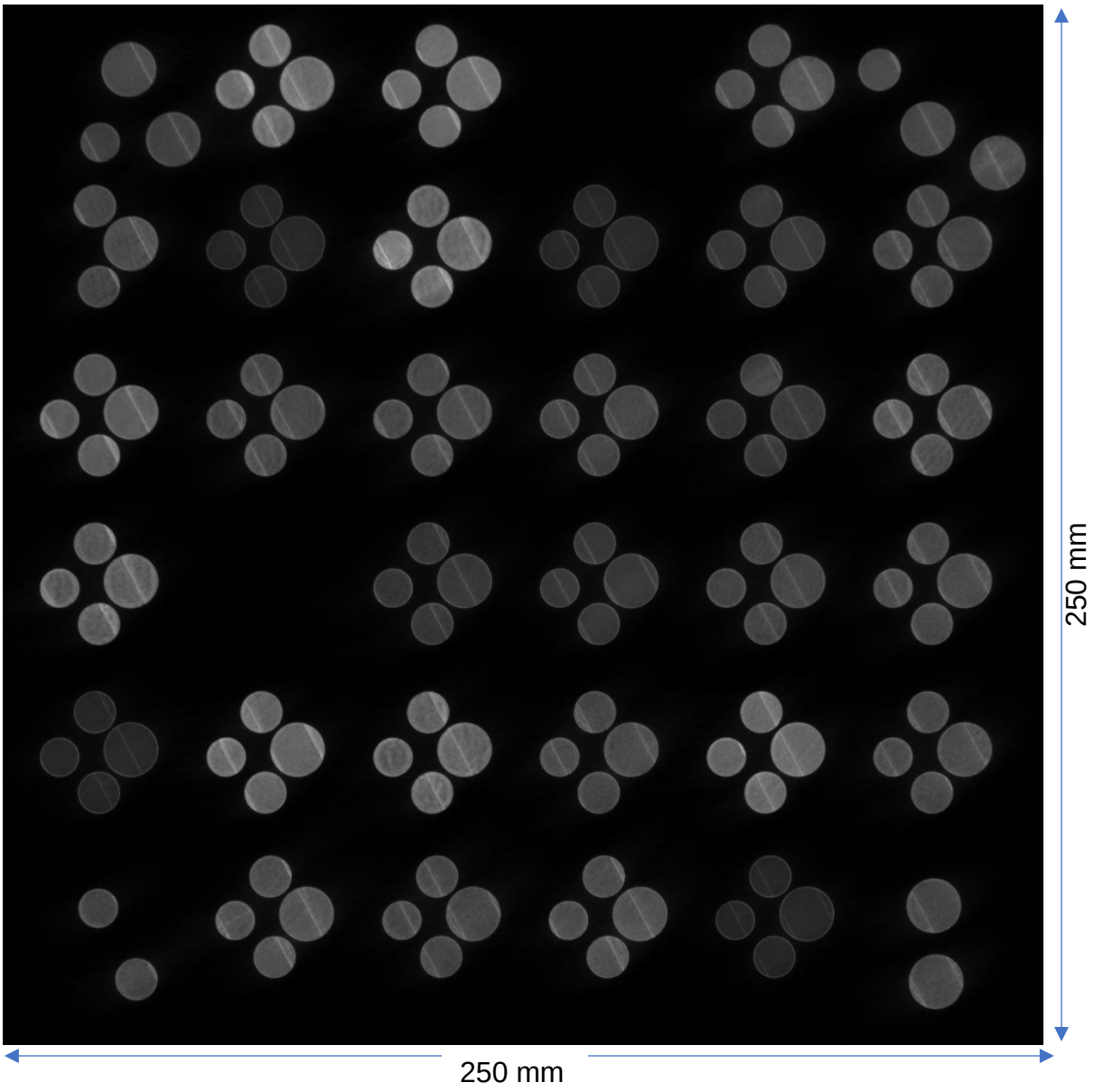

Figure 6.13 First In-Situ Image from Build #3 (250 mm x 250 mm).

parameters by looking back at Table 4.1 where the DOE combinations are presented and Figure 4.3, that shows the layout of the combinations in the panel. Figure 6.14 shows the last three in-situ images before the final failure occurred and the machine stopped. Figure 6.15 is the last image before the failure occurred. It is believed that an overheating event was occurring at those times causing the machine to stop, but it isn't clear what the cause was.

The CT scans of samples for runs 8 and 25 did not show any defects. The effective pixel pitch for the scans was 67 microns which is the feature size in the part that would occupy one pixel on the detector, or essentially the resolution. As a rule of thumb, it is preferable to have 3 pixels inside a feature to consider it detectable, so the detectable feature size would be 200 microns. The two samples evaluated had an energy density of 98.84, which was the highest value and expected to be the worst case for this matrix of samples.

6.2.4 Density Measurements

To reduce the number of samples to be built and fit them all on one build panel, it was necessary to eliminate the density samples that were originally planned. But after making the builds it was determined that some of the samples that were built could be used to make the measurements and calculate density. The cylindrical tensile coupons that were intended to be machined into test samples, were used in advance of the machining. These coupons had a small area near the bottom that was tapered to make them easier to remove from the panel which made the measurements and calculations

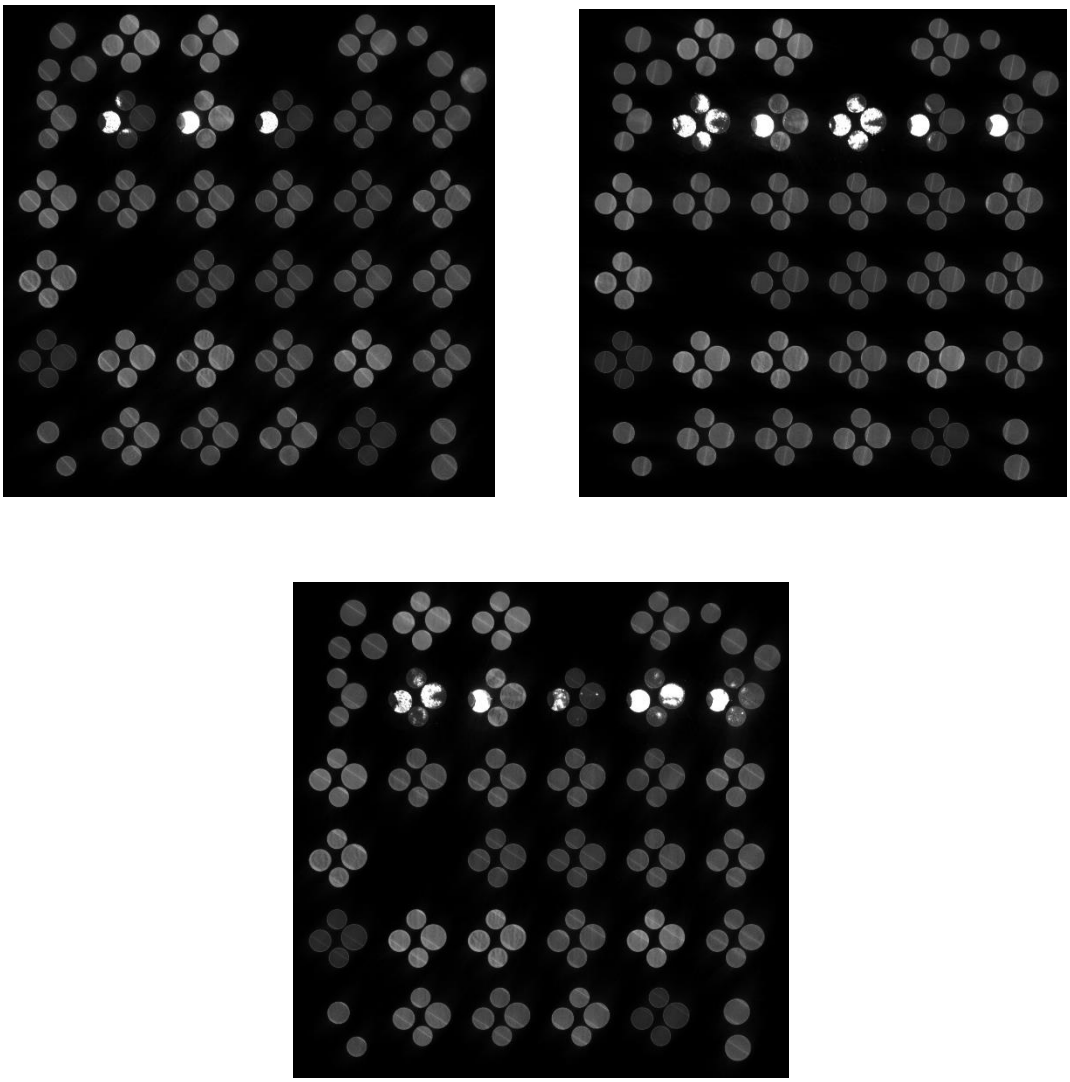

Figure 6.14 Three Images as the Final Failure Occurs and the Machine Stops (each scan is 250 mm x 250 mm).

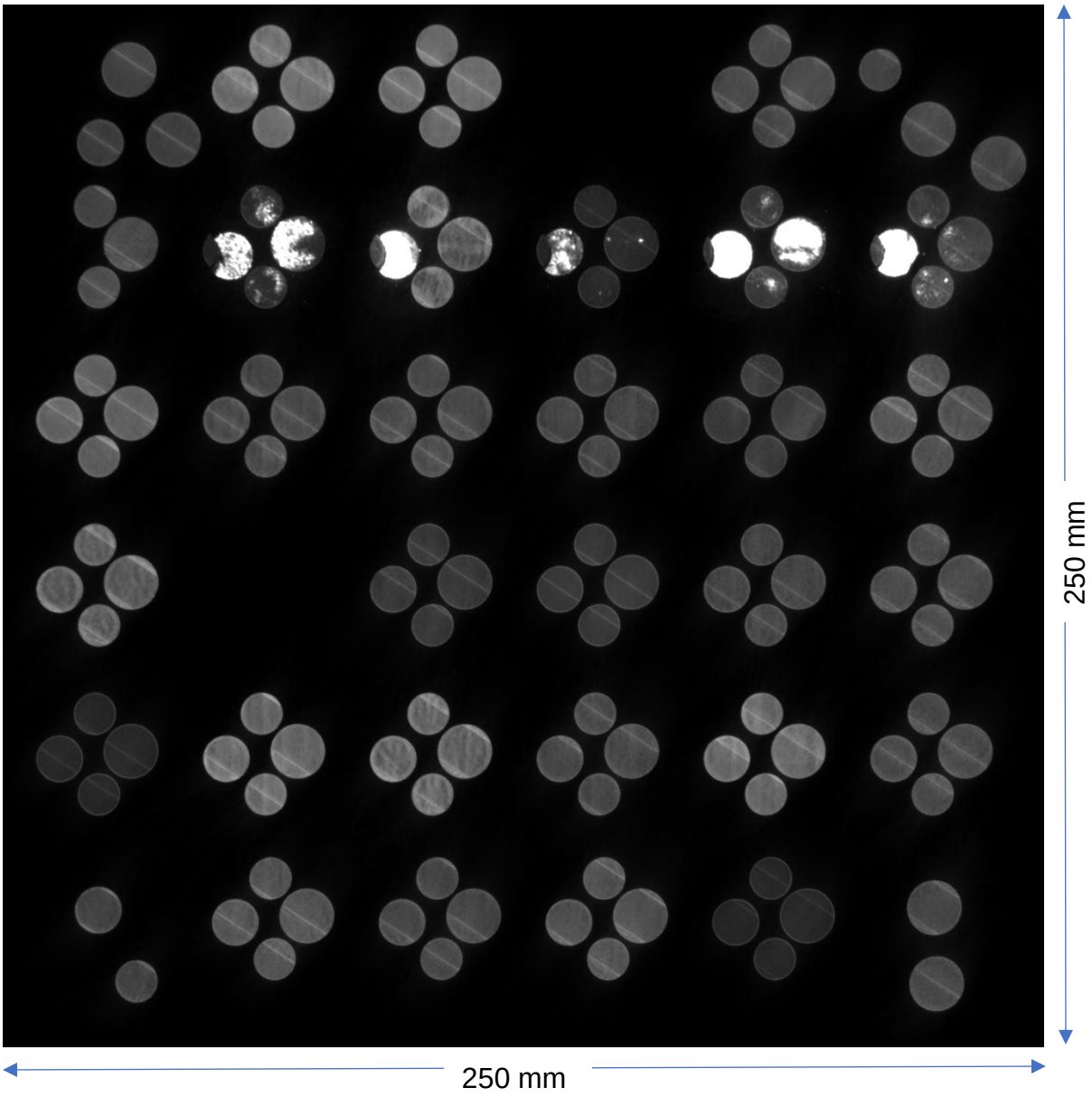

6.15 The Last Image from Build #3 before the Failure Occurred (250 mm x 250 mm)

slightly more complicated. Figure 6.16 shows the configuration of the sample used to perform the density calculations.

[69]A Mettler Toledo balance was used to weigh each of the blanks for calculating the densities. Archimedes' Principle was used to calculate the density and the formulas used were taken from the Mettler Toledo user manual after making the mass measurements using a precision balance in both air and in water.

A set of digital calipers was used to make the dimensional measurements of the metal samples. Then the calculations were made using the following formulas:

Density of a solid is determined with the aid of a liquid whose density is known, in this case, water:

$$\boldsymbol{\rho} = \left\{\left[\frac{\boldsymbol{A}}{\boldsymbol{A-B}}\right](\boldsymbol{\rho}_o - \boldsymbol{\rho}_1)\right\} + \boldsymbol{\rho}_1 \qquad \textbf{Equation 6.1}$$

where ρ = density of sample

A = weight of sample

B = weight of sample in water

ρ = m/V

ρ_0 = density of water

where m = mass of water at the test temperature

V = volume of water at the test temperature

Figure 6.16 Configuration used for density measurements

m = 65.71 at T = 21 C

Such that ρ_0 = 0.997999

ρ_1= density of air = 0.0012 g/cm^3

$$V_1 = \pi r^2 h \qquad \textbf{Equation 6.2}$$

Where r = D/2

D = the average diameter

h = overall length

$$V_2 = \pi h(D^2 + Dd + d^2)/12 \qquad \textbf{Equation 6.3}$$

Where h = overall length

D = the average diameter

d = the small diameter

Three diameter measurements were made along the length of the specimen and averaged to get the large diameter measurement for the length of the specimen. The small diameter, overall length, and drop length were each measured once.

Table 6.1 presents the values measured and all the calculated values used to determine the density for each combination of parameters used.

The expected density for NASA HR-1 is approximately 8.09. Except for one combination that turned out to have a great deal of defects, the density appears to decrease with increasing laser power, scan speed and hatch spacing. Figures 6.17, 6.18, and 6.19 present the trend analysis of the density test results. Figure 6.3 presents a ranking of all

Table 6.1 Density Data and Measurements from Samples

Sample	Mass		Large Diameters D			Overall Length	Small Diameter	Drop Length
	(g) in air	(g) in H2O	1	2	3			
20	65.7114	57.6216	0.484	0.4825	0.483	2.426	0.1255	0.3865
30	65.5695	55.6524	0.482	0.4835	0.481	2.434	0.125	0.3785
13	65.7501	57.6717	0.4835	0.4825	0.4825	2.425	0.1505	0.386
16	65.6839	57.6068	0.484	0.4815	0.481	2.4335	0.124	0.3805
26	65.6222	57.5601	0.4825	0.482	0.4825	2.435	0.0945	0.375
17	65.2502	56.6768	0.48	0.4825	0.4805	2.428	0.108	0.3715
22	65.6888	57.6183	0.4825	0.482	0.4825	2.426	0.1095	0.3845
2	65.4639	57.4167	0.4815	0.4805	0.481	2.4345	0.117	0.3785
4	65.7641	57.6694	0.4825	0.4835	0.475	2.447	0.1055	0.3655
32	63.6436	55.4738	0.4815	0.4825	0.4835	2.437	0.114	0.379
10	65.7627	57.6809	0.4825	0.482	0.484	2.435	0.099	0.385
7	65.3775	57.3158	0.4815	0.4815	0.482	2.4275	0.1025	0.3885
31	65.7293	57.6333	0.482	0.485	0.4795	2.423	0.101	0.3825
15	65.5259	57.4029	0.4825	0.483	0.482	2.438	0.1415	0.368
14	65.7544	57.6439	0.5105	0.512	0.5095	2.462	0.122	0.402
9	65.7815	57.6749	0.4835	0.4835	0.483	2.4315	0.125	0.3815
11	65.6922	57.6008	0.5135	0.5105	0.5105	2.4545	0.115	0.414
19	65.486	55.9992	0.484	0.4825	0.482	2.436	0.11	0.384
5	65.7354	57.629	0.485	0.483	0.482	2.447	0.102	0.3815
21	65.7114	57.6077	0.4835	0.4825	0.4815	2.427	0.105	0.313
28	65.7266	57.6424	0.4825	0.482	0.4825	2.438	0.1065	0.3715
24	65.4899	57.4525	0.4815	0.4815	0.4815	2.427	0.126	0.382
29	65.3511	57.323	0.4815	0.4815	0.482	2.4225	0.1145	0.3765
27	65.6823	57.6022	0.482	0.4835	0.483	2.445	0.1035	0.3915
23	64.0293	55.9258	0.484	0.483	0.484	2.436	0.1325	0.3825
1	65.4237	57.3569	0.4805	0.4815	0.479	2.427	0.125	0.3665
6	64.0685	55.9559	0.4825	0.482	0.4845	2.432	0.124	0.372
12	65.7549	57.6573	0.4825	0.4825	0.484	2.438	0.1175	0.3835

Table 6.1 (continued)

Average diameter	V1= pi x r^2 x h	V2 = pi * h*(D^2+Dd+d^2)/12	V = V1 + V2	rho =(A/A-B) * (rho0-rhoL)+rhoL
0.4832	0.4446	0.0313	0.4759	8.0979
0.4822	0.4442	0.0305	0.4747	6.5918
0.4828	0.4438	0.0332	0.4770	8.1141
0.4822	0.4441	0.0306	0.4747	8.1073
0.4823	0.4447	0.0282	0.4729	8.1147
0.4810	0.4410	0.0287	0.4696	7.5876
0.4823	0.4431	0.0299	0.4730	8.1145
0.4810	0.4421	0.0298	0.4720	8.1101
0.4803	0.4432	0.0280	0.4712	8.0995
0.4825	0.4454	0.0298	0.4752	7.7663
0.4828	0.4456	0.0293	0.4749	8.1123
0.4817	0.4421	0.0297	0.4718	8.0849
0.4822	0.4422	0.0292	0.4714	8.0939
0.4825	0.4456	0.0309	0.4765	8.0421
0.5107	0.5040	0.0356	0.5396	8.0825
0.4833	0.4459	0.0309	0.4768	8.0898
0.5115	0.5041	0.0361	0.5403	8.0940
0.4828	0.4458	0.0300	0.4758	6.8819
0.4833	0.4487	0.0293	0.4780	8.0843
0.4825	0.4435	0.0241	0.4677	8.0840
0.4823	0.4452	0.0287	0.4740	8.1054
0.4815	0.4417	0.0308	0.4725	8.1232
0.4817	0.4412	0.0296	0.4708	8.1154
0.4828	0.4474	0.0301	0.4775	8.1040
0.4837	0.4473	0.0316	0.4789	7.8773
0.4803	0.4396	0.0294	0.4689	8.0855
0.4830	0.4454	0.0300	0.4754	7.8733
0.4830	0.4465	0.0305	0.4770	8.0955

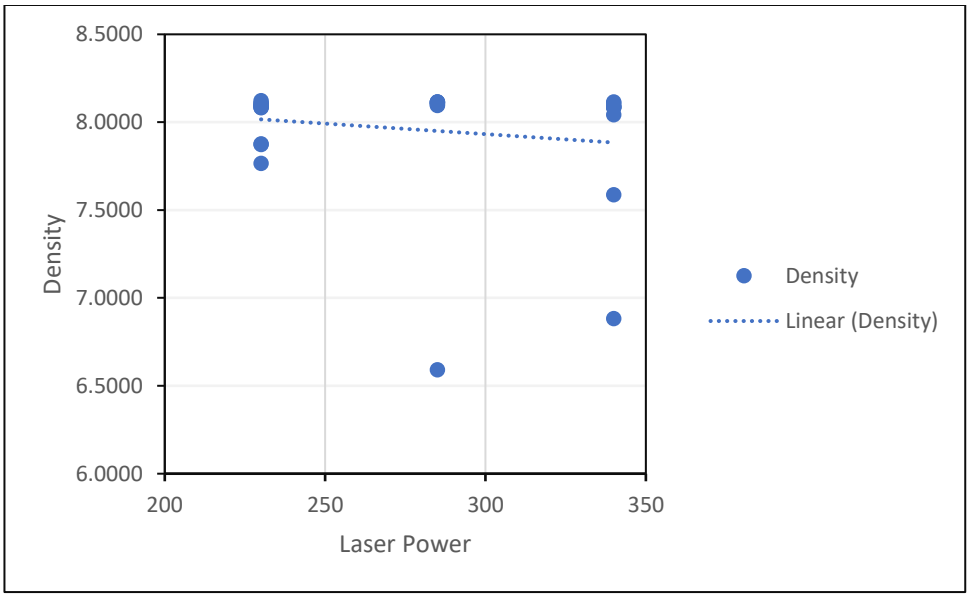

Figure 6.17 Density versus Laser Power

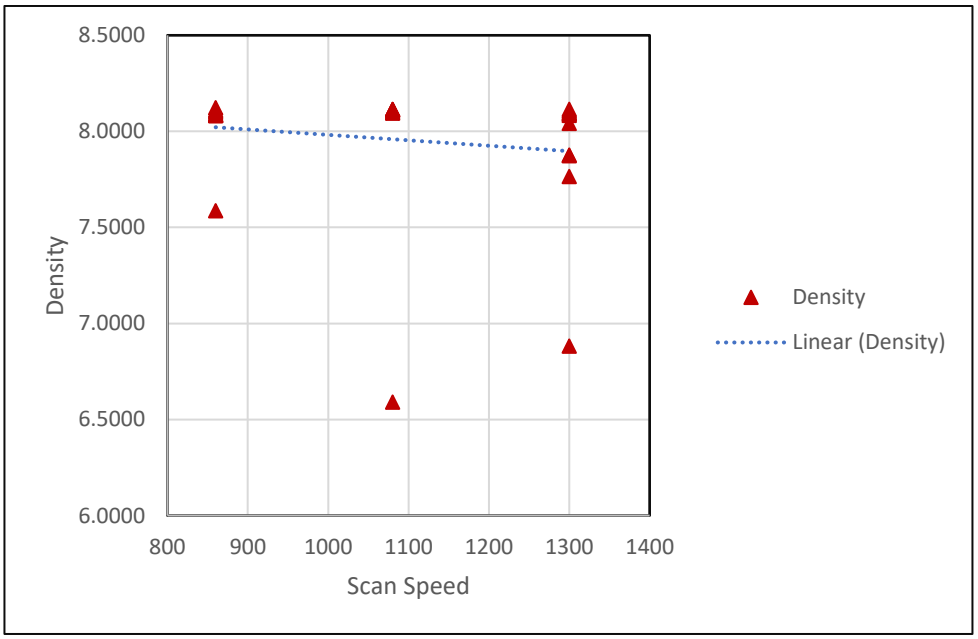

Figure 6.18 Density versus Scan Speed

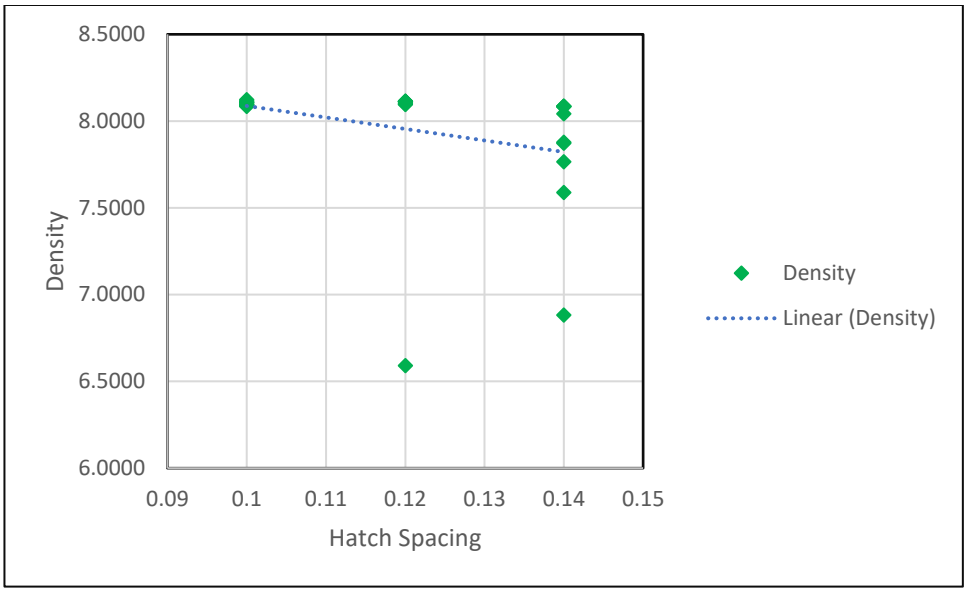

Figure 6.19 Density versus Hatch Spacing

the calculated densities.

6.2.5 Metallography

Metallographic examination was performed on a sample from each of ten of the samples that were produced in the DOE. The samples used were intended to be as built tensile coupons but since the builds all stopped early, none of these samples were completed to the point of being useable for that purpose. Figure 6.20 shows the sample configuration that was used for eight of the metallographic sections. These were eight different combinations that made it through until the machine stopped. Figures 6.21, 6.23, 6.24, 6.25, 6.26, 6.28, 6.29, and 6.30 show higher magnification photographs of the defects found in these eight combinations. Figures 6.22 and 6.27 show the whole cross section of the samples prepared for runs #3 and #18. These were the hot combinations that caused the build #1 to stop prematurely and resulted in only very small pieces of the samples attempted.

Most of the metallography only revealed porosity type defects. Figure 6.28 from Run #23 shows lack of fusion and is the only metallography sample that showed this type of defect.

The lower magnification photographs were analyzed using ImageJ to evaluate the volume of defects in each of the cross sections and the percentage of the area that was defective. Table 6.3 presents the data evaluation performed on the ImageJ application.

Table 6.2 Ranking Based on Density Measurements

Sample	Density	Laser Power (W)	Scan Speed (mm/s)	Hatch Spacing (mm)
24	8.123234192	230	860	0.1
29	8.11540914	340	1300	0.1
26	8.114708101	285	1080	0.12
22	8.114489169	285	1080	0.12
13	8.114118871	285	1080	0.12
10	8.112259842	285	1080	0.12
2	8.110122474	230	860	0.1
16	8.107254889	340	1300	0.1
28	8.105400677	285	1080	0.12
27	8.104047869	230	860	0.1
4	8.099506168	285	1080	0.12
20	8.09791782	230	1300	0.1
12	8.095473417	285	1080	0.12
11	8.093951482	230	860	0.1
31	8.093921153	340	1300	0.1
9	8.089757864	230	1300	0.1
1	8.085452709	340	860	0.14
7	8.08485454	340	860	0.14
5	8.084288783	340	1300	0.1
21	8.084029796	230	860	0.14
14	8.082537775	230	860	0.14
15	8.042062028	340	1300	0.14
23	7.877317493	230	1300	0.14
6	7.873299264	230	1300	0.14
32	7.766341629	230	1300	0.14
17	7.587584134	340	860	0.14
19	6.881934295	340	1300	0.14
30	6.591774113	285	1080	0.12

Figure 6.20 Sample configuration used for Metallographic sectioning

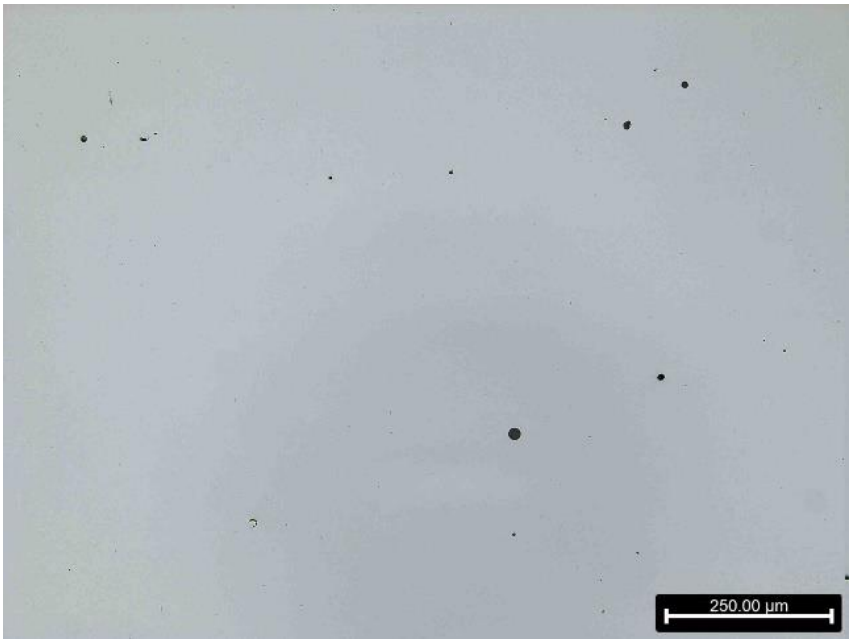

Figure 6.21 Defects from the Run #1 Core 2 sample from XZ direction, 100x

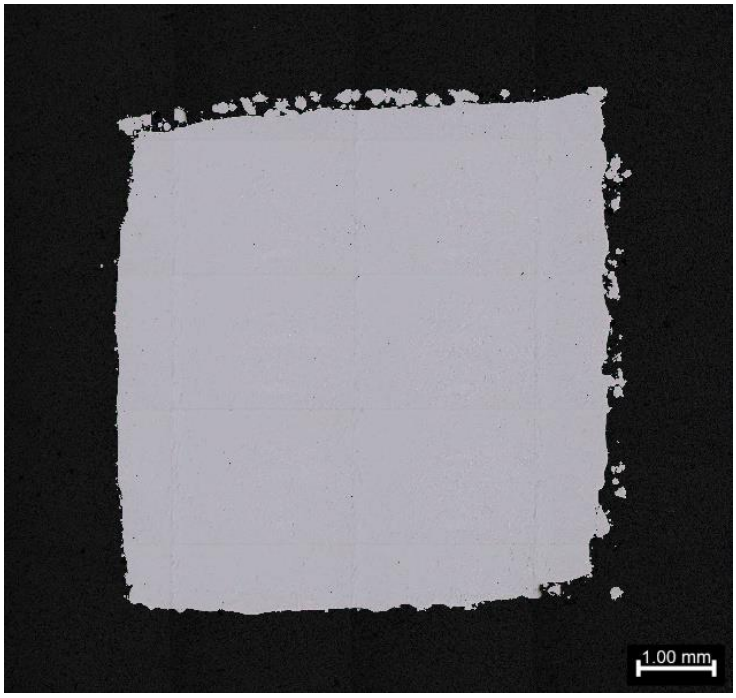

Figure 6.22 Defects from the Run #3 Tilescan sample, 50x

Figure 6.23 Defects from the Run #5 from Core1 XZ direction, 100x

Figure 6.24 Defects from the Run #9 Core1 XZ Direction, 100x

Figure 6.25 Defects From the Run #14 Core1 From XZ Direction, 100x

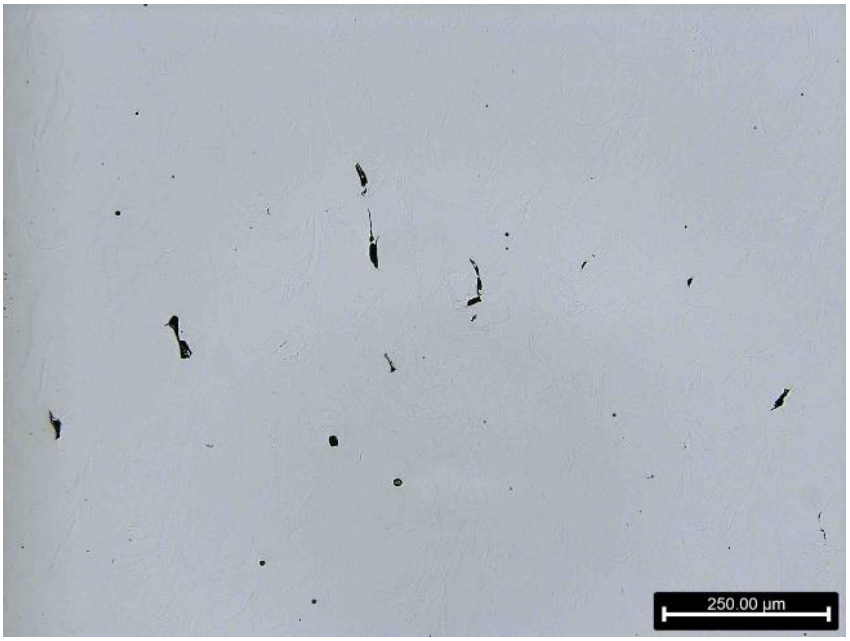

Figure 6.26 Defects From the #15 Core1 from the XZ Direction, 100x

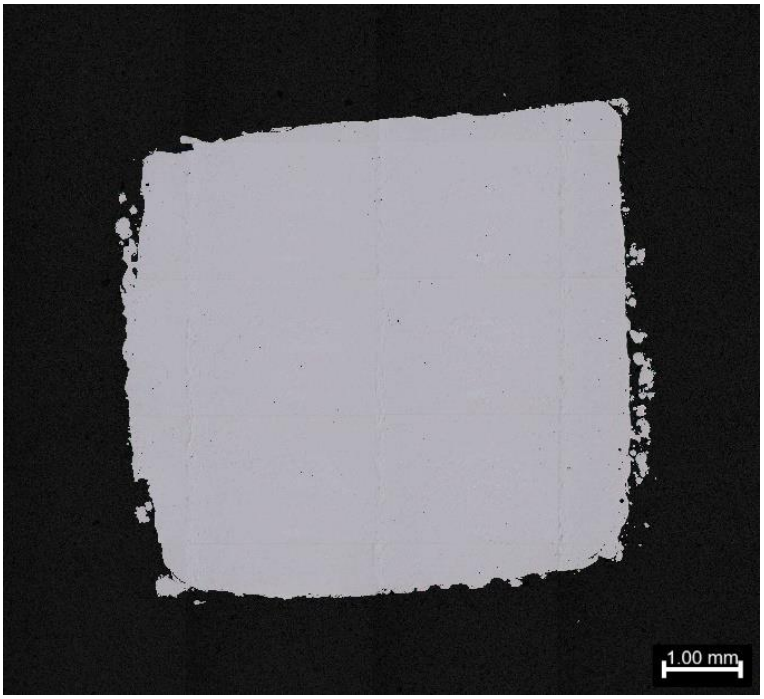

Figure 6.27 #18-1 Tilescan 50x_Overlay001

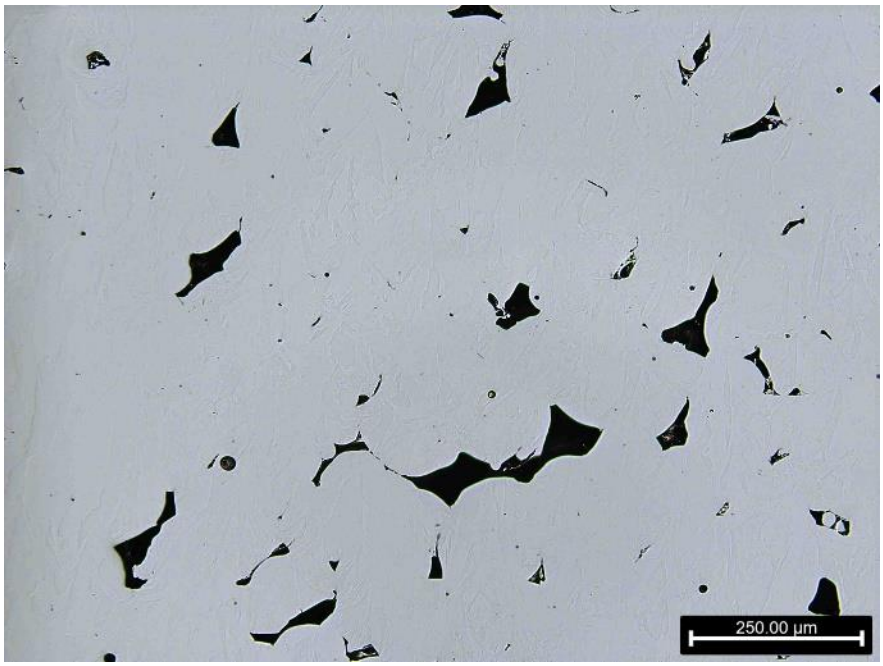

Figure 6.28 Defects #23 Core1 100x

Figure 6.29 Defects #27 Core2 100x

Figure 6.30 Defects #30 XZ Core2 100x

Figure 6.31 Sample Configuration for the pieces used for metallographic sectioning of Runs #3 and #18

Table 6.3 Defect Counts and Areas using ImageJ

Slice	Count	Total Area	Average Size	%Area	Laser Power	Scan Speed	Hatch Spacing
#1 Tilescan 50x_Overlay001.jpg	2486	0.047	1.90E-05	0.032	340	860	0.14
#3-1 Tilescan 50x_Overlay001.jpg	531	0.01	1.88E-05	0.026	340	860	0.1
#5 Tilescan Second 50x_Overlay001.jpg	2619	0.094	3.58E-05	0.063	340	1300	0.1
#9 Tilescan 50x_Overlay001.jpg	9535	0.543	5.70E-05	0.292	230	1300	0.1
#14 Tilescan 50x_Overlay001.jpg	5955	0.373	6.27E-05	0.17	230	860	0.14
#15 Tilescan 50x_Overlay001.jpg	6764	0.508	7.51E-05	0.29	340	1300	0.14
#18-1 Tilescan 50x _Overlay001.jpg	440	0.009	1.94E-05	0.025	340	860	0.1
#23 Tilescan 50x_Overlay001.jpg	16105	8.274	5.14E-04	4.323	230	1300	0.14
#27 Tilescan Second 50x_Overlay001.jpg	4348	0.093	2.14E-05	0.044	230	860	0.1
#30 Tilescan Second 50x_Overlay001.jpg	4195	0.171	4.07E-05	0.101	285	1080	0.12

Figures 6.32 through 6.37 show the trends for the percentage area and the average pore size. Table 6.4 shows the sorted values for pore count, total area and % area, and Table 6.5 shows the sorted values for average size. The #18 and #3-1 samples may have been biased by the size of the specimen evaluated. These are the two very hot runs from run 1. It was necessary to look at them because they were the only ones available from those combinations, but the results did not seem to follow the trends of the other samples at all. It would have been expected for them to have more defects because of the high heat.

Tables 6.4 and 6.5 also show the ranking of the results from the ImageJ assessments.

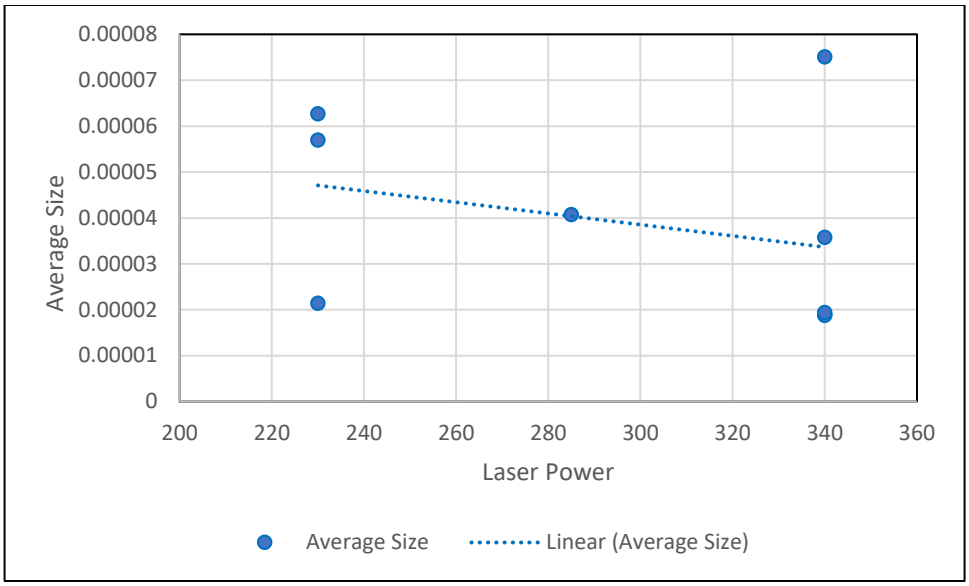

Figure 6.32 Average Pore Size Versus Laser Power

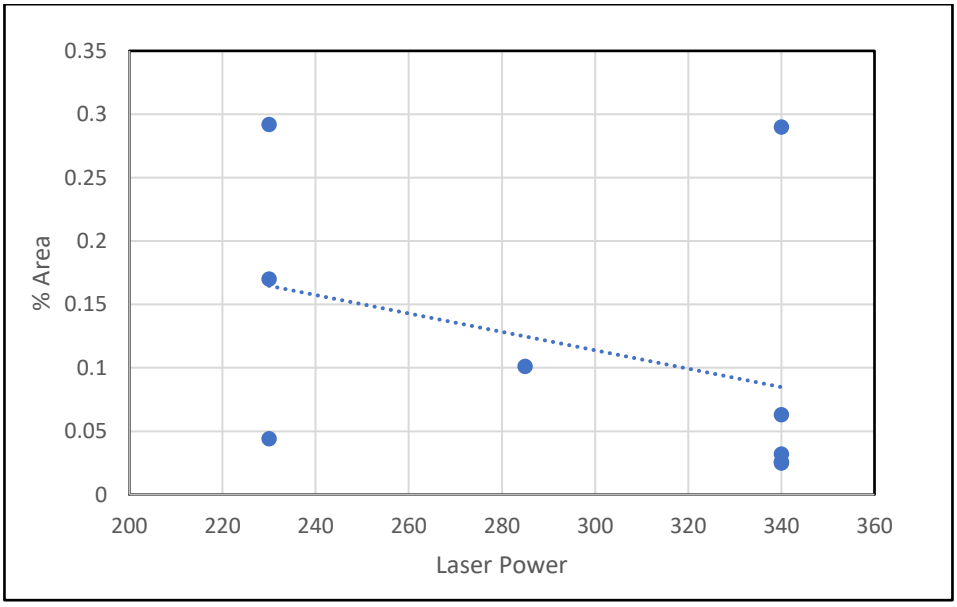

Figure 6.33 Percentage Area of Porosity Versus Laser Power

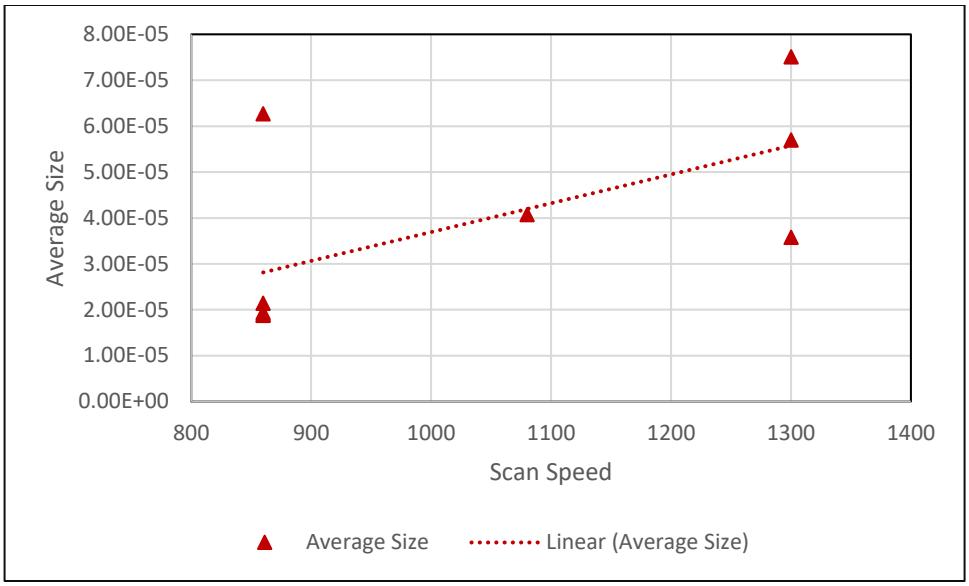

Figure 6.34 Average Pore Size Versus Scan Speed

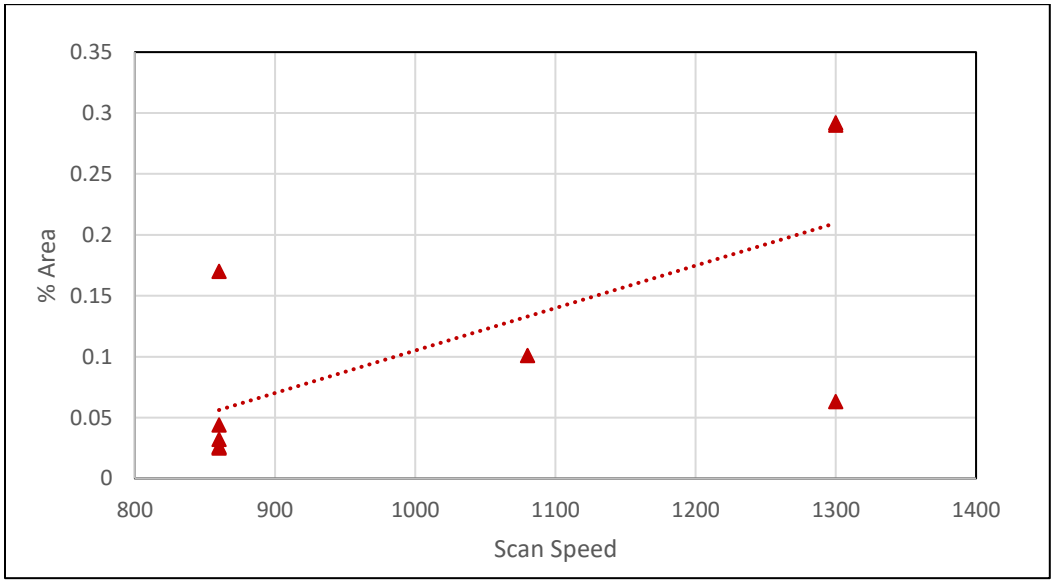

Figure 6.35 Percentage Area of Porosity versus Scan Speed

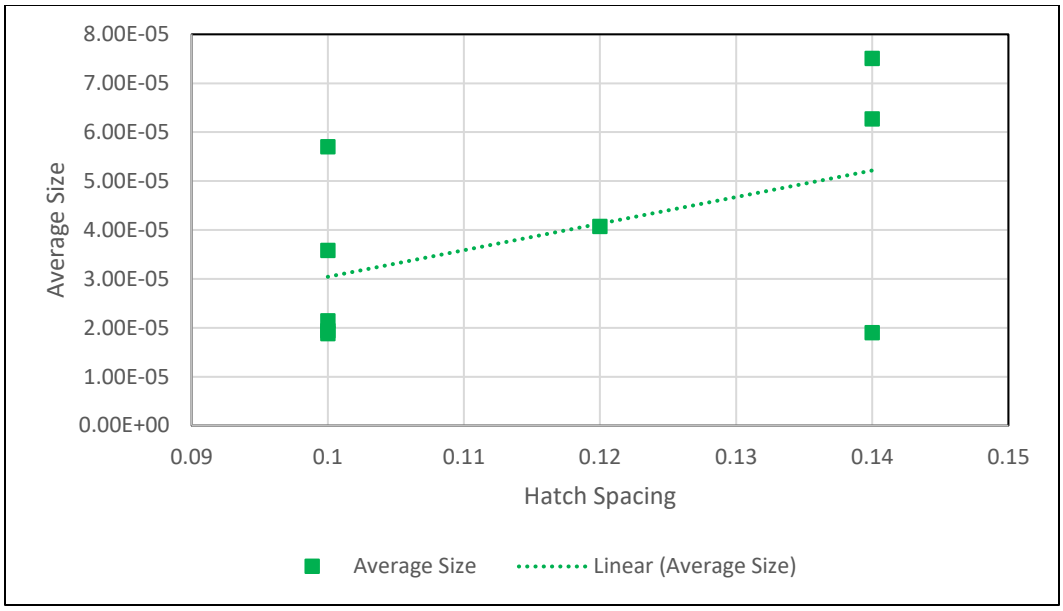

Figure 6.36 Average Pore Size versus Scan Speed

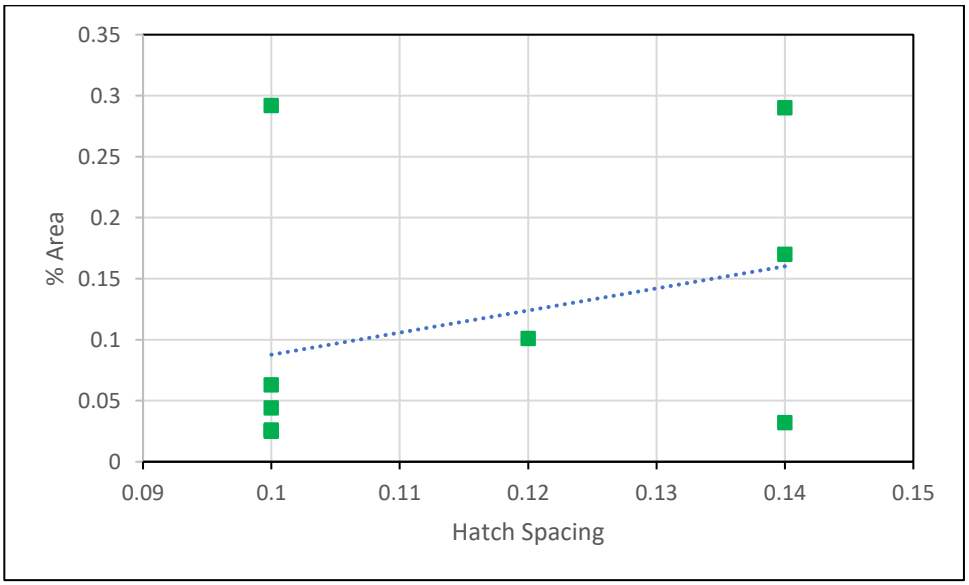

Figure 6.37 Percentage Area of Porosity versus Scan Speed

Table 6.4 Sorted by Count, Total Area, and % Area

Slice	Count	Total Area	Average Size	%Area	Laser Power (W)	Scan Speed (mm/s)	Hatch Spacing (mm)
#18-1 Tilescan 50x _Overlay001.jpg	440	0.009	1.94E-05	0.025	340	860	0.1
#3-1 Tilescan 50x_Overlay001.jpg	531	0.01	1.88E-05	0.026	340	860	0.1
#1 Tilescan 50x_Overlay001.jpg	2486	0.047	1.90E-05	0.032	340	860	0.14
#5 Tilescan Second 50x_Overlay001.jpg	2619	0.094	3.58E-05	0.063	340	1300	0.1
#30 Tilescan Second 50x_Overlay001.jpg	4195	0.171	4.07E-05	0.101	285	1080	0.12
#27 Tilescan Second 50x_Overlay001.jpg	4348	0.093	2.14E-05	0.044	230	860	0.1
#14 Tilescan 50x_Overlay001.jpg	5955	0.373	6.27E-05	0.17	230	860	0.14
#15 Tilescan 50x_Overlay001.jpg	6764	0.508	7.51E-05	0.29	340	1300	0.14
#9 Tilescan 50x_Overlay001.jpg	9535	0.543	5.70E-05	0.292	230	1300	0.1
#23 Tilescan 50x_Overlay001.jpg	16105	8.274	5.14E-04	4.323	230	1300	0.14

Table 6.5 Sorted by Average

Slice	Count	Total Area	Average Size	%Area	Laser Power (W)	Scan Speed (mm/s)	Hatch Spacing (mm)
#3-1 Tilescan 50x_Overlay001.jpg	531	0.01	1.88E-05	0.026	340	860	0.1
#1 Tilescan 50x_Overlay001.jpg	2486	0.047	1.90E-05	0.032	340	860	0.14
#18-1 Tilescan 50x _Overlay001.jpg	440	0.009	1.94E-05	0.025	340	860	0.1
#27 Tilescan Second 50x_Overlay001.jpg	4348	0.093	2.14E-05	0.044	230	860	0.1
#5 Tilescan Second 50x_Overlay001.jpg	2619	0.094	3.58E-05	0.063	340	1300	0.1
#30 Tilescan Second 50x_Overlay001.jpg	4195	0.171	4.07E-05	0.101	285	1080	0.12
#9 Tilescan 50x_Overlay001.jpg	9535	0.543	5.70E-05	0.292	230	1300	0.1
#14 Tilescan 50x_Overlay001.jpg	5955	0.373	6.27E-05	0.17	230	860	0.14
#15 Tilescan 50x_Overlay001.jpg	6764	0.508	7.51E-05	0.29	340	1300	0.14
#23 Tilescan 50x_Overlay001.jpg	16105	8.274	5.14E-04	4.323	230	1300	0.14

Chapter 7

Conclusions and Recommendations

This chapter includes the conclusions and recommendations for this study. This includes benefits and observations from the study as well as recommendations for continuation and additions to any future work. Another study would be very beneficial to try to get a full factorial experiment that could be statistically analyzed. There is also additional work that could be done on the existing unused specimens. The loss of the "hot parameters" was very unfortunate as well as all the other issues that occurred, but a great deal of good information was provided by the study and a lot was learned about in-situ monitoring.

A huge thanks to all the folks in my acknowledgements list and especially Dr. Yu and my Committee!

7.1 Conclusions

- The EOS machine does stop when the run becomes extremely hot, but not extremely cold which will also produce defects in the final product.
- The cold runs or issues are obviously visible while monitoring the in-situ data real time which allows the machine to be stopped manually even though it does not stop automatically.
- The defects produced by cold parameters are in fact worse than the ones produced by hot parameters.

- Table 7.1 lists the best combinations as they were predicted by the different methodologies studied.
- The Mukherjee method did not predict the combination that is currently in use for the Hr-1 alloy. It was predicted by Energy Density. But it is not clear whether that is the best combination of parameters for this alloy or not. Perhaps a tighter DOE without the hot parameters would be worth doing to find the best combination.

7.2 Recommendations

- Since I was unable to complete all the work planned originally for this study, I think there is much value in completing some of the work that remains, specifically the mechanical tests. I also have another set of coupons that could be used to complete additional density measurements that I would like to complete.
- Future work should include additional runs of similar DOE's that include more of the colder combinations and less of the hot combinations to evaluate how cold the run must be to fall off of the cliff, as it did in run 23

Table 7.1 Best Combinations as predicted by the different methods.

Laser Power (W)	Scan speed (mm/s)	Hatch Spacing (mm)	Method for prediction
285	1080	0.12	Energy Density
230	860	0.1	Material Density
340	1300	0.1	Material Density
285	1080	0.12	Material Density
340	860	0.14	Microscopy Pore Count
340	1300	0.1	Microscopy Pore Count
285	1080	0,12	Microscopy Pore Count
340	860	0.14	Microscopy average pore size
340	860	0.14	Microscopy average pore size
340	860	0.14	Mukherjee number
340	860	0.14	Mukherjee number w/ calculated Density

List of References

[1]Bi Zhang, Yongtao Li, Qian Bai. *Defect Formation in Selective Laser Melting: A Review.* Chinese Mechanical Engineering 2017 30:515-527

[2]Federico M. Sciammarella and Benyamin Salehi Najafabadi. Processing Parameter DOE for 316L Using Directed Energy Deposition. *Journal of Manufacturing and Materials Processing.* 2018**,** 2(3), 61; https://doe.org/10.3390/jmmp2030061.

[3]Pavel Hanzl, Miroslav Zetek, Thomas Baksa, Tomas Kroupa. The Influence of Processing Parameters on the Mechanical Properties of SLM Parts. *Elsevier Ltd.: Procedia Engineering 100.* 2015**,** pp 1405-1413.

[4] Lukas Fuchs, Christopher Eischer. *In-process monitoring systems for metal additive manufacturing.* A white paper from EOS GmbH, Germany, www.eos.info

[5]ASTM F 2792 Standard Terminology for Additive Manufacturing Technologies

[6]Sarah K. Everton, Matthias Hirsch, Petros Stravroulakis, Richard K. Leach, and Adam T. Clare. *Review of in-situ monitoring and in-situ metrology for metal additive manufacturing.* Elsevier Ltd.: Materials and Design. 2016, pp 431-445.

[7]Jacob Alldredge, John Slotwinski, Steven Storck, Sam Kim, Arnold Goldberg, and Timothy Montalbano. *In-Situ monitoring and modeling of metal additive manufacturing powder bed fusion,* AIP Conference Proceedings 1949, 020007 (2018), https://doi.org/10.1063/1.5031504. Published online: 20 April 2018.

[8]David H. Freedman, *Layer by Layer,* MIT Technology Review, December 19, 2011, https://www.technologyrevuew,cin/s/426391/layer-by-layer/

[9]Corey Dunsky, Process Monitoring in Laser additive manufacturing, September 12, 2014, https://www.industrial-lasers.com/articles/print/volume-29/issue-5/features/process-monitor

[10]EM20 MSFC Technical Standard, *Specification for Control and Qualification of Laser Powder Bed Fusion Metallurgical Processes,* October 18, 2017, 4.3.2.1 through 4.2.3.4, pp 22-24.

[11]Hossein Taheri, et al, “Powder-based Additive Manufacturing – A Review of Types of Defects, Generation Mechanisms, Detection, Property Evaluation and Metrology.” *International Additive and Subtractive Materials Manufacturing,* Vol.1, No. 2, 2017.

[12]Fulfa, Simina, et al, “Identification of in-line defects and failures during Additive Manufacturing Powder Bed Fusion processes.” *MATEC Web of Conferences 94***,** 030059 (2017), *CoSME’16.*

[13]Lu, B H, Li, D C. “Development of the additive manufacturing (3D printing) technology. *Machine Building Automation,* 2013, (4):1-4.

[14]Li, D C, He, J K, Tian, X Y et al, “Additive Manufacturing: integrated fabrication of macro/micro-structures.” *Chinese Journal of Mechanical Engineering,* 2013, (6):129-135.

[15]Zhao, J F, Ma, Z Y, Xie, D Q, et al. “Metal Additive Manufacturing Technique, *Journal of Nanjing University of Aeronautics and Astronautics,* 2014, 46(5): 675-683.

[16]Thijs, L, Verhaeghe, F, Craeghs, T, et al. “A Study of the Microstructural Evolution during Selective Laser Melting of Ti-6Al-4V, *Acta Materialia*, 2010, 58(9):3303-3312.am

[17]Steiner, Dirk and Urbanski, Jeff. “CT Inspection: An Inside Look at CT-Based Nondestructive Testing,” *Quality Magazine,* August, 2018.

[18]Aboulkhair N T, Everitt N M, Ashcroft I, et al. “Reducing porosity in $AlSi_{10}Mg$ parts processed by selective laser melting,” *Additive Manufacturing,* 2014, 1-4: 77-86.

[19]Gong H J, Rafi K, Gu H F, et al. “Analysis of Defect generation in Ti6Al4V parts made using powder bed fusion additive manufacturing processes,” *Additive Manufacturing,* 2014, 1-4: 87-98.

[20]Volaro T, Colin C, Cartout J D. “As-fabricated and hear-treated microstructures of the Ti6Al4V alloy processed by selective laser melting”, *Metallurgical and Materials Transactions A,* 2011, 42(10): 3190-3199.

[21]Liu Q C, Elambasseril J, Sun S J, et al. “The Effect of Manufacturing defects on the Fatigue Behavior of Ti6Al4V specimens Fabricated Using Selective Laser Melting”. *Advanced Materials Research,* 2014, 891-892: 1519-1524.

[22]Kempen K, Vrancken B, Buls S, et al. “Selective Laser Melting of Crack-Free High Density M2 High Speed Steel Parts by Baseplate Preheating.” *Journal of Manufacturing Science and Engineering*, 2014, 136(6).

[23]Carter L N, Essa K, Attallah M M. “Optimization of Selective Laser Melting for a High Temperature Ni-Superalloy,” *Rapid Prototyping Journal,* 2015, 21(4): 423-432.

[24]Zhang S, Gui R Z, Wei Q S, et al. “Cracking behavior and Formation Mechanism of TC_4 Alloy Formed by Selective Laser Melting,” *Journal of Mechanical Engineering,* 2013, 49(23): 21-27. (in Chinese)

[25]Li R D, Shi Y S, Wang Z G, et al. “Densification Behavior of Was and water Atomized 316L, Stainless Steel Powder During Selective Laser Melting,” *Applied Surface Science,* 256(13): 4350-4356.

[26]Gu D D, Hagedorn Y, Meiners W, et al. “Densification behavior, microstructure evolution, and wear performance of Selective Laser Melting Processed Commercially Pure Titanium,” *Acta Materialia,* 2012, 60(9): 3849-3860.

[27]Carter, L N, Wang X, Read N, et al. “Process Optimization of Selective Laser Melting Using Density Model for Nickel Based Superalloys.” *Materials Science and Technology,* 2015: 1-5.

[28]Yadroitsev I, Bertrand P, Smurov I. “Parametric analysis of the Selective Laser Melting Process,” *Applied Surface Science,* 2007, 253(19): 8064-8069.

[29]Xu W, Brandt M, Sun S, et al. “Additive Manufacturing of Strong and Ductile Ti6Al4V by Selective Laser Melting Via In Situ Martensite Decomposition,” *Acta Materialia,* 2015, 85: 74-84.

[30]Wang L, Wei Q S, He W T, et al. “Influence of Powder Characteristic and Process Parameters on SLM Formability.” *University of Science and Technology (Natural Science Edition)*, 2012, 40(6): 20-23.

[31]Thijs L, Kempen K, Kruth J, et al. “Fine-structured Aluminum Products with Controllable Texture by Selective Laser Melting of Prealloyed $AlSi_{10}Mg$ Powder,” *Acta Materialia*, 2013, 61(5): 1809-1819.

[32]Read N, Wang W, Essa K, et al. “Selective Laser Melting of AlSi10Mg alloy: Process Optimization and Mechanical Properties Development. *Materials & Design,* 2015, 65: 417-424.

[33]Wang D, Yang Y Q, Huang Y L, et al. “Density Improvement of Metal Parts Directly Fabricated via Selective Laser Melting,” *Journal of South University of Technology (Natural Science Edition),* 2010(6): 107-111.

[34]Yang Y Q, Song C H, Wang D. “Selective Laser Melting and its Application on Personalized Medical Parts,” *Journal of Mechanical Engineering,* 2014(21): 140-151.

[35]Vrancken B, Thijs L, Kruth J, et al. “Heat Treatment of Ti6AL4V Produced by Selective Laser Melting: Microstructure and Mechanical Properties”. *Journal of Alloys and Compounds,* 2012, 541:177-185.

[36]Rafi H K, Karthik N V, Gong H J, et al. “Microstructures and Mechanical Properties of Ti6Al4V Parts Fabricated by Selective Laser Melting and Electron Beam Melting”. *Journal of Materials Engineering and Performance,* 2013, 22(12): 3872-3883.

[37]Attar H, Calin M, Zhang L C, et al. “Manufacture by Selective Laser Melting and Mechanical Behavior of Commercially Pure Titanium.” *Materials Science and Engineering: A,*2014, 593: 170-177.

[38]Simonelli M, Tse Y Y, Tuck C, “Effect of the Build Orientation on the Mechanical Properties and Fracture Modes of SLM Ti-6Al-4V”, *Materials Science and Engineering: A,* 2014, 616: 1-11.

[39]Wu M W, Lai P, Chen J. “Anisotropy in the Impact of Toughness of Selective Laser Melted Tl6Al4V Alloy”. *Materials Science and Engineering: A.* 2016, 650: 295-299.

[40]Edwards P, Ramulu M. “Fatigue Performance Evaluation of Selective Laser Melted Ti-6Al-V.” *Materials Science and Engineering: A*, 2014, 598: 327-337.

[41]Hooreweder B V, Boonen R, Moens D, et al. “On the Determination of Fatigue Properties of Ti-6Al-4V Produced by Selective Laser Melting.” *Journal of Thermal Analysis & Calorimetry,* 2013, 113(113): 97-103.

[42]Rekedal K D, Liu D. “Fatigue Life of Selective Laser Melted and Hot Isostatically Pressed Ti-6Al-4V Absent of Surface Machining”. *56th AIAA/ASCE/AHS/ASC/Structures, Structural Dynamics, and Materials Conference, AIAA SciTech*, AIAA 2015-0894.

[43]Wycisk E, Emmelmann C, Siddique S, et al. “Effects of defects in Laser Additive Manufactured Ti6Al4V Alloy Processed by Selective Laser Melting”. *Advanced Materials Research,* 2013, 816-817: 134-139.

[44]Wycisk E, Solbach A, Siddique S, et al. “Effects of Defects in Laser Additive Manufactured Ti6Al4V on Fatigue Properties”. *Physics Procedia,* 2014, 56:371-378.
[45]Leuders S, Vollmer M, Brenne F, et al. “Fatigue Strength Prediction for Titanium Alloy Ti6Al4V Manufactured by Selective Laser Melting”. *Metallurgical and Materials Transactions A,* 2015, 46A(9):3816-3823.

[46]Kruth J P, 2009, *Procedure and Apparatus for In-situ Monitoring and Feedback Control of Selective Laser Powder Processing,* 2032345B1

[47]Wohlers T T, Wohlers Report, Wohlers Associates, 2015.

[48]AM Special Interest Group, in T.S. Board (Ed.). Shaping our national competency in additive manufacturing. Online: UK Government, 2012.

[50]Purtonen T, Kalliosaari A, Saliminen A, “Monitoring and Adaptive Control of Laser Processes,” *Phys. Procedia*, 56 (1) (2014) 1218-1231.

[51]”AM for Space,” *3D Printing Media Network, Space Additive Manufacturing, the next frontier for 3D printing,* https:// 3dprintingmedia.network/category/space-exploration/

[52]Hurley, Billy, Digital Editorial Manager, “3D Printing and Space Exploration: How NASA Will Use Additive Manufacturing,” *Tech Briefs, Engineering Solutions for Design and Manufacturing,* January 17, 2020.

[53]Alldredge, Jacob, et al, “In-Situ Monitoring and Modeling of Metal Additive Manufacturing Powder Bed Fusion,” *AIP Conference Proceedings 1949, The Johns Hopkins University Applied Physics Laboratory, https://doi.org/10.1063/1.5031504* published online: 20 April 2018.

[54]EOS M 290 Industrial 3D Printer, Technical Data Sheet, 1/2019.

[55]Chen, Yao, et al, “Defect Inspection Technologies for Additive Manufacturing,” *International Journal of Extreme Manufacturing,* **3**(2021) 022002 (21pp), https://dol.org/10.1088/2631-7990/abe0d0

[56]Zhong M L, et al, ”Boundary Liquation and interface cracking characteristics in laser deposition of Inconel 738 on directionally solidified Ni-based superalloy,” *Scripta Materialia,* April 25, 2005,159-164.

[57]Gunther J, et al, “Fatigue Life of additively manufactured Ti-6Al, 4V in the very high cycle fatigue regime,” *International Journal of Fatigue,* 2016, 94 236-245.

[59]Ojo O A 2007 “Intergranular Liquation Cracking in Heat Affected Zone of a Welded Nickel Based Superalloy in As Cast Condition,” *Materials Science and Technology,* 231149-55.

[60]Dye D, et al, 2001, “Numerical Analysis of the Weldability of Superalloys,” *Acta Materialgia,* 49 683-97.

[61]Mukherjee T, Wei H L, De A, DebRoy T, “Heat and fluid flow in additive manufacturing—Part I: Modeling of powder bed fusion,” *Computational Materials Science,* 150 (2018) 304-313.

[62]Mukherjee T, DebRoy T, “Mitigation of lack of fusion defects in powder bed fusion additive manufacturing,” *Journal of Manufacturing Processes,* 36 (2018) 442-449.

[63]NSI North Star Imaging, An *ITW* Company. https://4nsi.com/systems/x5000

[64]Xu Z. W. et al, “High Cycle Fatigue Performance of AlSi10Mg Alloy Produced by Selective Laser Melting,” *Mechanics of Materials,* June 2020.

[65]EOState Exposure OT user manual, EOS GmbH - Electro Optical Systems, 2020

[66]Jayakumar, Manikandan, “When and How to Use Plackett-Burman Experimental Design,” https://www.isixsigma.com/tools-templates/design-of-experiments-doe/when-and-how-to-use-plackett-burman-experimental-design/

[67] EOSTATE Exposure OT Monitoring software for laser-sintering systems
EOS GmbH - Electro Optical Systems
Robert-Stirling-Ring 1
D-82152 Krailling / Munchen
Telephone: +49 (0)89 / 893 36-0
Fax: +49 (0)89 / 893 36-285
Internet: www.eos.info
E-Mail: info@eos.info
Original operating instructions
Software – EOSTATE Exposure OT
Article number: 9258-3851
Edition: 05.20

[68] EOSTATE MeltPool Monitoring software for laser-sintering systems
EOS GmbH - Electro Optical Systems
Robert-Stirling-Ring 1
D-82152 Krailling / Munchen
Telephone: +49 (0)89 / 893 36-0
Fax: +49 (0)89 / 893 36-285
Internet: www.eos.info
.
Translation of the original operating instructions
Software – EOSTATE MeltPool
Article number: 9251-3841
Edition: 10.19

[69]Mettler Toledo User Manual, www.mt.com/GWP, Mettler-Toledo AG Laboratory & Weighing Technologies CH-8606 Greifensee, Switzerland, Mettler-Toledo AG 01/2011.

[70]WWW.EngineeringToolBox.com, “Metals, Latent Heat of Fusion.”

[71]Trapp, Johannes, et al, “In Situ absorptivity measurements of metallic powders during laser powder-bed fusion additive manufacturing,” *Applied Materials Today,* 9, (2017), 341-349.

[72]Chen, PoShou, Mitchell, M., HR-1 Alloy, *ASM Handbook,* 2005

Vita

Tina White Malone was born November 7, 1960 in Gadsden, AL. She received her BS in Materials Engineering from the University of Alabama in Birmingham and her MS in Systems Management from Florida Institute of Technology. She has worked for the National Aeronautics and Space Administration at Marshall Space Flight Center for almost 37 years. She has been married to William Malone for almost 40 years, has four children and four grandchildren. She loves music and plays several instruments including the piano. She also enjoys singing and gardening in her spare time. She is a member of Blanche United Methodist Church.